Queensland University of Technology

A NOVEL IDENTIFICATION METHOD FOR ULTRA TRACE DETECTION OF BIOMOLECULES USING FUNCTIONALISED- SURFACE ENHANCED RAMAN SPECTROSCOPY (SERS)

JUANITA MAREE HUGHES
B. APP. SC. (CHEM.) MRACI

Principal supervisor: Emad Kirakous

Submitted in partial fulfilment of the requirements for the degree of
Master of Applied Science (Research)

Discipline of Nanotechnology and Materials Science
Science and Engineering Faculty
Queensland University of Technology
2014

KEYWORDS

Biomolecular analysis

Caffeine

Doping in Sports

Erythropoietin (EPO)

Nanobiotechnology

Surface Enhanced Raman Spectroscopy (SERS)

Ultra trace analysis

ABSTRACT

The ultra trace detection of both simple and large organic biomolecules is sought after for many different applications. The aim of this research was to develop a simple, rapid and cost-effective technique for the detection of ultra trace amounts of simple organic molecules as well as complex biomolecules, using functionalised Surface Enhanced Raman Spectroscopy (SERS). Two models were developed using caffeine and erythropoietin (EPO) respectively.

Caffeine, the world's most widely used legal stimulant, is found in both beverages and pharmaceuticals. With its ubiquity, its assay is an important chemical analysis. Caffeine serves as an excellent simple organic molecule exemplar for this analytical technique.

Erythropoietin is a complex protein hormone produced by the kidneys to initiate red blood cell production and found in blood serum and urine. Detection and quantification of both human EPO and recombinant human EPO (rHuEPO) is required for medical purposes. Their distinction is also required, as rHuEPO is banned by both the World Anti-Doping Agency (WADA) and in animal racing. RHuEPO's proscribed use by athletes has been well documented in several infamous cases, e.g., in cycling. As a complex protein, EPO is also a valuable complex biomolecule exemplar for this technique.

For this work, antibody functionalised nanoparticles were developed and characterized, reacted with the analyte solutions, and then characterized by Raman spectroscopy. This thesis presents the results of the nanoparticle characterization, the Raman spectra, and the univariate statistical and/or chemometrics analysis.

It demonstrates the ability of this new technique to detect ultra low levels of the nominated analytes with significant improvement over existing methods. Caffeine detection was improved from 2×10^{-4} g (FT-Raman) down

to 2×10^{-13} g. The detection of EPO improved from 7×10^{-11} g (IEF) down to 3×10^{-16} g.

This novel technique quantifies the analytes in trace amounts, encompassing those levels required for the analysis of the nominated analytes (2×10^{-10} M to 3.5×10^{-13} M for EPO and 1×10^{-4} M to 1×10^{-9} M for caffeine), with application in many fields (such as, food analysis, clinical diagnostics, and in the racing and sports industries). Moreover it distinguishes between human EPO and rHuEPO, with a substantial improvement on current techniques, 71% (IEF) and 40% (MAIIA); distinguishing rHuEPO in urine at 2.5% of the total EPO. And so has widespread applicability for the ultra trace analysis of biomolecules.

TABLE OF CONTENTS

LIST OF FIGURES

LIST OF TABLES

LIST OF ABBREVIATIONS

APTMS	(3-Aminopropyl)-Trimethoxysilane
BHK	Baby Hamster Kidney
CHO	Chinese Hamster Ovary
EPO	Erythropoietin
ESA	Erythropoiesis Stimulating Agents
HLOQ	Higher Level of Quantification
HUEPO	Human Urinary EPO
IEF	Isoelectric Focusing
IS	International Standard
LLOQ	Lower Level of Quantification
LSPR	Localised Surface Plasmon Resonance
MAIIA	Membrane-Assisted Isoform Immunoassay
PBS	Phosphate Buffered Saline
pI	Isoelectric point
rHuEPO	Recombinant Human Erythropoietin
SERS	Surfaced Enhanced Raman Spectroscopy
TEM	Transition Electron Microscopy
THPMP	3-(Trihydroxysilyl) Propyl Methylphosphonate
UV-VIS	Ultraviolet and Visible
WADA	World Anti-Doping Association
IR	(Mid) Infrared
NIR	Near Infrared
FT	Fourier Transform

STATEMENT OF ORIGINAL AUTHORSHIP

The work contained in this thesis has not been previously submitted to meet requirements for an award at this or any other higher education institution. To the best of my knowledge and belief, the thesis contains no material previously published or written by another person except where due reference is made.

QUT Verified Signature

Signature:

Date: 4/6/2014

ACKNOWLEDGEMENTS

My heartfelt gratitude to my supervisors for your patience, advice and hard work on my behalf:

I would like to thank Emad Kirakous for the initial idea for this research, your input and helping with finding research that was applicable, your patience with me, and the hard work that you did to get the grant that we have now.

My thanks go to Godwin Ayoko for finding time from your very busy schedule and your willingness to help me wherever necessary. Thank you also for your great expertise which has been invaluable.

My gratitude to Bill Lott for your enthusiasm and inspiration, for believing in me and the worth of my research project, for helping me to aim high, and for your unqualified help to develop me into a beginning scientific writer. (However, any mistakes are mine.)

In addition, but not last, I would like to thank Martin Sillence for your enthusiasm about the EPO project and your advice on this project's real-life application and its industry linkage.

I would like to thank Llew Rintoul for your training and help on the Raman instrument. I am grateful to Jamie Riches for your help with training on the Transition Electron Microscopy (TEM) instruments and obtaining TEM measurements for me at Queensland University when our instruments were not available. Thank you also to Rachel Hancock for your initial training in electron microscopy. If I've forgotten any other technical staff who have helped me along this timeline please accept my apologies as I'm also thankful to you for what you have done.

Thank you to QUT for granting me a Strategic Masters Scholarship. Without this financial help I would not have been able to continue.

Thank you to my fellow students, and early career researchers who shared lab and office space and have to put up with me. You have been a good sounding board, and have provided technical help, encouragement and excitement with my progress. You have helped to keep my sanity during the stress of this project and I'll not forget you.

And, a massive Thank you to my family. Firstly I wish to express my gratitude to my sons for patience and understanding during the times that I have not been able to give you all the attention and help you need. I cannot thank enough my parents for your immeasurable help. You have relieved me of my parenting duties where necessary and have helped in so many innumerable ways to allow me the time to finish this work; I would not have finished this thesis without you. Thank you from the bottom of my heart.

Chapter 1: Introduction

1.1 BACKGROUND TO ANALYTICAL METHOD USED

1.1.1 Historical Background

Discovery of the Raman Effect

The phenomenon that is now known as the 'Raman Effect', which refers to light that has been inelastically scattered upon encountering molecules of interacting substances, was discovered and elucidated early in the 20th century. C.V. Raman, for whom it is named, became interested in the molecular scattering of light after reading Professor Joseph Larmor's paper, 'Molecular Scattering of Radiation'. He was also inspired by the work of Lord Rayleigh and his son, who proposed that the colour of the sea was simply a reflection of the colour of the sky [1].

Attempting to confirm Rayleigh's theory, Raman performed a simple experiment by observing the ocean through a Nicol prism in such a way that excluded reflection of light from the sky. He found that the sea's blue colour was not extinguished by this experiment, thus disproving the Rayleigh's theory. This observation laid the foundation for his future work, which led to the ultimate discovery of the Raman Effect [1]. Raman's initial experiments elucidating the molecular scattering of light employed concentrated sunlight and a pair of complimentary filters [fig.1.1.1]. Later an 18 cm telescope (short focus) objective lens was used to focus the light, and a direct vision spectroscope was used to view the emerging light.

A series of over 80 different liquids (aromatic, aliphatic and inorganic), several gases (ether and pentene vapours, CO_2 and N_2O) and ice crystals were examined. New polarized light beams that were not present in the incident beam were detected for each substance, and the scattered light had less energy than the incident light; and a gap of unoccupied space between the non-scattered and scattered light rays was visible through the direct vision spectroscope. Even the most careful experimental work could not extinguish

these effects, so they concluded that this phenomenon was characteristic of each substance [1]. The initial discovery of polarised scattered light, the consistent loss of energy in the scattered light, and the weak effect of the scattered light all pointed to a hitherto unknown phenomenon, which was the optical equivalent of the Compton Effect [1].

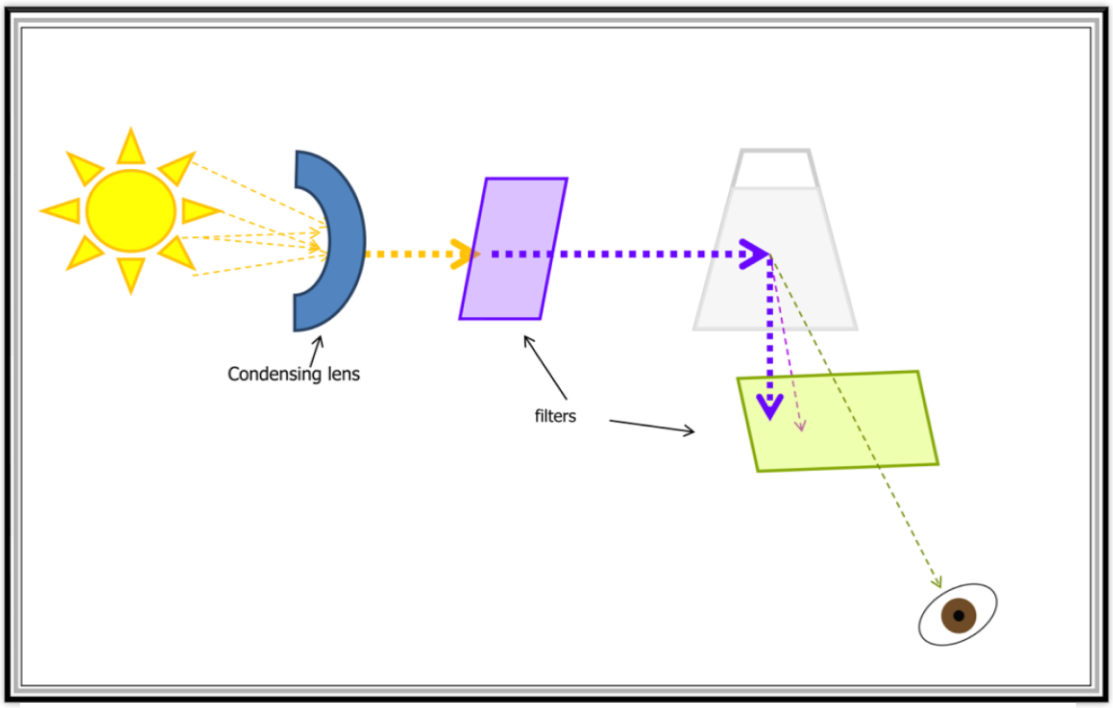

Figure 1.1.1 Experimental design for Raman's early experiments

In his first experimental observation confirming the 'Raman Effect', made on February 28, 1928, Raman used a monochromatic mercury arc lamp as the light source. (All visible light except that above indigo at 4358 Å was excluded by this lamp.) He used a direct vision spectroscope to view the emerging light. This showed several sharp blue/green lines, with a remarkable similarity in wavelength between related chemicals, i.e. pentane, heptane and octane [1]. He also showed that the difference in wavelength of the scattered light due to toluene was equivalent to its infrared (IR) absorbance, and that different molecules produced different wavelength shifts [1].

Raman was internationally credited with the discovery of the effect, which led to his election as Fellow of the Royal Society in 1924,[2] the granting of his knighthood in 1929 [1] and the Nobel Prize for physics in 1930. His Nobel prize

was awarded "for his work on the scattering of light and for the discovery of the effect named after him" [3]. His Nobel Lecture was entitled "The Molecular Scattering of Light" [4].

Chemists recognised the technique as a valuable analytical tool, and during this time 2500 different chemical compounds were studied using it, but its popularity waned due to the technical limitations associated with the arc lamp light source. The development of lasers in the 1960s as an intense coherent light source led to a resurgence in Raman research [1]. The Surface Enhanced Raman Spectroscopy (SERS) technique described in this thesis was accidentally discovered in 1974 by Fleischmann, *et al* [5].

The Surface Enhanced Raman Spectroscopy (SERS) Innovation

Fleischmann and his colleagues used pyridine deposited on a silver electrode in an attempt to use the Raman Effect to study a single molecular layer of analyte. To increase the surface area, they electro-chemically roughened a silver electrode. They ascribed the enhanced Raman signal that they observed to this increased surface area [5, 6]. The mechanism of enhancement was subsequently described and recognised as what is now known as the SERS effect, following its initial description in the late 1970s.

The first indication of the importance of Fleischmann's discovery was noted with the publication in the *Journal of the American Chemical Society* in July 1977 [7, 8] by M.G. Albrecht and J.A. Creighton. In November of the same year R.P. Van Duyne and D.L. Jeanmarie also published their findings on surface enhanced Raman spectroscopy in the *Journal of Electroanalytical Chemistry* [8, 9]. These two articles' theoretical explanations of the enhanced Raman signal were the foundation of the two current competing explanations for the SERS effect.

Since that time there have been several waves of interest in this research topic. The first upsurge in research interest in this topic was an intense research effort that refined the methodology and largely refined theory behind it. A second groundswell in SERS research activity started in the late 1990s, and the

publication of articles about SERS has grown exponentially since approximately 2000, led by improvement in instrumentation, the 'nano' revolution, and the enticement of single molecule detection [5, 10].

The SERS enhancement of spectral intensity led to the development of Raman spectroscopy for single molecule detection (SM SERS). Several laboratories have since independently claimed success [11].

Many technical developments have also supported the rise in Raman spectroscopy. Since their initial availability in the 1960s, lasers have continuously developed, increased in accuracy and flexibility and have diminished in size. This has allowed portable instrumentation to be developed [8]. Raman spectroscopy can now be performed outside the laboratory when required. So what is Raman spectroscopy?

1.1.2 **A background in Raman Spectroscopy**

When light interacts with matter, the majority of light that is scattered by the molecules is done so elastically; i.e. no energy is lost in the process and the angle of the emitted and incident light are conserved. This is commonly known as Raleigh scattering.

Only very few of the incident photons that interact with the substance molecules will lose or gain energy before being re-emitted. In such cases, the angle between the incident and emitted light is no longer conserved. Inelastically scattered light is called Raman scattering, and energy loss is more common than energy gain. These two types of inelastic scattering are called Raman Stokes scattering and Raman Anti-Stokes scattering, respectively [Fig. 1.1.2].

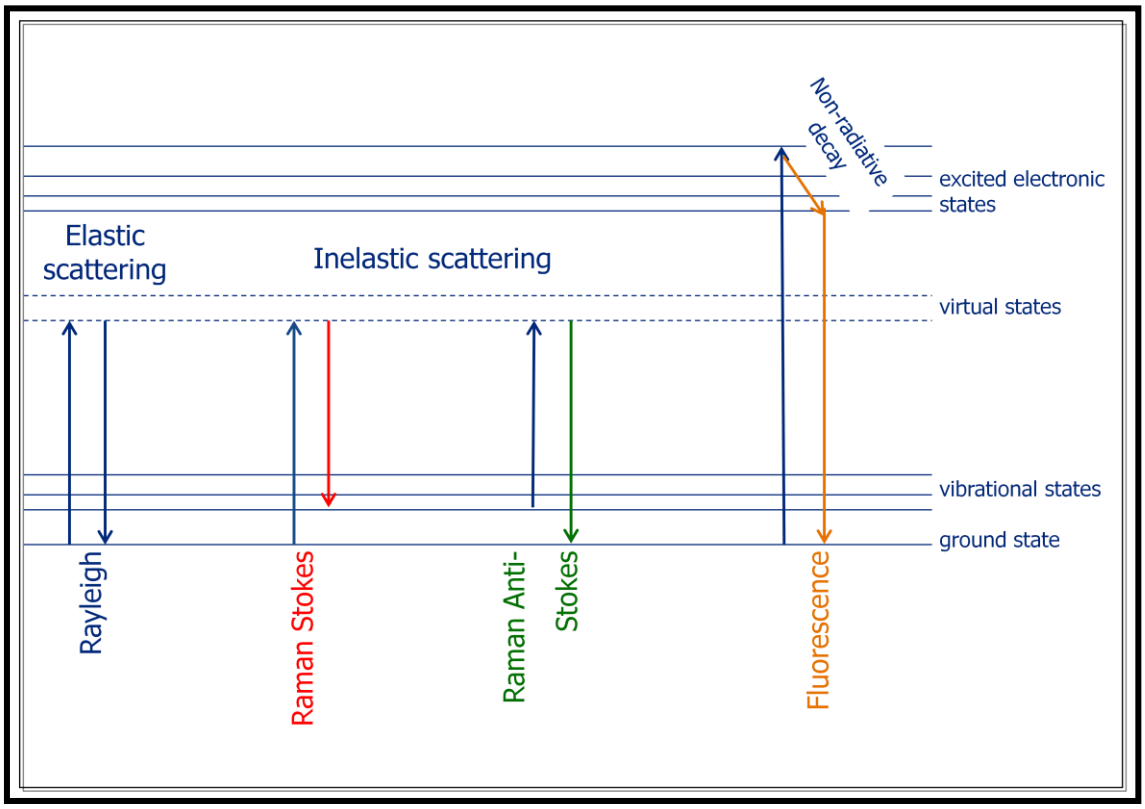

Figure 1.1.2 Simplified Jablonski diagram of energy transitions in molecules with the absorption and emittance of light, comparing elastic-Rayleigh scattering, inelastic-Raman Stokes and anti-Stokes scattering and fluorescence. The arrow pointing up is the energy of incident light with the arrow pointing down the energy of the emitted light.

The difference between the energy of the incident and emitted light in Raman scattering is neither random nor continuous. Rather, the quantum of energy that is absorbed or donated by the molecules reflects the status of the electrons in the bonds between the atoms of the molecules. Analysis of the energy differences is therefore diagnostic of the molecule, and can detect very subtle differences in molecular structure. In this way it forms a 'molecular fingerprint' of the molecule.

In general, fluorescence emission accompanies the Raman emission. Fluorescence is caused when the energy of the incident light undergoes rapid non-radiative decay, i.e. losing some energy as heat, before the incident photons are re-emitted [Fig 1.1.2]. Fluorescence emission is much stronger than Raman scattering and will swamp the relatively weak Raman signal for many samples. This limits the use of Raman spectroscopy.

As with all vibrational spectroscopy, not all molecules can be detected using Raman scattering. A Raman active molecule must have anisotropic polarizability to respond to incident light and generate Raman photons. The absorbed energy then induces a dipole moment in the molecules' bonds. The induction of a dipole moment within the molecule determines whether the molecule is 'visible' or 'invisible' to Raman.

Mid-infrared spectroscopy is complimentary to Raman Spectroscopy. Mid-infrared spectroscopy requires a permanent dipole in the molecule, whereas Raman spectroscopy induces a temporary dipole. Importantly, water is essentially 'invisible' in Raman spectroscopy, as it is already very polar. This means that Raman spectroscopy can be performed directly on analytes in aqueous solutions including biological fluids. This is a significant advantage when compared to infrared spectroscopy where trace amounts of water interfere with the analysis. Raman spectroscopy is generally characterized by sharp bands of good resolution, which makes the technique ideal for the distinction of closely related molecules such as structural isomers.

However, because Raman is such a weak effect, many molecules do not react strongly enough to be detected. Surface Enhanced Raman Spectroscopy (SERS) is a modified Raman technique that overcomes much of this difficulty.

1.1.3 **Surface Enhanced Raman spectroscopy**

Surface Enhanced Raman Spectroscopy (SERS) is a Raman Spectroscopic technique that greatly enhances Raman signals from Raman-active analyte molecules that have been adsorbed onto certain specially prepared metal surfaces[8]. SERS is observed primarily for analytes adsorbed onto coinage metals (Au, Ag and Cu) with the excitation wavelength in the near infrared (NIR) or visible region. Alkali (Li, Na, and K) metal surfaces have been proposed as even better enhancers, but their applicability is limited owing to their extreme reactivity with water. For excitation in the near ultraviolet region, Pd and Pt facilitate signal enhancements of about 10^2 - 10^3 fold.

Two primary explanations for SERS enhancement compete in the literature: an electromagnetic enhancement, based on the original interpretation by Van Duyne and his group [8, 9], and a Chemical Enhancement, as initially proposed by Albrecht and Creighton [7, 8].

Chemical Enhancement results from the interaction of analyte with the metallic surface to form a charge transfer complex. The metal-analyte proximity may allow pathways of electronic coupling from which novel charge-transfer intermediates emerge that have higher Raman scattering cross-sections than does the analyte when not adsorbed onto the surface. This effect it is limited to molecules that can chemically bond to the metallic surface.

The greater part of the overall enhancement of SERS is believed to be due to an electromagnetic enhancement mechanism that is a direct consequence of roughness of the metal surface. These features can be developed in a number of ways; for example: oxidation-reduction cycles on electrode surfaces; vapour deposition of metal particles onto substrate; metal spheroid assemblies produced via lithography; metal colloids; and, metal deposition over a deposition mask of polystyrene nanospheres. All of these methods leave the metal surface with small metal particles or aggregates of particles that serve as metal roughness features. The electromagnetic field at the particle's roughness results in an electromagnetic enhancement caused by the resonance oscillation of the free electrons on the metallic surface with the incident light. This forms an electric field at the particle surface called the localised surface plasmon resonance (LSPR) [8].

When the analyte molecule is within the effective range of the LSPR, the large electric field induces a dipole moment in the molecules, which yields the SERS enhancement [8]. The LSPR and the consequent SERS enhancement is only observed very close to the nanoparticle surface, and exponentially decays with increasing distance from the surface, with the effective range <10 nm [12]. The SERS enhancement can be as large as 10^5 - 10^6 fold [7, 9].

If multiple metallic nanoparticles are close enough together, their LSPR will merge and exhibit exponential enhancement. This can increase the enhancement of the SERS up to 10^{12} fold. These regions of extraordinary

enhancement are known as 'hotspots'. In most technological SERS applications, many analyte molecules and nanoparticles are measured simultaneously, because the spot size of the interrogating laser is many orders of magnitude larger than the nanoparticles or analytes. Because of the extraordinary enhancement value of 'hotspots' they will dominate any spectra.

SERS enhancement of Raman spectra is very good for pure analytes. However, many analytes co-exist with other interfering substances in complex matrices. This is particularly true when examining biological analytes, which are often found in very complex biological matrices. Biological fluids often contain multiple compounds that can bind to the metal surface, causing chemical enhancement and resulting in complicated and confusing spectra. Even when they cannot bind to the surface, all analytes within the effective range for electromagnetic enhancement will contribute to the Raman spectrum and may deliver interfering fluorescence emission that will also complicate the spectra. These limitations have led to further modification of the technique.

1.1.4 **Functionalised- Surface Enhanced Raman spectroscopy**

The restrictions in SERS selectivity has led to several improvements on the SERS method of Raman spectroscopy enhancement, including shell isolated nanoparticles and Raman reporters. These improvements are often combined in the same nanoparticles structure.

Shell isolated nanoparticles are metallic nanoparticles that have been coated with an inert outer shell. The outer shell can be polymer based [13] or silica and prevents non-specific binding to the nanoparticle surface [14]. The outer shell can then be functionalized with molecules with a specific affinity for the target analyte.

Raman reporters are dye molecules that can be attached to the metal surface of shell isolated nanoparticles [15, 16]. Raman Reporters demonstrate a very strong Raman signal, and the enhancement is maximised by binding the reporter to the metal surface. The technique can be referred to as indirect SERS detection when Raman reporters are used, as binding of the analyte is assumed rather than directly observed. Thus the analyte is indirectly detected through the detection of the Raman reporter molecule [17]. This represents a significant disadvantage, as the spectrum being acquired is not of the analyte itself, but of the Raman reporter molecule. Consequently, the Raman reporter approach has very little value for the SERS screening of analytes, unless it is coupled with another method to ensure that the analyte is bound. A 'sandwich' based method is common for this purpose, in which the analyte is anchored to the nanoparticle with one antibody and a second antibody that recognises a different epitope is used for detection. [fig. 1.1.3]

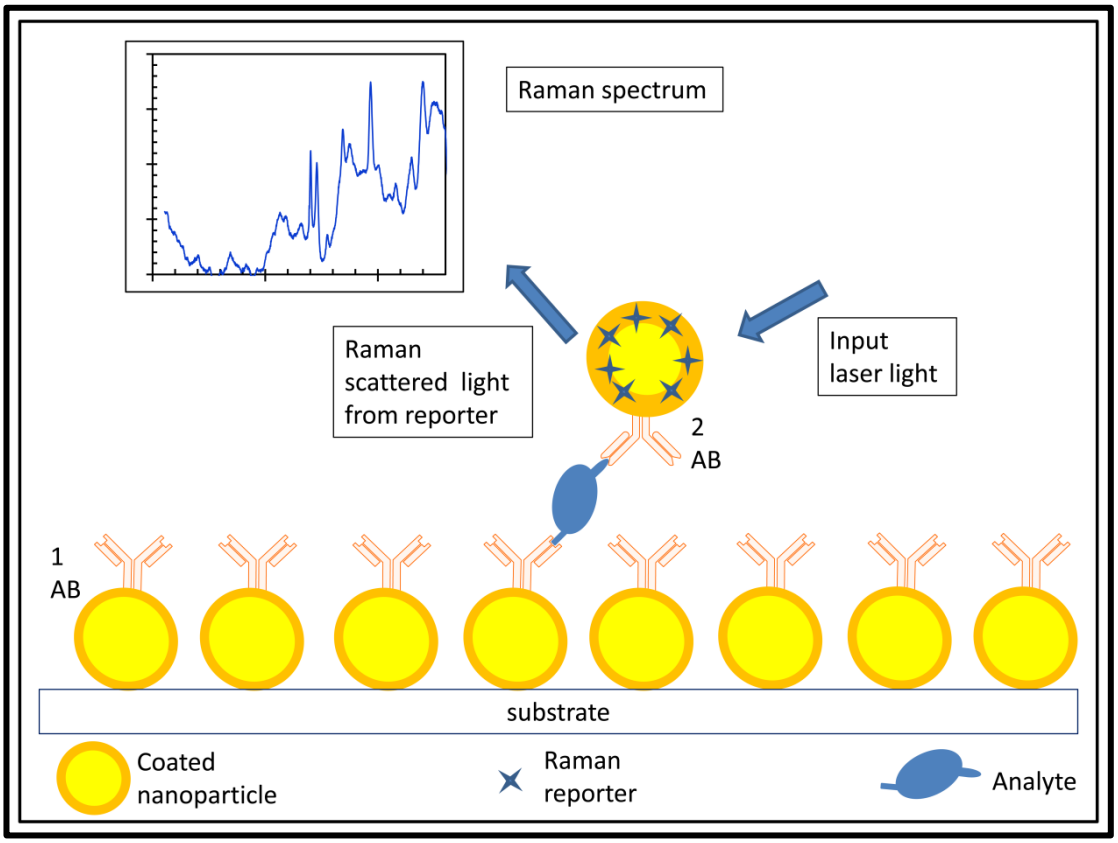

Figure 1.1.3 Common setup for indirect sandwich style Raman. Note: the 1st antibody (1 AB) could be attached directly to the substrate, or to an unanchored nanoparticle.

1.1.5 Other Methods Currently Used for Detection of Biological Analytes, Their Advantages and Problems

Several different techniques are currently available to detect biological analytes in solution. For proteins, biochemists traditionally use the antibody based techniques like the Western blot or the enzyme-linked immunosorbent assay (ELISA) [18-22]. For nucleic acids, techniques such as Southern blot and polymerase chain reaction (PCR) based techniques can be used [18, 23]. The detection mode in these methods is usually colorimetric [20-22, 24], fluorescent [25-27], or radioactive.

The SERS techniques typically require much smaller quantities of analyte, less time to complete the analysis, and reach lower detection limits than the currently used techniques for the analysis of biomolecules. The sensitivity and rapidity of SERS techniques are particularly evident when compared with conventional ELISA. See table 1.1.1. A direct comparison of SERS detection techniques with an equivalent ELISA detection method found that the SERS technique increased the sensitivity by 5 to 6 orders of magnitude with a wider detectable concentration range, used lower reagent consumption, and required a shorter induction time [22].

The SERS techniques in table 1.1.1 all employed a Raman tag, i.e. indirect SERS. The direct SERS technique proposed in this study will retain all the benefits of these techniques, but will, in addition, directly confirm analyte binding and will collect information about the analyte within the SERS spectrum. This additional information will allow discrimination between very similar molecules, even when antibody cross-reactivity is present.

Table 1.1.1 Analysis of the Strengths and Weaknesses of the Current Techniques, and Proposed New Techniques

Method	separation/ purification/ amplification	detection	time required	sample	sample size	Lower limit of detection		Ref
							M	
current methods								
ELIZA	immuno sandwich	colorimetric	16 hr	human IgG & rabbit IgG	10 µL	10 ng/mL, 25 ng/mL		[22]
ELIZA	immuno sandwich	colorimetric	14 hr	antibodies to malachite green (raman tag)	100µL	20 µg/mL		[20]
ELIZA	immuno sandwich	colorimetric	~5hr	(fluoro) quinolone anti-biotics in food	5g	4 -200 µg/kg		[21]
flow injection	flow injection	Chemilumin-escence	30 sec	Levofloxacin antibiotic in urine or serum	500 µL	0.3 ng/ml		[28]
Capillary Electrophoresis	hydroxyl propyl-β-cyclodextrin	fluorescence	3 min	Levofloxacin antibiotic in PBS or urine	-		10×10^{-9} in PBS	[25]
reversed-phase HPLC	Organic extraction, chiral mobile phase	UV	>30 min	Levofloxacin antibiotic in urine or serum	plasma 250 µL, urine 10 µL)	0.08 - 23 µg/mL (plasma, urine)		[29]
Other suggested methods								
exonuclease protection assay	aptamer with EPA Real-Time PCR	fluorescence	4 hours	$thrombin_{(aq)}$	1µL	$\sim 10^2$ mole-cules	1.7×10^{-16}	[26]
Aptamer DNA Arrays	Aptamer imbedded array	Confocal fluorescence microscopy	2-3 min.	$thrombin_{(aq)}$ and in BSA	100 µL		2×10^{-10}	[27]
Electrochemical Assay	Aptamer with magnetic separation	Electro-chemical	minimum 1 hour	thrombin in buffer, serum & plasma	450 µL		0.5×10^{-9} (buffer), $<5 \times 10^{-9}$ (bio-fluids)	[30]
circulating-flow piezoelectric biosensor	Au nano-particle PCR amplification	piezo-electric	varied >2.5 hr	*E coli* in PBS, apple juice, milk, beef	1mL, 1 g beef	1.2×10^2 CFU/mL		[23]
Proposed Raman tagged SERS methods								
Raman tagged SERS	Az–p53 complexing	Raman tag	5 hr	wild-type and mutant p53 proteins in serum	200 µL		500 fM, 5 pM in serum	[19]
Raman tagged SERS	Aptamer with magnetic separation	Raman tag	1.5 hr	thrombin in buffer,spiked 1% fetal bovine serum(FBS)	25 µL		0.27 pM	[31]
Raman tagged SERS	immuno sandwich	Raman tag	4 hr	antibodies to malachite green (raman tag)	100µL	50 pg/ml		[20]
Raman tagged SERS	immuno with magnetic separation	Raman tag	1 hr	Viruses in PBS	50µL	5 fg/mL	-	[17]
						25 pg/mL	-	
Raman tagged SERS on microarray chip	immuno sandwich	Raman tag	1:45 hr	human IgG & rabbit IgG	0.75 µL	10 fg/mL, 10–100 fg/mL		[22]
Raman tagged SERS with complimentary DNA	sandwich to glass slide, DNA extracted from sample	Raman tag	1hr + DNA extract-ion time	genetically modified rice	-	0.1 pg/mL		[18]

1.2 AIMS OF THE PRESENT STUDY

The overarching aim of my thesis is to develop a technique capable of detecting ultra trace levels of biologically relevant molecules in biological fluids and/or aqueous solutions. This technique should be able to:

- Provide sufficient information about the molecule to adequately identify it.
- Distinguish between very similar molecules.
- Be impervious to water to simplify the method.
- Measure ultralow quantities of analyte.
- Carry out rapid on-site screening.

However it should not:

- Exhibit non-specific cross-reactivity.
- Mask and/or swamp the analyte spectrum.

Raman spectroscopy with its characteristic features is competent for the required detection. Functionalised metallic nanoparticles allow for the rapid SERS screening of ultra trace amounts of analytes in various aqueous matrices. However, the indirect detection method described above has important limitations. Direct SERS detection of analytes by functionalized nanoparticles is preferred, as it ensures that the method is actually detecting the analyte not just implying its presence.

Critical innovations to the nanoparticle structure are required to enable the direct detection of analytes. This research presents the development of functionalized nanoparticles with the desired features for the detection of ultra trace amounts of caffeine and erythropoietin (EPO) in aqueous and biological matrices by SERS.

1.3 WHAT WILL BE ATTEMPTED AND RESEARCH QUESTIONS ANSWERED

In this study we developed a proof of concept for the direct, ultra trace detection of biologically relevant molecules in solution, using SERS detection of antibody functionalised nanoparticles. This was developed using two model analytes: caffeine in caffeinated beverages and erythropoietin (EPO) in human urine. Here we demonstrate that the technique is applicable to a wide range of biologically relevant molecules, from small organic biomolecules to much larger and far more complicated proteins.

The questions that are answered in this proof of concept include:

- Does the technique detect the analyte?
- Will the nanoparticle manufacturing process interfere with the antibody's reaction site?
- Is blocking needed to prevent non-specific cross reaction?
- What is the optimal nanoparticle reaction time for best analytical results?
- Is the technique sufficiently sensitive for the desired application?
- Can the technique distinguish between closely related analytes that might cross react with the functionalised nanoparticles?
- Can the technique quantitatively determine the concentration of the analyte that is present?

1.4 SIGNIFICANCE AND SCOPE OF THE RESEARCH

The ultra trace detection of both small and large organic biomolecules is sought for many different applications. While inductively coupled plasma mass spectrometry (ICP MS) is capable of trace detection of metal ions to a detection limit as low as 1×10^{-5} ng/g, but varying widely between minerals [32], few methods are capable of trace or ultra trace detection of organic molecules. ICP MS is only useful for organic molecules where the molecule is organometallic. A technique that is capable of ultra trace detection is urgently needed.

Biological molecules are frequently found in aqueous solutions. When the analyte is in trace concentration, it is commonly found in a complex matrix with many possible interfering species. Often extensive pre-analysis separation and/or concentration techniques are required to enable detection or to prevent false identification. This increases the complexity of the analysis and the amount of time required. A technique that allows direct measurement in biological fluids without this pre-preparation would be a valuable advance.

One important example application where this technology could be used is for medical diagnostics and anti-doping purposes. Many biomarkers for disease detection and monitoring are found in ultra trace levels within complex biological fluid matrices. Detection of doping in sport often has the same limitations as medical diagnostics.

The anti-doping effort often requires techniques that are capable of measuring ultra trace concentrations of doping agents or their metabolites. These doping agents are often found in biological fluids, and noninvasively obtained biological fluids, such as urine or saliva, are preferred.

Other examples of where technique could potentially assist include environmental monitoring of water for public health and homeland security; industrial/manufacturing processes where the determination of a particular analytes concentration in a mixture is required for quality control; and forensic applications where detection of trace level contaminants at a crime scene is sometimes required. In fact, the scope of this technique's applicability is only limited by the user's imagination.

TWO independent but related studies were used in this project. An initial study using caffeine as the analyte was used to establish and troubleshoot the technique, followed by the main study, which analysed erythropoietin. The corresponding chapters will provide the background specific to that particular study. They will also present the results and discussion of the individual studies performed. The following outlines the specific details of the remaining chapters:

Chapter 2 describes the experimental design. This chapter details the materials and instruments used for general nanoparticle manufacture and characterisation.

Chapter 3 presents the results and discussion for the caffeine model analyses, including the characterisation of the caffeine specific nanoparticles and the initial studies to develop the general technique.

Chapter 4 provides a background literature review of erythropoietin (EPO), recombinant human EPO (rHuEPO) and its misuse by athletes, and the current techniques used to detect this misuse. It then provides the results and discussion and summary for the EPO model analyses.

Chapter 5 provides an overall summary of this work and indicates the future directions of the research.

Chapter 2: Materials and Methods

This chapter describes the experimental design and procedures used to achieve the aims and process objectives stated in Section 2 of Chapter 1: to develop appropriately featured functionalized nanoparticles enabling detection and distinction of biologically relevant molecules at ultra trace levels in biological fluids. This chapter discusses the materials used in the study; the instruments used for analysis; nanoparticle manufacture and characterisation; Raman spectroscopy and the data analysis.

2.1 MATERIALS

Caffeine standard (≤100%) and Gold III Chloride ($AuHCl_4$) (99.9985%) were purchased from ProSciTech. Trisodium Citrate (99%) ACS grade; Silver Nitrate (≥99.5%) (AT) Puriss p.a. Grade; (3-aminopropyl)-trimethoxysilane (APTMS) (97 %); Sodium Silicate (27%) Reagent Grade; 3-(trihydroxysilyl) propyl methylphosphonate (THPMP) 50 wt.% in H_2O; and Glutaraldehyde (25 wt.%) grade I premium and Ethylamine (~70wt.%) were purchased from Sigma-Aldrich.

For erythropoietin, the lyophilized World Health Organisation (WHO) human urinary reference erythropoietin standard (HUEPO, 2nd International Reference Preparation), containing 10 international units of purified human urinary HUEPO and the lyophilized WHO recombinant erythropoietin standard (rHuEPO, 3rd International Reference Preparation) containing 1650 international units (11 µg) of Epoetin α, were sourced from the National Institute for Biological Standards and Control, UK.

Mouse monoclonal anti-Caffeine antibody (ab15221), manufactured by abcam, was purchased from Sapphire BioScience Pty. Ltd. Mouse monoclonal antibody anti-Erythropoietin antibody (3F6, 5.7 mg/mL) was purchased from MAIIA Diagnostics, Uppsala, Sweden. The 3F6 antibody recognises endogenous EPO as well as recombinant epoetins α, β, δ, Ω, and darbepoetin.

Beverages containing caffeine (regular coke and diet coke from Coca Cola Company and a short black from a barista) were purchased and analysed using

the developed SERS nanoparticle method for their caffeine content. Caffeine-Free diet coke (a caffeine free beverage from Coca Cola Company) was also analysed for comparison purposes.

Self-donated urine was analysed for human erythropoietin content by the developed SERS nanoparticle method. The use of self-donated human urine complies with QUT ethical regulations.

2.2 INSTRUMENTATION

Eppendorf Microcentrifuge (model 5430) (1.5 mL tubes), and Bransonic Ultrasonic Cleaner (model 1510E – MTH) from Branson Ultrasonics Corp were used for the separation and re-dispersion of the prepared nanoparticles during synthesis and following binding to the respective target analytes.

UV-VIS Spectrometer:

The Cary 100 spectrometer (Agilent Technologies, USA) was used for UV-Vis characterisation of the nanoparticles.

Transmission Electron Microscope:

The nanoparticles where characterised using the JEOL JEM-2100F TEM (JEOL, USA).

Raman Spectrometer:

A Renishaw inVia Raman Microscope, with microscope spot size 1 μm and excitation wavelength of 785nm was used for the Surface-Enhanced Raman Spectroscopy (SERS) measurements.

2.3 NANOPARTICLE MANUFACTURE

2.3.1 Bare gold nanoparticle

Bare gold nanoparticles were initially manufactured using the traditional Turkevich method [33]. Briefly, 20 mL of 1 mM $AuHCl_{4(aq)}$ was heated to boiling with vigorous magnetic stirring in a beaker covered with a watch glass to minimise evaporation. Two mL of warmed 1 wt% trisodium $citrate_{(aq)}$ was added

to the boiling $AuHCl_4$ solution. During the course of the reaction, the colour changed from colourless to black, then purple, then to a clear red with a slight blue tinge. The mixture was heated for about 5 min, until colour change was complete.

In subsequent gold nanoparticle manufacture, the Turkevich synthesis method was replaced with the method reported by Xia *et al* [34]. This method was used to control the spherical shape of the gold nanoparticles. For the synthesis of the nanoparticles by the Xia method, a saltwater (NaCl) bath was heated with magnetic stirring until it commenced to boil. Twenty mL of distilled water was placed in a two-neck round bottom flask fitted with a reflux condenser and heated in the saltwater bath to 95°C with rapid magnetic stirring. $AuHCl_{4(aq)}$ (14.73 wt.%, 117.8 µL) and 17 µL of 0.1 wt.% $AgNO_{3(aq)}$ were mixed at room temperature with magnetic stirring. Two mL of 1 wt.% trisodium $citrate_{(aq)}$ was added to the $AuHCl_4$ mixture and stirred for 3 min. The aqueous $AuHCl_4$ mixture was then quickly added to the heated water and stirred for five minutes after the solution colour change was complete. The colour changes were from colourless to black, then to purple almost instantaneously. The mixture then turned to a transparent red within 10 sec. The solution was allowed to cool to room temperature. (Note: all concentrations designated wt.% were mass reagent in total mass of solution (i.e. wt/wt))

The trace amount of silver nitrate (8.5×10^{-5} wt.%) was added to increase the rate of oxidation of trisodium citrate to sodium acetone dicarboxylate (SADC), which increased the rate of nucleation and narrowed the nanoparticle size distribution. Silver ions also encourage more spherically shaped nanoparticles by slowing the rate of gold deposition on particular polycrystalline facets that would otherwise lead to irregularly shaped nanoparticles. The trisodium citrate, $AuHCl_4$ and $AgNO_3$ solutions were added and mixed at room temperature for several minutes to minimise the pH buffering effect of the citrate ions and induce a more homogenous nucleation[34].

2.3.2 **Silica coating**

For the addition of a pacifying silica coat onto the gold nanoparticles, the reagents described by Liz-Marzán *et al* [35] and methods described by Li *et al* [36] were used. Briefly, the gold nanoparticle solution produced in section 2.3.1 was mixed with 131.25 µL of 1 mM APTMS under vigorous magnetic stirring for 15 min. Eighty four µL of activated sodium silicate$_{(aq)}$ (0.54 %(v/v)) was added. The pH of the solution was lowered to 10-11 using 1M HCl). The solution was rapidly heated to 90°C in a saltwater bath and vigorously stirred for 20 min. It was then allowed to cool to room temperature. The silica coated nanoparticles were centrifuged (25 minutes) and the supernatant was removed. Centrifugation (at this stage and hereafter) was done at maximum speed for the instrument. The silica-coated nanoparticles were then washed by resuspending in an equal amount of ethanol under sonication, followed by centrifugation. This process was repeated twice more. After the final wash, the supernatant was removed and the nanoparticles were allowed to evaporate to dryness.

2.3.3 **Functionalization of the silica-coated nanoparticles with antibodies**

The nanoparticles were functionalised with the appropriate antibodies according to the method described by Freitag *et al* [37] with a slight modification of the buffer and blocking agent used at the final step. The process consisted of the following steps:

A-Priming the nanoparticle

The silica-coated nanoparticles were re-suspended in distilled water. They were concentrated during the re-suspension process from 24 x 1.5 mL centrifuge tubes by re-suspending 8 tubes at a time, then transferring resuspended nanoparticles to the next set of 8 and repeating this for the final 8 tubes. The resuspended nanoparticles were then transferred to a flask. The emptied centrifuge tubes were washed with a further 2 aliquots of 1 mL deionised water

and the washings were added to the flask for a total of 14 mL of nanoparticle solution.

THPMP (5 % (v/v), 1.68 mL) was added and mixed under vigorous magnetic stirring for one hour at room temperature. The nanoparticles were then centrifuged (20 minutes), washed and evaporated to dryness. (Twelve tubes)

B-Adding pre-linker

The THPMP-primed nanoparticles were resuspended in distilled water and concentrated by resuspending 4 tubes at a time to make a total of 8 mL of primed nanoparticle solution. Eight mL of 1 mM APTMS solution (pH 5-6, acidified with CH_3COOH) was added and mixed under vigorous magnetic stirring for 30 min at 35° C. The nanoparticles were then centrifuged (20 minutes), washed with Phosphate Buffered Saline (PBS, pH 7.4) and evaporated to dryness. (Ten tubes)

C-Adding Glutaraldehyde linker

The pre-linked nanoparticles were re-suspended in glutaraldehyde solution, 10% (v/v) concentrated then sonicated for 30 minutes. The nanoparticles were then centrifuged (15 minutes) and washed with PBS (pH 7.4) and evaporated to dryness.

D-Immobilization of antibody and blocking of un-reacted glutaraldehyde linker

The appropriate antibody was diluted with PBS, giving 3 x 1.5 mL tubes (caffeine antibody, 1:200) and 4 x 1.5 mL tubes (EPO antibody, 1:300). One tube of the glutaraldehyde-functionalised nanoparticles was re-suspended in an aliquot of the diluted antibody. The mixture was allowed to react at 4°C overnight. The nanoparticles were then centrifuged (10 minutes) and washed with PBS. The resultant antibody-functionalised nanoparticles were re-suspended in 1.5 mL of 0.7 % (v/v) ethylamine solution (in PBS) by sonication. The solution was kept at

4°C for 30 min to allow the ethylamine to bond with any remaining aldehyde groups of the glutaraldehyde linker. The blocked nanoparticles were then centrifuged and washed with PBS.

2.4 NANOPARTICLE CHARACTERISATION

The nanoparticles were characterised by UV-Vis spectroscopy to determine their plasmonic properties. Transmission Electron Microscopy (TEM) was used to determine the size and shape of the gold nanoparticles (before and after the coating procedures and immobilization of the antibodies) as well as the thickness of the silica coat.

For the TEM technique, 1:10 dilutions of the nanoparticles were used for each type, except for the complete antibody-functionalized nanoparticles, which were analysed undiluted. To load the sample onto the TEM grid, a drop of the diluted nanoparticle sample was dropped on a Cu grid, coated with carbon, allowed to set for 3 min. The surplus fluid was removed by absorption onto filter paper. If the coating was subsequently found to contain insufficient nanoparticles for analysis, the loading process was repeated for a further 5 min.

2.5 RAMAN SPECTROSCOPY

The completed antibody-functionalized gold nanoparticles were directly analysed by Raman spectroscopy without dilution to acquire a background SERS spectrum of the nanoparticles prior to their interaction with the target analyte. For the detection of the target analytes in standard solutions by SERS, the appropriate antibody-functionalized nanoparticles were mixed 1:1 with the target analyte solution to produce a 20 µL sample and spun down with brief centrifugation to ensure that the sample and nanoparticle were mixed. After mixing, the solution was allowed to react for the predetermined optimal time for each antibody, loaded on a glass microscope slide, covered with aluminium foil, and then air dried.

The above procedure was repeated for caffeinated beverages and urine. The samples were then washed (by several replications of centrifugation, removal of supernatant and resuspension) to remove the unbound proteins and other interfering molecules that may produce interference fluorescence during the SERS measurements. As loss of nanoparticles may occur during the washing process, 60 µL total volumes were used to compensate, and the nanoparticles were resuspended in 20 µL of PBS before transfer to the slides.

Since human urine has a wide pH range, PBS was used as a buffer to regulate the urine medium to pH 7.4 to ensure the stability of the bond between the glutaraldehyde linker and the antibodies [38].

The Raman spectroscopy measurements were carried out using excitation laser at 785 nm, at 5% of maximum (450 mW) laser power, i.e. 22.5 mW. Unless otherwise indicated, spectra were collected within the spectral region 350 cm^{-1} to 1700 cm^{-1}. All spectra were obtained using a 10 second exposure time. The initial caffeine experiment used a single accumulation, while subsequent experiments acquired 10 accumulations per sample measurement. A minimum of 6 measurements per sample was carried out for all Raman measurements.

2.6 DATA ANALYSIS

2.6.1 Collection, Pre-treatment and Initial examination of results

The spectral data for each sample were collected and data pre-treatment was carried in Microsoft Excel 2007 as described below.

The data points for each spectrum were baseline corrected, by subtracting the intensity of the lowest point of the spectra between 350 cm^{-1} and 1600 cm^{-1} from each data point. They were then normalized according to a published method [39]. The formula for these transformations for the i^{th} spectral point (where hi is the peak intensity for the i^{th} peak and 100 is an arbitrary scaling factor for ease of handling and display) is as follows:

$$hi\ (normalised)\ = \frac{hi\ (baseline\ corrected)\ X\ 100}{\sum_{i=1} n\ hi\ (baseline\ corrected)}$$

An Excel spread sheet was designed to collect the results for the initial analysis, the major peaks of the analyte's reaction with its antibody, as well as the hierarchical PCA (HPCA) data. The data were then used in the relevant chemometrics analysis.

Preliminary examination of individual spectra and averages of the 6 spectral replicates of analytic samples was performed by visual inspection to detect any obvious trends in the data. Excel 2007 was used for this analysis.

2.6.2 **Quantitative analysis**

The r^2 value for each of the major peaks of the analyte verses the analyte concentration was calculated using the RSQ function in Excel 2007. Excel's RSQ function returns the square of r (the Pearson product moment correlation coefficient) where r is defined as:

$$r = \frac{\sum (x - \bar{x})(y - \bar{y})}{\sqrt{\sum (x - \bar{x})^2 \sum (y - \bar{y})^2}}$$

The major peaks with the highest r^2 value (i.e. ≥ 0. 7) were chosen for each analysis. High values of r^2 suggested that the spectra of the samples at that wavelength correlated best with the concentration of the analyte in the samples. Linear or logarithmic calibration curves were constructed to determine which gave the best r^2 value.

2.6.3 **Chemometrics analysis**

The software used for the Chemometrics analyses was SIMCA P+ 13 from Umetrics AB, Sweden.

Principal component analysis (PCA)

PCA was performed using all of the major peaks. The PCA model was refined by identifying the outliers and/or peaks that were poor predictors as identified in the software's built-in functions.

Hierarchical PCA (HPCA)

For the HPCA model, the spectra were divided into 10 to 14 approximately evenly sized blocks encompassing the spectral regions of interest. For example, the interference studies were performed using the regions known to vary with the analyte concentration, while ignoring those spectral regions known to be associated with the background nanoparticle. PCA was performed on each block and a maximum of 3 significant PCs were recorded. The significant PCs from the initial PCA were used as the variables to perform a subsequent PCA, i.e. the HPCA.

Partial Least Squares (PLS) using Major Peaks

The data was divided into training and test sets. Preliminary PCA was performed on the data, using the wavenumber values of the major peaks as x values. The values of the major peaks are indicated in section 2.6.4. For the PLS analysis, the concentrations of the standard solutions were used as the y variable. Successive models were executed with various combinations of the x variables to identify the combination with the highest R this ^{2} values, lowest Root Mean Square Error of Estimation (training set), and Prediction (test set) [RMSEE and RMSEP] values.

2.7 STUDIES PERFORMED

2.7.1 Unreacted nanoparticle and concentrated analyte

An initial study for the analyte and its unreacted nanoparticle was performed to identify the major Raman peaks, and to distinguish between major Raman peaks that were related to the unreacted nanoparticle and those that

were related to the reaction of the analyte with the antibody. In all studies, visual inspection was performed using the averaged pre-processed spectra. A previously optimised reaction time of 30 minutes was used.

2.7.2 Effect of time on the binding between the analyte and the antibody-functionalized gold nanoparticles

The optimal reaction time for the binding reaction between the analyte and the antibody-functionalized gold nanoparticles was determined empirically. A standard solution of the analyte, caffeine ($1x10^{-6}$ M) and EPO ($1x10^{-8}$ M), respectively, was mixed with the relevant antibody-functionalized gold nanoparticles and the solution was incubated for a series of times, spanning 5 to 60 minutes for caffeine and 0 to 600 minutes for EPO (where 0 minutes = air drying immediately after mixing). These samples were then analysed by SERS.

The spectra were overlaid and the major peaks were visually inspected to determine the time point beyond which there was no further significant change in signal intensity with increasing time. This optimal reaction time, determined to be approximately 10 minutes for caffeine and 30 minutes for EPO, was then used for all further studies with the respective analyte.

2.7.3 Development of calibration curves for the quantifications of the target analytes

To develop a calibration curve for each analyte, standard solutions of the target analytes (caffeine (10^{-4} M - 10^{-10} M), EPO ($2x10^{-10}$ M - 10^{-15} M) were reacted with the relevant antibody-functionalized gold nanoparticles for the nominated optimum reaction time (10 minutes for caffeine and 30 minutes for EPO). The solutions were then screened by SERS, and the acquired spectra were analysed as indicated in section 2.6.4. If there were multiple peaks that fulfilled the criteria outlined (RSQ ≥ 70%) PLS (as in section 2.6.5) was attempted to determine if this would give a better R^2 result than univariate regression.

Calibration curves for caffeine and EPO were constructed by plotting the normalized signal intensity against the concentration of the analyte on a log scale.

2.7.4 **Interference study**

Initial study EPO vs. rHuEPO only

The initial EPO interference study was performed using the 2nd international reference standard for human urinary EPO (HUEPO) and the 3rd international reference standard for rHuEPO. $1x10^{-13}$ M solutions of the international reference standards were prepared, reacted with the relevant antibody-functionalized gold nanoparticles and screened using SERS, and the acquired spectra were inspected visually and a PCA of the relevant major Peaks was performed to determine whether there was any significant interference.

Interference study using real-life samples

The interference study was performed/ repeated using the relevant beverages/ biological fluid containing the analyte. For the EPO model, spiked biological fluids were also used. The spiking was done by mixing, 1:1, the biological sample and standard solutions (HUEPO IS and rHuEPO IS, at $1X10^{-12}$ M and $1x10^{-14}$ M). The samples were then reacted with the relevant antibody-functionalized gold nanoparticles and washed (as described in section 2.5) to remove the unreacted/interfering substances (e.g. proteins from the matrix of the biological sample).

The washed nanoparticles were then screened by SERS as described in section 2.5. After visual inspection of the spectra, PCA models of the relevant major Peaks / HPCA analyses were developed as described in section 2.6.5 to determine whether there was any relevant interference with endogenous components or cross reactivity. The specific comparisons for the caffeinated beverages and EPO are described in chapters 3 and 4 respectively.

2.7.5 **Reactivity of antibody before and after immobilization onto the gold nanoparticles nanoparticle (Caffeine model only)**

To determine whether the immobilization of the antibody onto the gold nanoparticles would result in blocking of the antibody binding sites and potentially destroy its reactivity towards the target analyte, a standard solution of caffeine (1×10^{-6} M) was mixed with an aliquot of the caffeine antibody prior to linking the antibody to the nanoparticles. A second aliquot of the caffeine standard solution was mixed with the antibody-functionalized gold nanoparticles solution, in the proportions outlined in section 2.6. The resulting mixtures were examined using SERS. Visual inspection of the spectral data and PCA analysis of the relevant major peaks was performed as described in section 2.6.5.

2.7.6 **Confirmation of blocking adequacy**

The caffeine studies were initially performed with unblocked nanoparticles. When the cross-reaction potential was intimated in the beverage studies the nanoparticles were mixed with ethylamine to bind to any un-reacted linker aldehyde groups that might remain following immobilisation of the antibody to the nanoparticle. Raman spectra of the un-blocked and blocked nanoparticles were then obtained and visually compared for variations that might indicate the blocking was inadequate. Repeat experiments were performed after blocking, using PCA and HPCA (using the data from the entire spectra) to confirm the adequacy of the blocking step.

Additional confirmation of the adequacy of blocking was performed with the EPO antibody attached nanoparticles using skim milk.

Chapter 3: Caffeine Model

3.1 BACKGROUND

Caffeine [fig. 3.1.1] is the world's most widely used legal stimulant [40, 41]. It stimulates both the cardiac muscle and the central nervous system, however, it may have negative effects on the gastrointestinal tract when consumed in large amounts. Caffeine can be found naturally in plants, where it serves as the plant's natural insecticide [42]. Synthetic caffeine or extracts from caffeinated plants are found in numerous commercially produced beverages and in coffee, tea and various naturally caffeinated herbal teas [43, 44]. Caffeine is also present in an increasing number of pharmaceutical and medicinal herbal and "energy" products [40, 43].

The inclusion of caffeine in a wide range of commercial products highlights the importance of developing cost-effective effective and facile methods for its rapid identification and quantification in food, supplement and pharmaceutical products [43, 45].

An interesting and important analytical application associated with naturally caffeinated plant products is provenance. With the increasing use and popularity of naturally caffeinated extracts in beverages, food and pharmaceuticals, there is the potential for falsification of the product by incorporating a cheaper and more available plant extract. This is suspected to be a concern with guarana extract containing products, due to their high popularity and the rare main source of this product. Greater than 80% of guarana is traditionally hand produced by the Amazon based Guarani Indians [43].

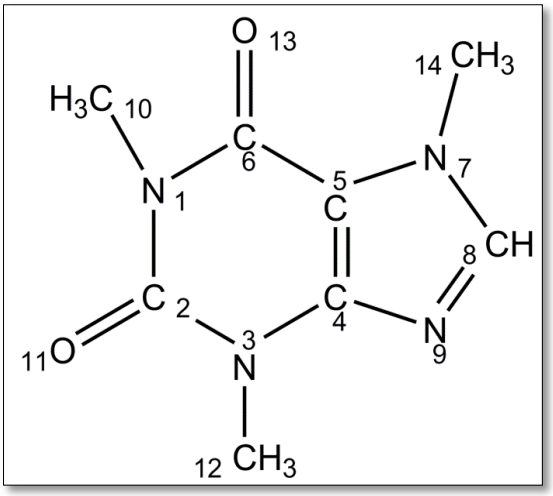

Figure 3.1.1 Diagram of caffeine with atoms numbered.

Multiple analytical protocols are available for caffeine detection and quantification, with chromatography-based separation techniques dominating the reported methods [40, 43, 46-49]. Vibrational spectroscopy has also been employed using various Fourier transform infrared spectroscopy (FT-IR) based methods [50-52] and near infrared spectroscopy (NIR) [53]. Most of these techniques require complicated extraction methods and/or mobile phases utilizing organic solvents (e.g. chlorinated solvents, methanol, acetonitrile or chloroform [40, 43, 46-50, 52, 53]), which are toxic to humans and not environmentally friendly. The solvent extraction procedure is essential in most methods, because caffeine is poorly soluble in water, and highly purified extracts are required to detect trace amounts of the substance [40, 43, 49].

Various FT-Raman techniques have also been applied to caffeine detection, and complex extraction/ clean up procedures are again required. FT-Raman analyses suffer from interference from other products that may co-exist with the target analyte in complex natural matrices (matrix effect) [43, 45]. However, Raman spectroscopy is still reported as a viable technique for identifying caffeine in caffeinated products [40, 43-45, 51]. Traditional solvent extraction techniques prior to Raman analysis failed to eliminate significant matrix effects with other molecules that were co-extracted with caffeine [43]. Solid-phase extraction techniques minimised, but could not eliminate, organic solvents, which were required to remove the concentrated caffeine from solid-phase. This solid-phase extraction technique also achieved an improved lower limit of detection (LLOD) of 18.1 mgL^{-1} (9.3×10^{-5} M) [40].

The present study employed surface-enhanced Raman spectroscopy (SERS), for caffeine detection. Our method employed an immuno-separation/capturing technique to ensure the selective detection of caffeine against a complex matrix background without purification, and eliminates the requirement for organic solvents. This technique offers significant sensitivity enhancement relative to other techniques, which stems from the SERS well-known ability to detect ultra-trace amounts of the target molecule, potentially down to the single molecule level [11, 12, 54, 55].

The sensitive environmentally friendly technique developed here is non-destructive and uses very small sample sizes without requiring a pre-purification step. While this technique could revolutionize caffeine analysis in food products, it could have much wider applicability for small molecule analysis and potentially analysis of much larger biomolecules. Here we present the SERS detection of caffeine as an application exemplar for a more general method to detect small molecules in solution.

3.2 AIMS OF THIS STUDY

In addition to the specialised interest in developing a rapid and sensitive method for the detection of caffeine as an important industrial substance that is involved in many commercial products, the caffeine analyte was selected to demonstrate proof-of-concept for an innovative surface enhancement Raman spectroscopy-based technique for the rapid, sensitive and selective detection of ultra-trace amounts of small molecules, such as drugs of abuse and illicit substances. It was chosen to determine the applicability of the proposed technique for detection and quantification of the small organic target analyte in complex matrices.

3.3 DEVELOPMENT OF FUNCTIONALIZED GOLD NANOPARTICLE MANUFACTURE FOR CAFFEINE DETECTION

Gold nanoparticles were synthesised by the traditional Turkevich method, the innovative method described by Xia, *et al* [34] and a modification of Xia's method. See section 2.3.1 for a detailed description. Briefly, for the Xia technique, Millipore water was heated in a salt water bath under reflux. A mixture consisting of concentrated gold (III) solution, sodium citrate and trace amounts of silver nitrate was added. The silver nitrate was omitted in the modified Xia method. A video showing the progress of the modified preparation process is provided in appendix A.

For the Turkevich method [33], dilute gold salt solution was heated under reflux and then the sodium citrate reducing agent was added to the reaction

mixture. The traditional Turkevich method was slightly modified to be performed under reflux to allow a more direct comparison between the three methods.

3.3.1 **Nanoparticle characterisation**

Visual Characterisation

The colloidal nanoparticles that were produced by the three different reaction routes were very similar in colour [Fig. 3.3.1].

Figure 3.3.1 Photograph of Gold nanoparticles made by (L-R) the modified method with trace Ag, the modified method without trace Ag, and the traditional Turkevich method.

UV -Vis Characterisation

The nanoparticles prepared by Xia's method (and its modification) showed an absorption band at 517 nm in the UV-Vis spectrum, while those prepared by Turkevich method have a band at 522 nm [fig. 3.3.2]. The band width at 517 nm was 47.5 nm at half-height, while the band at 522 nm was broader with a width of 49 nm at half-height. These data imply that Xia's method resulted in a narrow size distribution of the synthesized nanoparticles. This was attributed to the addition of silver nitrate to the reaction mixture [25].

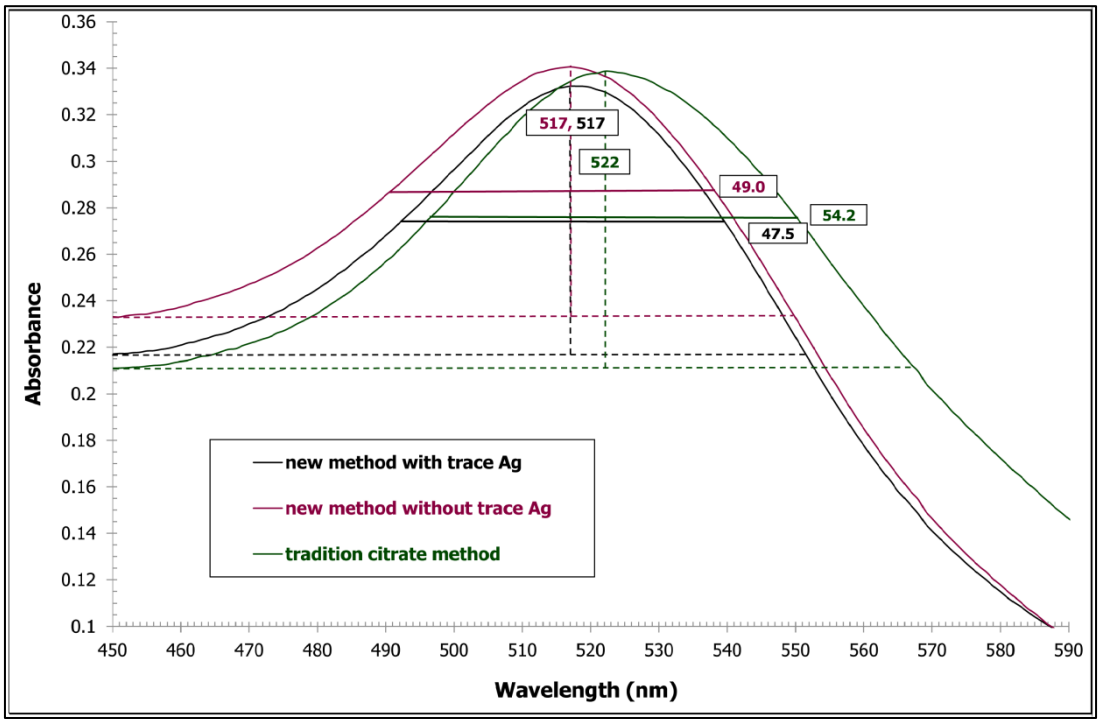

Figure 3.3.2 UV-Vis spectrograph of the traditional Turkevich citrate reduction method for gold nanoparticle manufacture vs. the proposed citrate reduction method (Xia) and its modifications. Peak width at half peak height is shown for the 3 methods by the solid straight lines with the measurement noted beside. The wavelength of maximum peak height is straddling the dotted line indicating the positions. The colours corresponding to the key are used in all lines and labels.

TEM Characterisation

The TEM characterization of the nanoparticles indicated that those produced by the traditional Turkevich [33] citrate reduction method were poly dispersed, with respect to size and shape, when compared to those prepared by Xia's method [figs. 3.3.3, 3.3.4].

The visual, UV-Vis and TEM characterisations collectively indicated that the modified citrate reduction method using trace silver nitrate is effective in

producing more mono-diverse nanoparticles, both in spherical shape and in size. Therefore, Xia's method was chosen for the preparation of the nanoparticles used in all of the SERS investigations of this study.

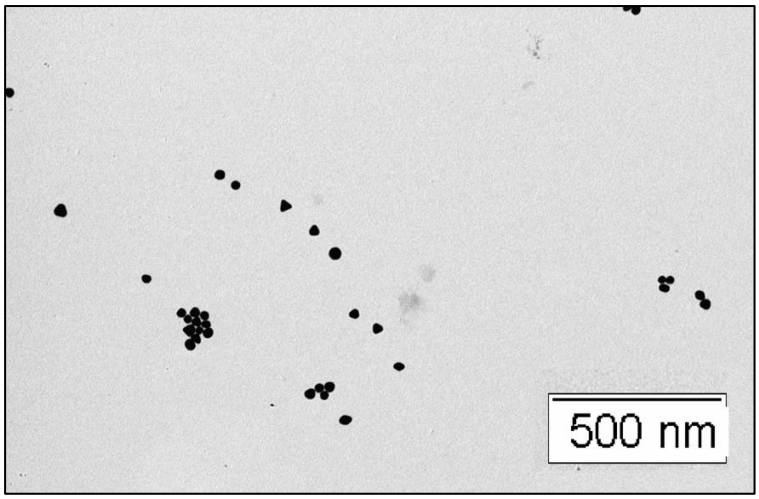

Figure 3.4.2 TEM of gold nanoparticles prepared by Xia's method.

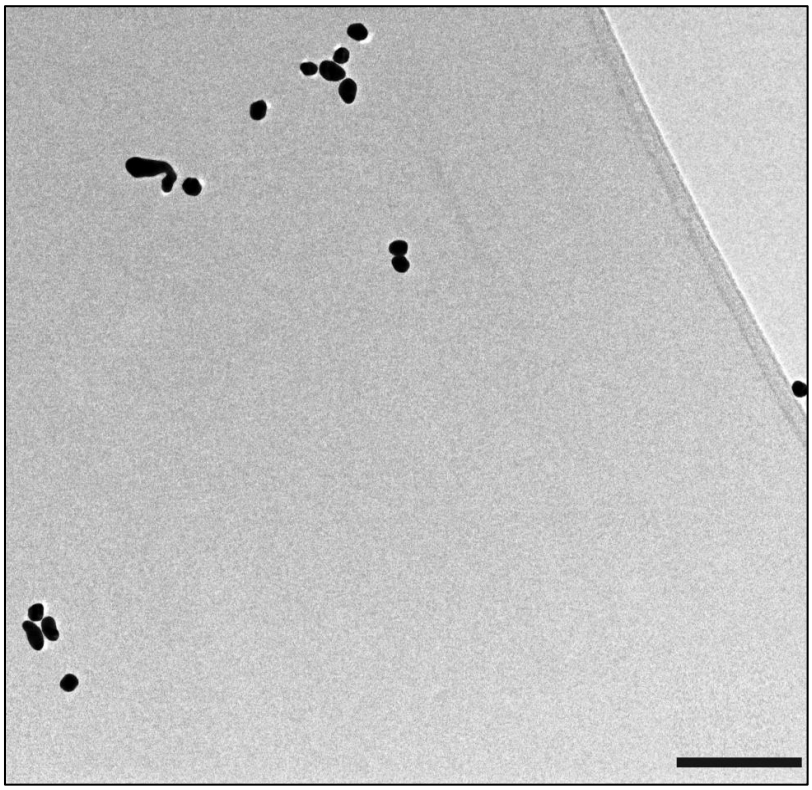

Figure 3.3.1 TEM of gold nanoparticles prepared by the Turkevich method. Note: bar = 500nm

3.4 CHARACTERISATION OF FUNCTIONALIZED NANOPARTICLES FOR CAFFEINE DETECTION

After the bare gold nanoparticles were prepared, their surfaces were coated with a passive silica layer to protect the GNP from interacting non- specifically with interfering analytes and to provide the surface for immobilizing caffeine

antibodies via silane chemistry. The procedures for silica coating and attachment of antibodies have been described in section 2.3 of this thesis. The nanoparticles used for the caffeine detection by SERS were characterised as described in section 2.4, with the exception that only the bare gold nanoparticles, the silica coated and functionalised gold nanoparticles were characterised.

3.4.1 **Visual Inspection**

The visual inspection of the nanoparticle colloid after the addition of the silica coat showed no change in colour. After the attachment of the caffeine antibodies to the silica coat, the colour of the nanoparticles colloid became black as indicated by figure 3.4.1

Figure 3.4.3 Photograph of (L-R) the Bare Gold nanoparticles, the Silica coated nanoparticles, and the completed nanoparticles with Caffeine antibody attached.

Note: the functionalised nanoparticle colloids when concentrated are black due to the agglomeration of nanoparticles, but they appear grey in this photograph because they have been diluted more than the other colloids.

UV-Vis characterisation

The UV-Vis spectroscopy showed that the bare and silica-coated Gold nanoparticles both showed an absorption band at approximately 530nm. There was no obvious absorption band for the nanoparticles after immobilization of the caffeine antibody attached to the silica surface [fig. 3.4.2], which suggests that there is a mixture of particle sizes with no one size dominating. In addition, the large nanoparticle clusters may cause light scattering which would complicate the UV-Vis spectrum.

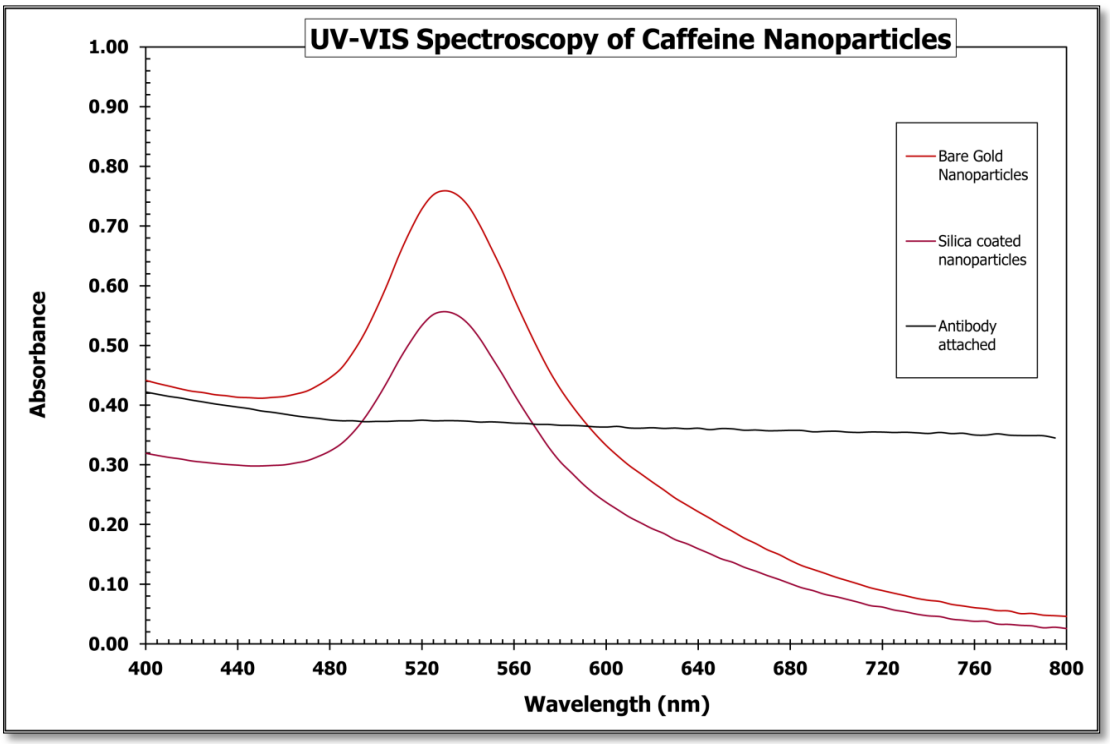

Figure 3.4.4 UV-Vis spectroscopy of the bare gold nanoparticles, silica coated nanoparticles and the completed nanoparticles with the caffeine antibody attached.

3.4.2 **TEM characterisation**

The bare Gold nanoparticles in figure 3.4.3 below, produced with trace silver nitrate in the Xia's[34] method are approximately spherical in shape, and contain only a small size range of sizes. This is consistent with the method used to generate the nanoparticles and potentially leads to greater reproducibility. The more consistent the size and shape of the nanoparticles are, the higher the probability of batch to batch reproducibility.

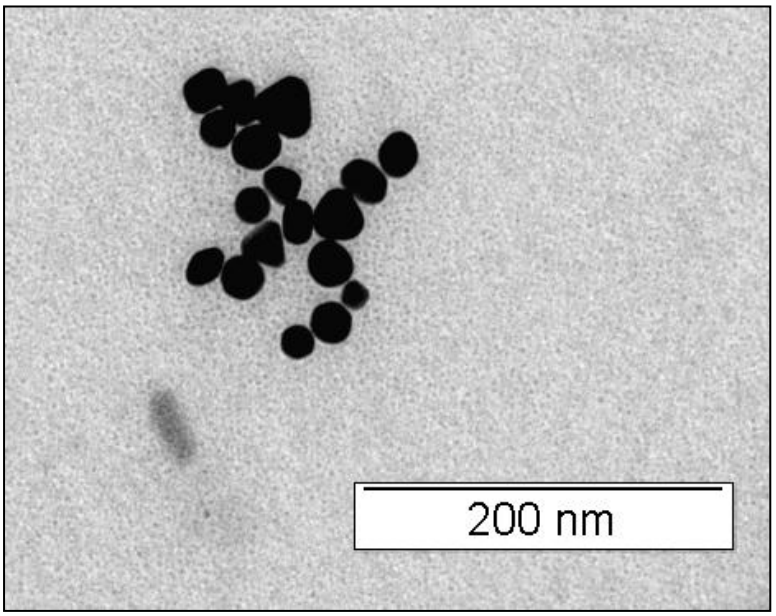

Figure 3.4.5 TEM of the bare gold nanoparticles produced by Xia's method using trace silver nitrate.

The TEM of the silica-coated gold nanoparticles is shown in figure 3.4.4. The silica coating method was chosen to produce a very thin coating (approximately 2 nm)[36]. As silica is a small molecule with low density, it is difficult to visualise in the TEM. However a slight increase of ~2 nm in the size of the nanoparticles was observed, relative to the bare gold nanoparticles [fig. 3.4.3] on measuring the nanoparticles in their TEM while expanded in Microsoft Office Picture Manager.

The TEM image of the antibody-coated gold nanoparticles following the caffeine antibody immobilization is shown in figure 3.4.5. The caffeine antibody-functionalised gold nanoparticles were observed to form large aggregates of gray

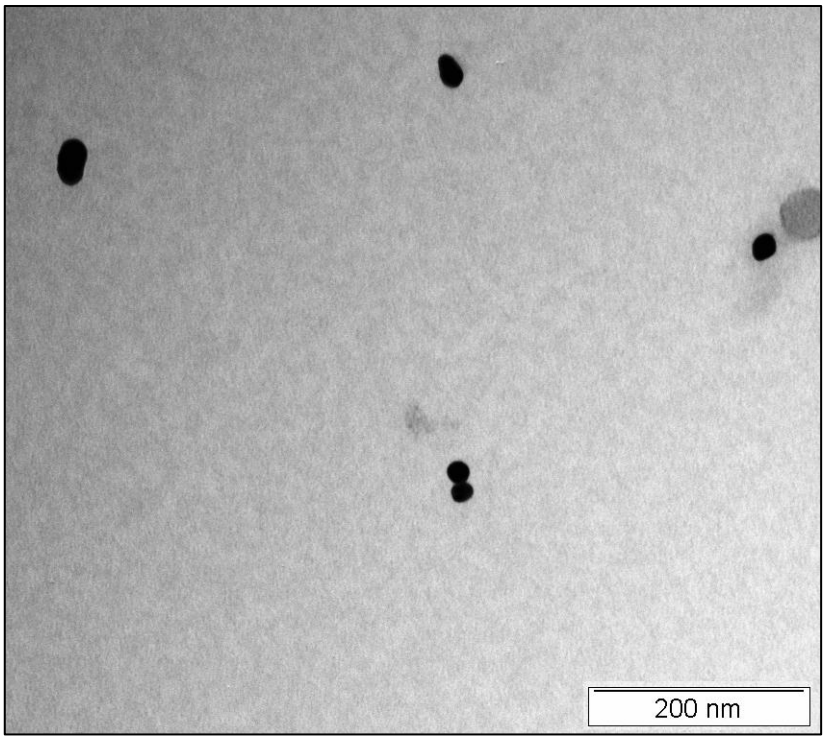

Figure 3.4.7 TEM of silica coated nanoparticles

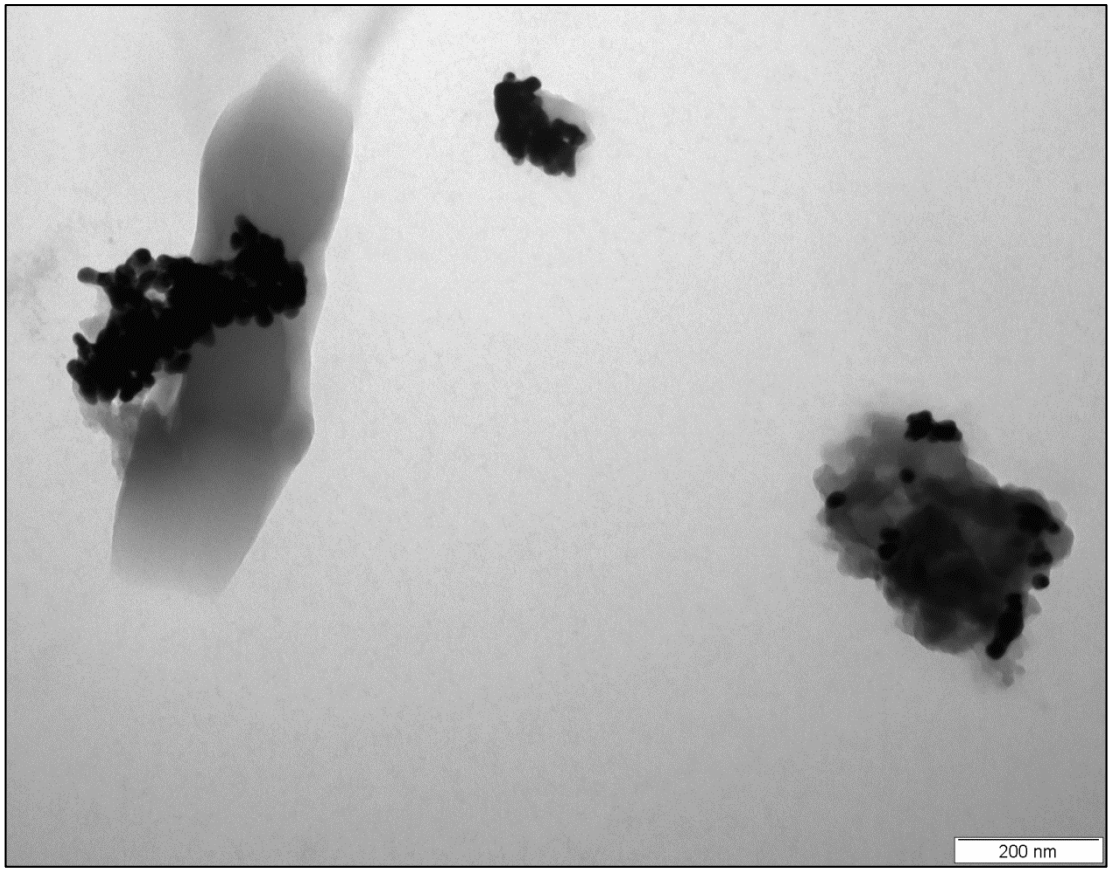

Figure 3.4.6 TEM of completed nanoparticle with caffeine antibody

colour [fig. 3.4.1]. The large size of the nanoparticles contributes to the light scatterings properties of these aggregates.

3.5 COMPARISON OF STANDARD RAMAN, SERS AND FUNCTIONALISED SERS SPECTRA OF CAFFEINE

Firstly, a Raman measurement of caffeine was obtained at 1×10^{-3} M using the drop-dry technique for the loading of the sample onto the gold nanoparticles. In this technique, an aliquot of the analyte solution was loaded onto the surface of an aluminium foil covered slide and allowed to dry. For the SERS method the nanoparticle solution was added and dried before adding the analyte solution to the deposited nanoparticles. The resulting analyte/nanoparticles mixture was then allowed to dry prior to the SERS measurements. Then SERS measurements of caffeine were collected at a series of concentrations from 1×10^{-3} M to 1×10^{-6} M on bare gold nanoparticles. This technique was also used for the SERS measurements of caffeine by the antibody-coated nanoparticles in the concentration range of 1×10^{-4} M to 1×10^{-10} M.

3.5.1 **Raman spectra of caffeine**

The Raman spectrum of caffeine at 10^{-3} M is shown in figure 3.5.1 below. The caffeine Raman spectrum shows a very prominent band at 556 cm^{-1} and a less prominent one at 1325 cm^{-1}. The band at 556 cm^{-1} is caused by the combination of the pyrimidine (six membered) ring breathing, in plane C_{14} - N_7 - C deformation, CH bending, CH_3 symmetrical bending and CH_3 rocking [41]. The band at 1325 cm^{-1} is caused by the Imidazole trigonal ring

stretching of the caffeine molecule [41]. Refer to the structure of caffeine in figure 3.1.1 above.

It is unlikely that 10^{-3} M of caffeine in solution could be detected by Raman spectroscopy, because of its inherent weak effect. Drying the solution before

Raman analysis allowed this detection by a phenomena known as the

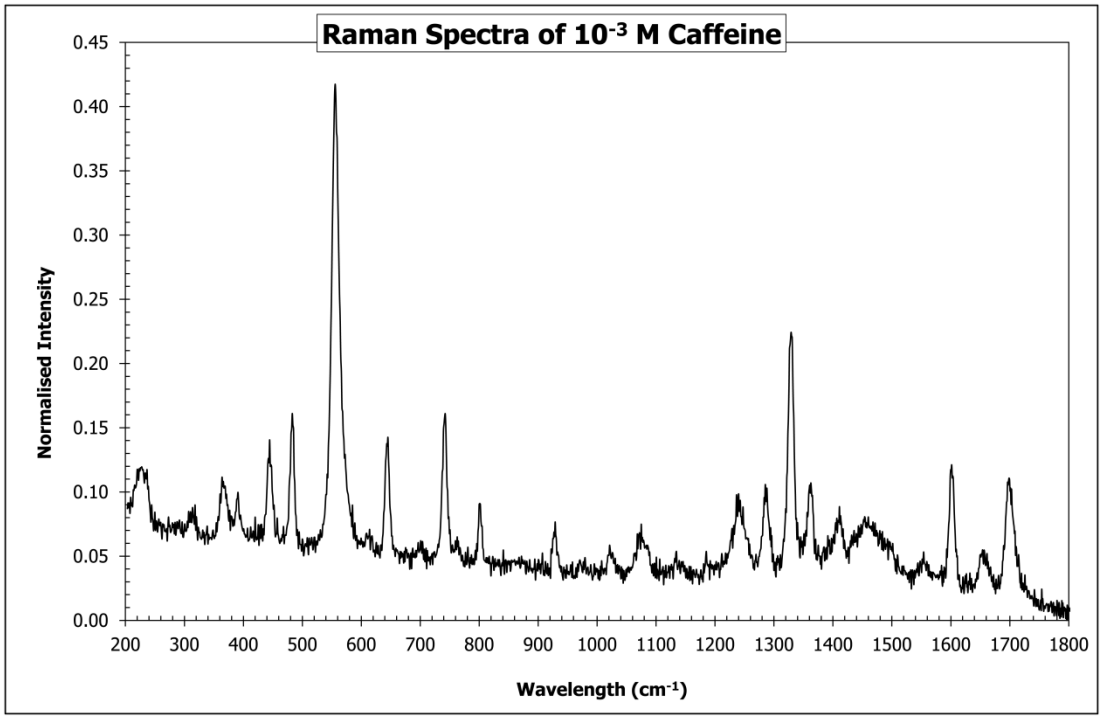

Figure 3.5.1 Raman spectra of 1 x 10^{-3} M Caffeine

coffee ring effect [56]. When a coffee drop is allowed to dry, the coffee concentrates by capillary action into a dark ring around the edge of the drop. This phenomenon is not exclusive to coffee, and has many important effects [57].

In our study, the small caffeine molecule was drawn to the edge of the ring, where it was concentrated and ultimately detected. This form of natural chromatography has been named nanochromatography [57]. Direct Raman measurement of a standard solution of caffeine at 1 × 10^{-4} M was also attempted, using the drop dry method as explained above. Considering the height of the peak at 556 cm^{-1}, (fig. 3.5.1), some evidence of this could have been expected with a 1: 10 dilution, but its detection was unsuccessful as the white ring of pure caffeine was too faint to determine its position. Thus the lower limit of detection (LLOD) for caffeine by direct Raman spectroscopy was confirmed to be 1 x 10^{-3} M.

3.5.2 **SERS spectra of caffeine using bare gold nanoparticle**

The ability to detect molecules with Raman spectroscopy can be significantly enhanced when the analytes are in contact with, or very close to, metal nanoparticles, particularly those of coinage metals (e.g. Ag and Au). Gold nanoparticles were prepared as described in section 3.4.1 [using Xia's method], and were used for SERS detection of caffeine across a series of standard solutions in the concentration range 1×10^{-3} M, 1×10^{-5} M and 1×10^{-6} M. The results are shown in figure 3.5.2. For comparison the bare gold nanoparticle background spectrum is also shown.

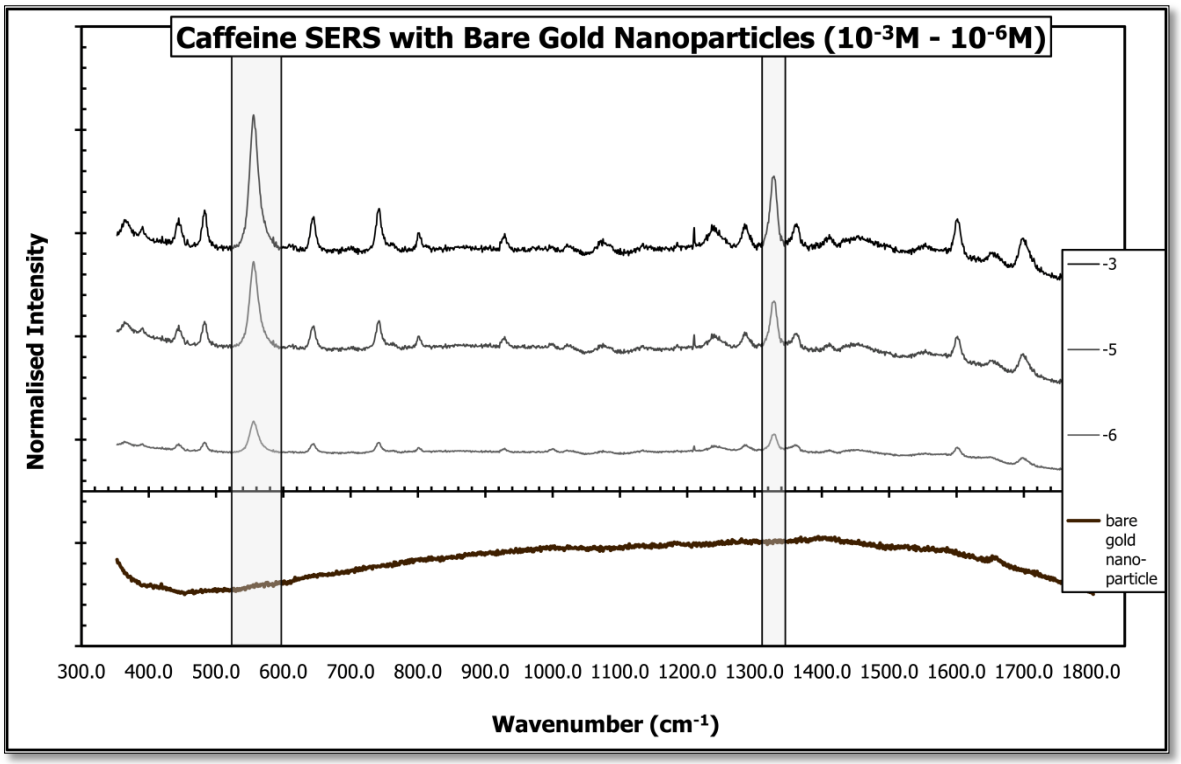

Figure 3.5.2 Stacked SERS Spectra of caffeine standards at 10^{-3} M, 10^{-5} M and 10^{-6} M and the bare gold nanoparticles for comparison. The gray boxes show the most prominent bands caffeine from the Raman spectra of caffeine. The 10^{-3} M and 10^{-5} M spectra have been raised and the background lowered for clarity.

A prominent result was found for the 10^{-3} M and 10^{-5} M caffeine standards. The spectra in fig 3.5.2 were consistent with the reference spectrum of caffeine as shown in the literature [41].Although the averaged SERS spectrum of the 10^{-6} M caffeine solution showed caffeine- specific Raman bands, only one of the eight spectra taken showed any caffeine with the remainder showing no evidence of caffeine at all, therefore confident detection of caffeine was only possible down

to 10^{-5} M [fig. 3.5.2], which we defined as the LLOD for caffeine on our bare gold nanoparticles

3.5.3 SERS spectra of caffeine with caffeine antibody functionalised gold nanoparticle

The functionalization of the gold nanoparticles with analyte-specific binding molecules adds selectivity to the already ultrasensitive detection of the target analyte [58-60].

Our antibody-functionalised nanoparticles were designed to specifically capture the caffeine molecule through the selective binding properties of the caffeine-specific antibody, while limiting or eliminating non-specific cross reaction with potentially interfering molecules. In addition, the thin silica passive shell around the gold surface of the nanoparticles prevents non-selective direct adsorption of interfering molecules onto the gold surface. Therefore, the antibody-functionalised nanoparticles immobilize and pre-concentrate the caffeine molecules close to the gold surface of the nanoparticles and enable the sensitive and selective SERS detection of caffeine [58-60].

The reference SERS spectrum of antibody-functionalised gold nanoparticles that have not been exposed to caffeine shows prominent bands at 1000 cm^{-1} and 1030 cm^{-1}. (See the nanoparticle background spectrum in Figure 3.5.3.) These bands are characteristic of pyridine ring vibrational modes [61] and arise as a result of our method of cross-linking the antibody to the modified silica surface. The glutaraldehyde linker attachment to the modified silica surface involves the reaction between glutaraldehyde and the terminal amine groups of the silica shell. The reaction of glutaraldehyde with amines has been reported to result in some dimerization [62, 63], such as the formation of quaternary pyridinium compounds [38]. The formation of the pyridinium species would give rise to pyridine bands in the SERS spectra of the antibody-functionalized NPs. Therefore any caffeine-specific Raman bands that fall in this spectral region could not be confidently used for analysis.

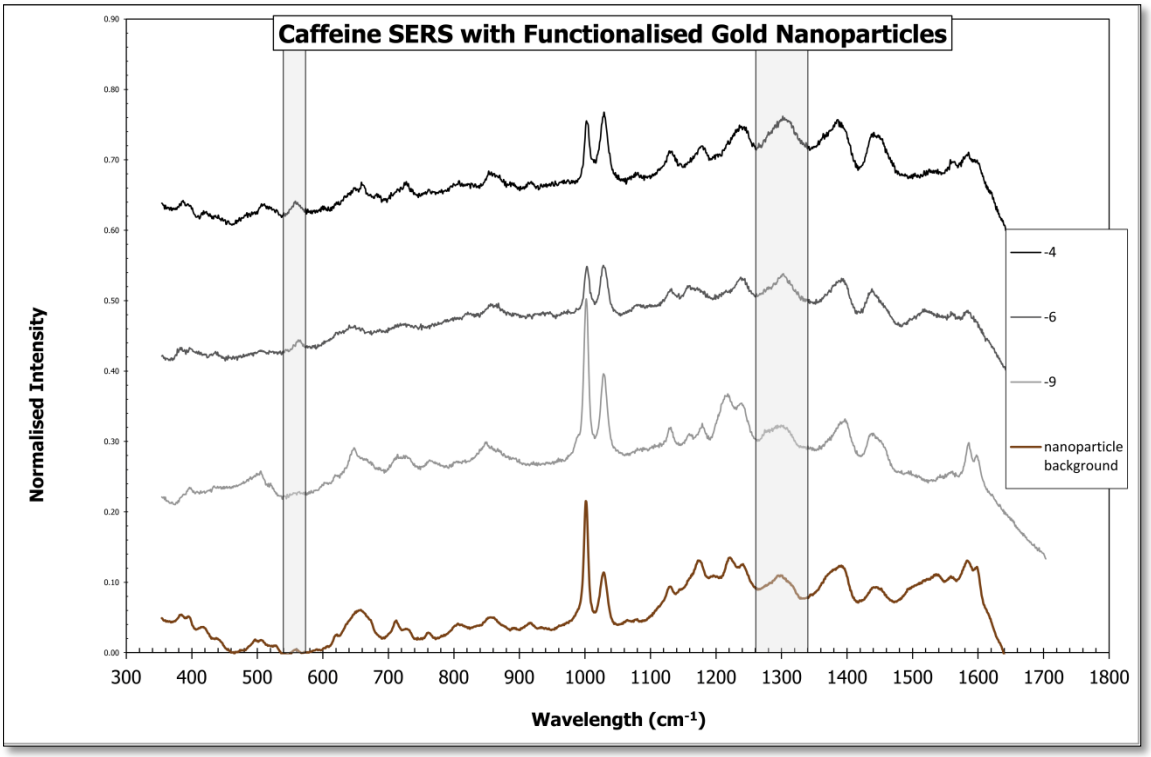

Figure 3.5.3 Stacked SERS Spectra of caffeine standards at 10^{-3} M, 10^{-5} M and 10^{-6} M and the bare gold nanoparticles for comparison. The gray boxes show the most prominent bands caffeine from the Raman spectra of caffeine. The 10^{-3} M and 10^{-5} M spectra have been raised and the background lowered for clarity.

A panel of standard caffeine solutions ranging from 1×10^{-4} M to 1×10^{-10} M was exposed to the antibody-functionalised nanoparticles. Figure 3.5.3 shows the SERS spectra of 1×10^{-4} M, 1×10^{-6} M and 1×10^{-9} M caffeine solutions after their interaction with the antibody-functionalized gold nanoparticles.

The caffeine-specific Raman bands at 560 cm^{-1} and 1300 cm^{-1}, however, remain evident at concentrations as low as 1×10^{-9} M. (While there are peaks in these regions, at 1×10^{-9} M the peak at 1300 cm^{-1} remains higher than the background.) These peaks were chosen as they correspond to the most prominent peaks in the Raman spectrum of caffeine [fig. 3.5.1].

The SERS spectra in figure 3.5.3 showed spectral differences compared to those obtained for caffeine by the bare gold nanoparticles [fig. 3.5.2]. The two characteristic caffeine Raman bands at 556 cm^{-1} and 1325 cm^{-1} in the Raman caffeine spectra [fig. 3.5.1] shifted to 560 cm^{-1} and 1300 cm^{-1}, respectively.

The specific causes of these shifts are unknown. The small shift from 556 cm^{-1} to 560 cm^{-1} might be attributed to instrumental variation. Pavel *et al*

attribute the caffeine Raman band at 1325 cm^{-1} to the imidazole (five membered) trigonal ring stretching. They report that that the shift of the band at 1325 cm^{-1} inward to approximately 1311 cm^{-1} is pH dependant. This peak shifts at about pH 6.5 and remains there at higher pH, see Table II and figure 2 in this reference [41]. We used buffering at pH 7.4 so this amount of shift is expected. The background has a peak ~ 1298 cm^{-1}. In figure 3.5.3, the peak at 1298 cm^{-1} marginally shifts to 1302 cm^{-1} with increasing concentration. So, the peak at 1300 cm^{-1} could be this caffeine peak at 1311 cm^{-1} superimposed on the background nanoparticle peak at 1298 cm^{-1}.

This spectral shift could also be partially due to the high affinity binding of caffeine to the antibody on the surface of the gold nanoparticles. Specific intermolecular interactions (e.g. hydrogen bonding) between the analyte moieties and the antibody could potentially shift the wavelengths of the analyte Raman bands. This ring's nitrogen atom moiety (N_9) [fig. 3.1.1] carries a lone pair of electrons that is available for hydrogen bond donation as well as other potential interactions with the antibody [43]. Further characterisation will be required to fully understand this spectral shift.

3.6 IS THERE INTERFERENCE WITH THE ANTIBODY'S ANTIGEN BINDING SITE WHEN LINKING THE NANOPARTICLE?

The caffeine antibodies were attached to the gold nanoparticles via a glutaraldehyde crosslinker, which reacts with primary amines [38]. In proteins, primary amines are found in the lysine side-chain and at the N-terminus of each peptide chain. The N-terminus of the each of the four antibody protein chains is located in the antigen binding sites. See figure 3.6.1 below [64]. If the antibody is attached to the nanoparticle through any of the primary amines within the antigen binding site there, steric hindrance might prevent the antibody from binding efficiently to the antigen. This would likely result in a significant difference in the Raman spectrum.

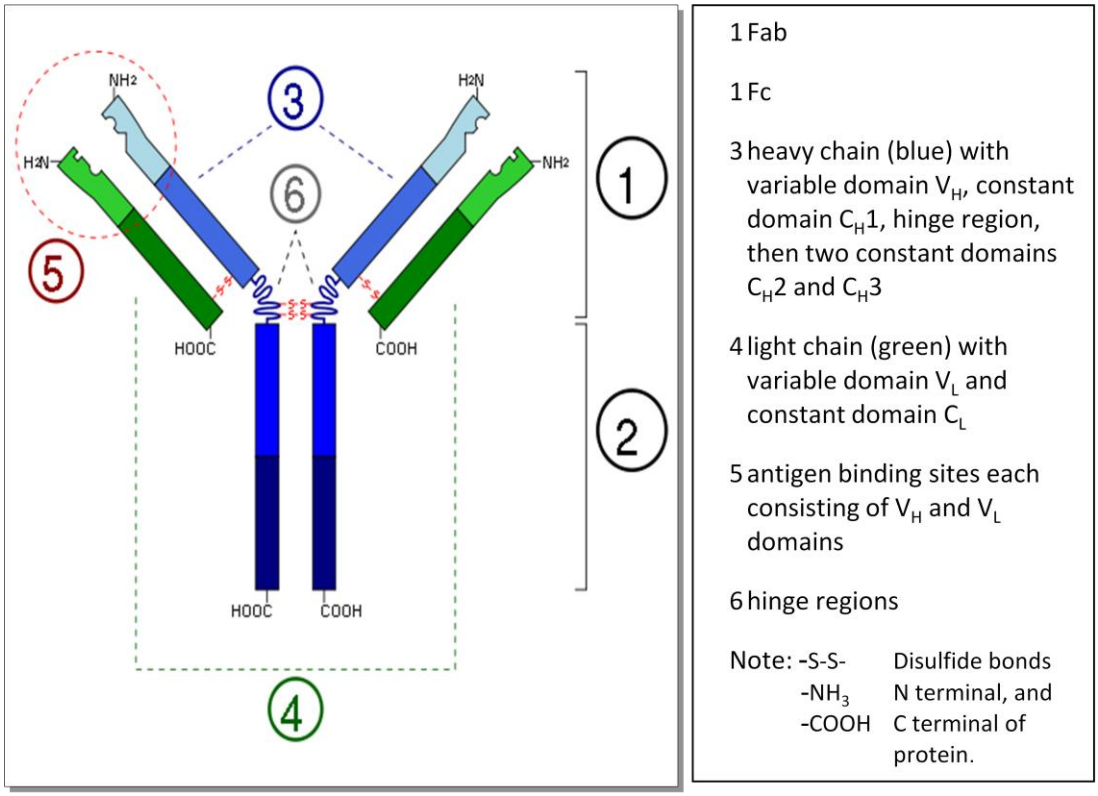

Figure 3.6.1 Schematic diagram of the basic units of an antibody (immunoglobulin) [61]

To determine whether the immobilization of antibodies on nanoparticles interferes with the ability of the antibody to react with the analyte, we compared the Raman spectra of caffeine solutions that were interacted with free caffeine antibodies prior to antibody immobilization (pre-bound) to spectra acquired by reacting caffeine solutions with antibody only after they had been immobilized on the gold nanoparticles (post-bound). Caffeine was also exposed to the antibody-functionalized gold nanoparticles from different manufactured batches. The prepared solutions were analysed by SERS as described in section 2.5 of the Materials and Methods chapter. All data analyses and multivariate statistical treatments of the acquired spectra were performed as indicated in section 2.6.

The results are reported in figure 3.6.2. These data compare the pre-bound nanoparticles with post-bound nanoparticles and the data show that all of the post-bound samples were consistent within the model. About half of

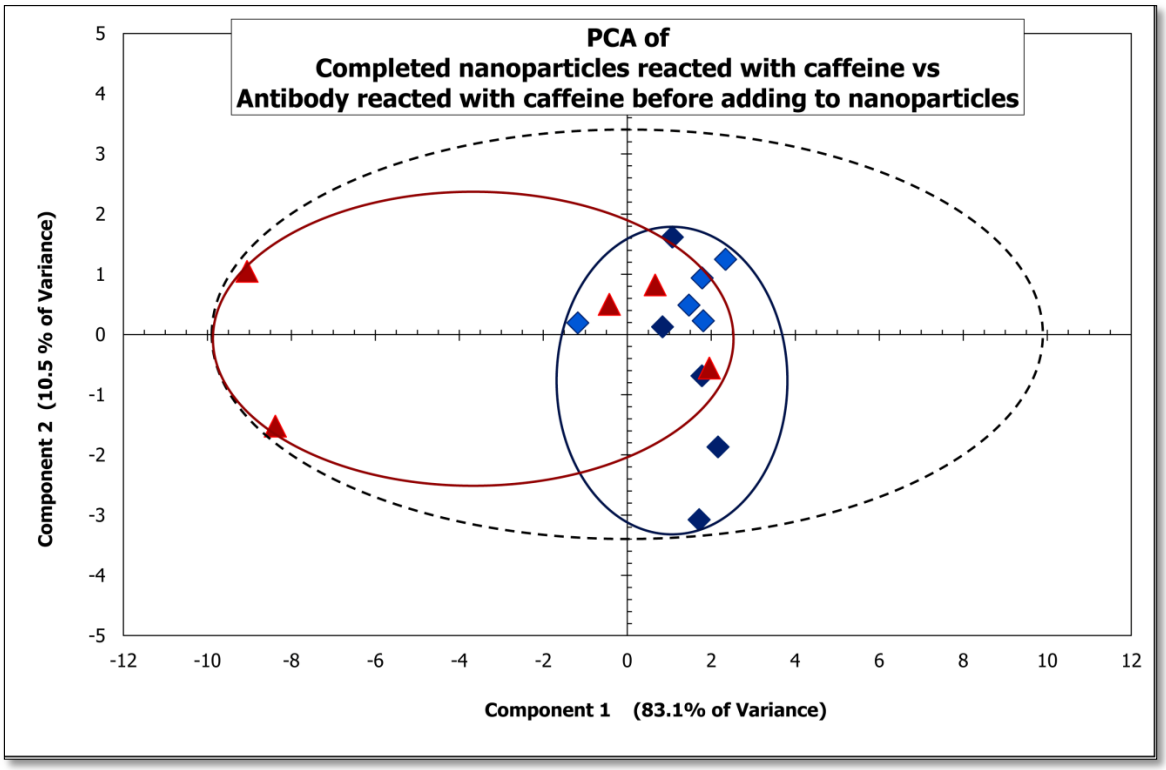

Figure 3.6.2 PCA of SERS spectra of caffeine solutions reacted with antibody-functionalized gold nanoparticles (light and dark blue diamonds) vs SERS spectra of caffeine solutions reacted with caffeine antibodies prior to immobilising on the nanoparticles (red triangles)

the pre-bound samples appeared to be different from the post-bound samples. The remaining pre-bound samples were statistically similar to the post-bound samples. From these data, we can safely assume that no significant interference to antigen binding occurs as a result of immobilizing the antibodies on the nanoparticles.

3.7 EFFECT OF TIME ON THE BINDING BETWEEN CAFFEINE AND ANTIBODY-FUNCTIONALIZED GOLD NANOPARTICLES

To determine the optimal reaction time for the complete binding between the caffeine molecules and the antibody-functionalized gold nanoparticles, a 1 x 10^{-6} M standard solution of caffeine was mixed with the antibody-functionalized gold nanoparticles and incubated under ambient temperature for different intervals of time (from five to 60 minutes). The incubated samples were then characterised by SERS as per the procedures in section 2.5. The caffeine-specific peaks at about 1300 cm^{-1} in the acquired spectra were used to determine the time at which no further appreciable changes in SERS signals intensities occurred.

The results are shown in figure 3.7.1. The peak at 1300 cm^{-1} correlates with a prominent peak in the Raman spectra of caffeine (1325 cm^{-1}), and it was baseline separated.

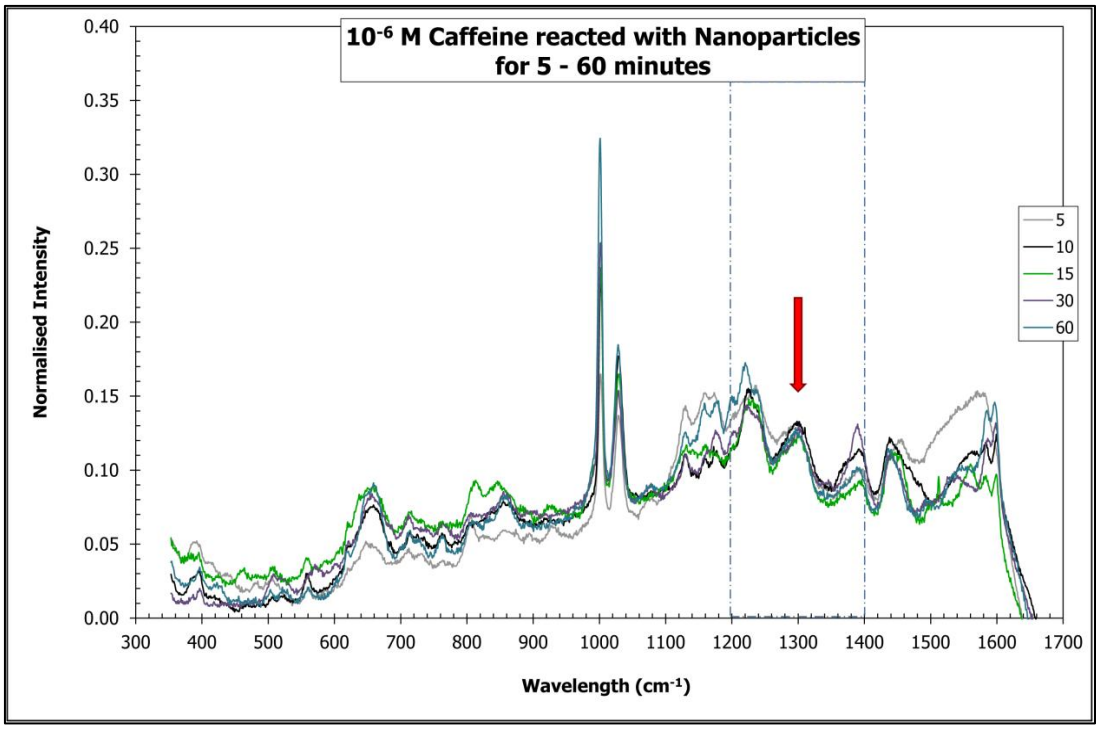

Figure 3.7.1 SERS measurements of caffeine (1x 10^{-6} M) at different time intervals. The caffeine solution was reacted with antibody-functionalized gold nanoparticles and incubated for different intervals of time (5, 10, 15, 30, 60 min respectively) prior to the SERS measurement. The red arrow indicates the monitored caffeine Raman band @ 1300 cm^{-1}.

NOTE: this peak shifts wavelength as in figure 3.5.3 with increasing reaction time (i.e. analogous to increasing concentration). See figure 3.7.2A change between 5 and 10min. The peak used for interrogation is indicated by the red arrows in figure 3.7.1, and figure 3.7.2 A.

The relationship between the peak intensity at 1300 cm^{-1} and the incubation time is shown in figure 3.7.2. The maxim intensity of the peak at 1300 cm^{-1} was observed after 10 minutes. Therefore, the optimal reaction time for the interaction between caffeine and the antibody-functionalized gold nanoparticles is 10 minutes. This time was then used for the rest of the study.

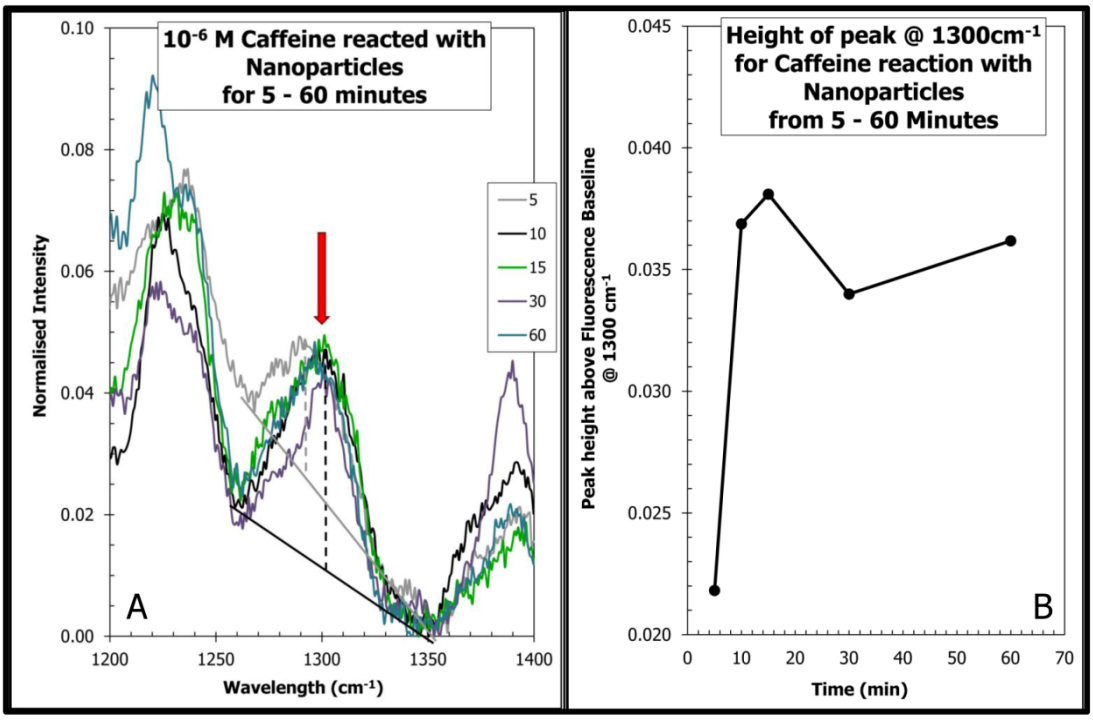

Figure 3.7.2 Relationship between caffeine signal intensity @ 1300 cm^{-1} and time A) Partial spectrum of 1×10^{-6} M caffeine reacted with nanoparticles (from 1200 - 1400 cm^{-1}). The red arrow indicates location of indicative peaks for the reaction of the nanoparticle with caffeine, @ 1300 cm-1. B) Peak height @ 1300 cm^{-1} corresponding to vertical dotted lines in A (grey = 5min, black = 10 min) Note: improvement (and minor wavelength shift) from 5 – 10 minutes and relative consistency of both from 10 minutes to 60 minutes.

3.8 QUANTIFICATION OF CAFFEINE BY ANTIBODY-FUNCTIONALIZED GOLD NANOPARTICLES

In this part of the study we investigated the quantification of caffeine by SERS with the aid of the antibody-functionalized gold nanoparticles. Standard solutions of caffeine in the concentration range 1×10^{-4} M to 1×10^{-10} M were prepared, interacted with antibody-functionalized gold nanoparticles and screened by SERS. The acquired spectra [fig. 3.8.1] were subjected to baseline subtraction and normalisation, see section 2.6.1.

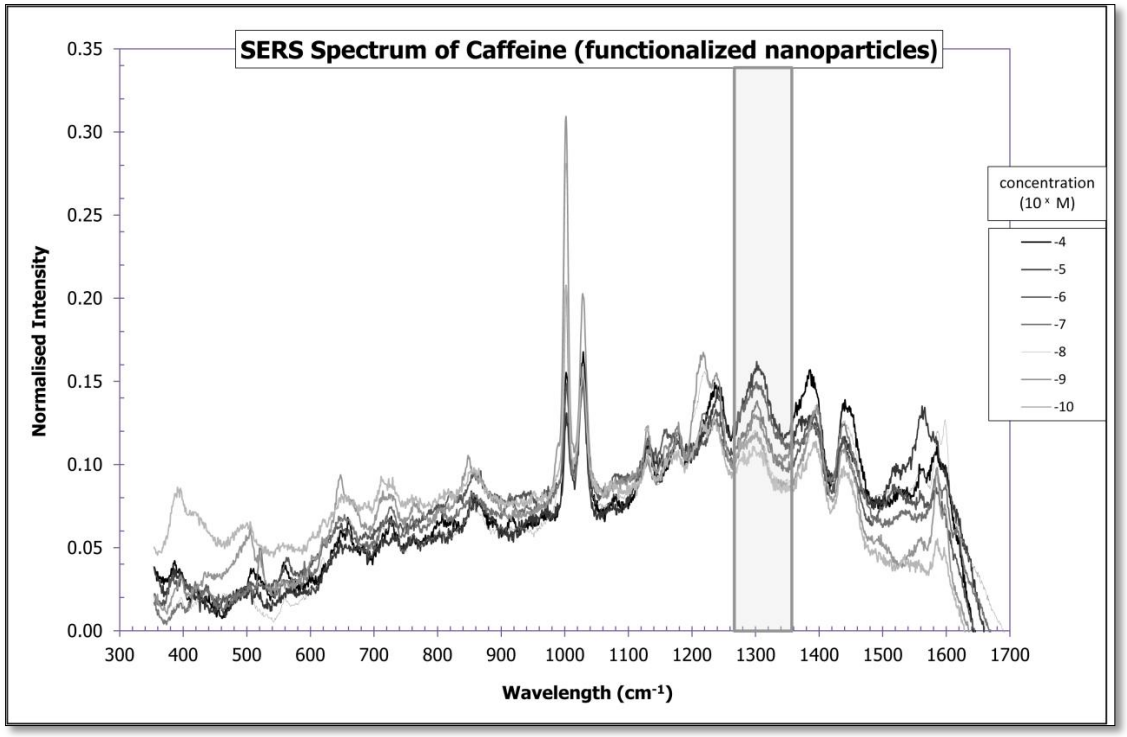

Figure 3.8.1 SERS spectrum of caffeine using antibody-functionalised gold nanoparticles. The grey highlighted box indicates the peak caffeine Raman band, at 1300 cm-1, that was used for developing the calibration in figure 3.8.2.

The signal intensity at 1300 cm^{-1} was found to be in excellent agreement with the ln function of the caffeine concentration in the concentration range 1×10^{-4} M to 1 $\times10^{-10}$ M [fig. 3.8.2., 6 measurements were taken for each data point on the curve]. The regression line showed excellent linearity with R^2= 0.9794 [fig.3.8.2]. These results confirmed the quantification of caffeine by the prepared antibody- functionalized gold nanoparticles.

The average height of the nanoparticles background at this wavelength was measured individually as for figure 3.8.2. Taking the LLOD as mean + 3*SD, LLOD of the caffeine that can be achieved by using our antibody-functionalized gold nanoparticles was an intensity of 0.035 which is equivalent to 5×10-11 M using the equation of the regression line, so conservatively we defined the LLOQ as 1×10-9 M. This LLOQ is five orders of magnitude lower than that achieved using the bare gold nanoparticles (without antibody attachment) for the SERS detection of the caffeine [fig. 3.8.2].

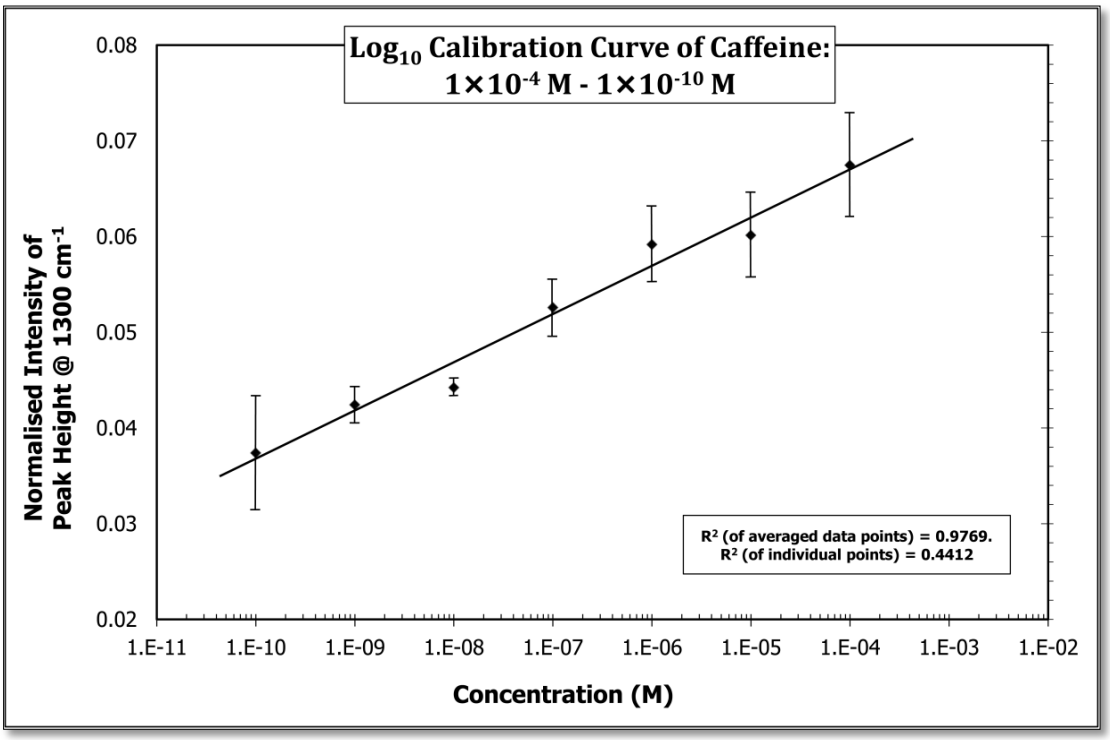

Figure 3.8.2 Relationship between signal intensity at 1300 cm^{-1} and the concentration of caffeine solutions in the concentration range 1×10^{-4} M to 1×10^{-10} M (n=6). The trend line indicates the ln relationship between concentration of caffeine and the peak intensity at 1300 cm^{-1}. Error bar = 1 SD

This improvement can be attributed in part to the immobilization and concentration of caffeine molecules close to the gold surface, which effectively increased the caffeine SERS signal intensity. This peak corresponds to a peak at 1325 cm-1 in the SERS spectrum for caffeine on bare gold nanoparticles, see grey shaded box in figure 3.7.1. This SERS peak for caffeine has shifted in wavelength which is evidence that the caffeine is bound to its antibody with potential hydrogen bonding to N9 (Fig 3.1.1). The implications for calibration are that with hydrogen bonding to this atom the molecular vibration (Imidazole trigonal ring stretching) that causes this peak would be inhibited /modified and the wavelength of the peak subsequently shifted. The second implication would be that the caffeine would be held as close as possible to the gold nanoparticles surface which would lead to maximum possible enhancement of this peak. Therefore this is an excellent choice as a peak for calibration purposes.

3.9 STUDY OF INTERFERENCE ON THE DETECTION OF CAFFEINE BY ANTIBODY-FUNCTIONALIZED GOLD NANOPARTICLES

A series of studies were performed to determine if other compounds that may co-exist with caffeine in beverages with complicated matrices can cause interference or completely compromise the detection of caffeine with the proposed method. As was mentioned in the Raman spectroscopy section, in this and subsequent studies washing was required to remove interfering large molecules prior to loading on the slide.

In this study various beverages that contain caffeine were screened by SERS with the aid of the antibody-functionalized gold nanoparticles. After gathering the spectra, PCA of the relevant major Peaks or HPCA (as indicated) was performed as outlined in section 2.6.5 to determine if there was any relevant interference to the spectrum from other molecules present in the beverage.

3.9.1 **Coke vs Diet Coke™**

Regular Coca-Cola™ and Diet Coke™ have similar content of caffeine. However, a major difference between the two products is the sweetener used in each. Coca-Cola contains sucrose, whereas Diet Coke uses aspartame as its sweetener. Aspartame is a molecule that contains a primary amine group. The Glutaraldehyde linker that is used in this study to attach the antibodies to the nanoparticles can react with primary amines. Therefore, any unreacted glutaraldehyde (not attached to an antibody molecule) can readily bind to the aspartame content in the diet coke beverage. This non-selective binding onto the surface of the antibody-functionalized gold nanoparticles may cause a significant interference to the caffeine spectrum.

This study was performed to check if it was necessary to block any un-reacted glutaraldehyde. The antibody-functionalized gold nanoparticles were originally designed without blocking molecules in order to keep their synthesis as simple as possible. However it was important to determine whether this was adequate for commercial products with complex matrices or if blocking of the un-reacted glutaraldehyde molecules is necessary to prevent uncontrolled cross

reaction with unknown interfering compounds. The results are shown in figure 3.9.1.

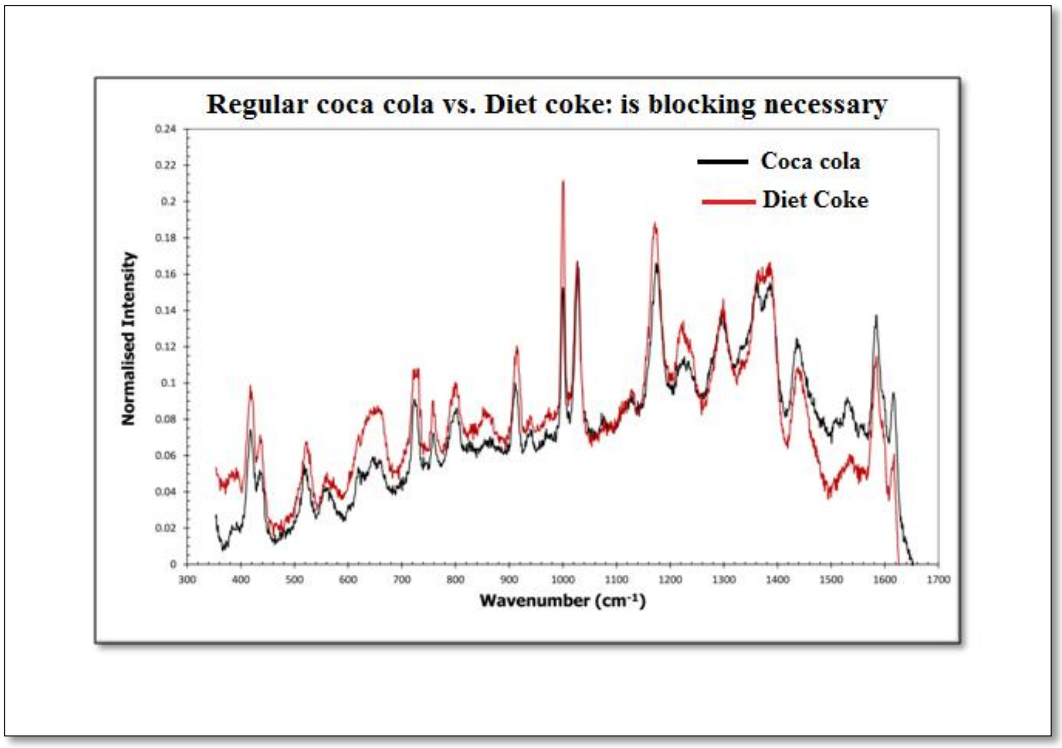

Figure 3.9.1 Spectra of regular Coca-Cola™ compared with Diet Coke™ reacted with the original unblocked antibody-functionalized nanoparticles [without background subtraction].

Careful inspection of the spectra in figure 3.9.1 indicated minor differences between some of the corresponding peaks of the Coca-Cola™ and Diet Coke™ averaged spectra. Height differences that do not appear to be solely the result of background variability are also present and may be more significant to the difference between the two samples, particularly if there has been non-specific binding to the unreacted glutaraldehyde.

To confirm whether these differences seen in the spectrum are significant, PCA analysis of the two samples was performed using the prominent positive peaks remaining after subtraction of the averaged background spectra from each individual spectrum before baseline correction and normalisation. The PCA analysis comprised two significant components: component 1 comprising 84.5% of the variation in the data, and component 2 comprising 6.9% of the variation in the data. The results are shown in figure 3.9.2.

The regular Coca-Cola™ and Diet Coke™ are clearly separated in this study. The major separating component is component 2 which comprises less than 10% of the variation. While on component 1, which has the majority of the

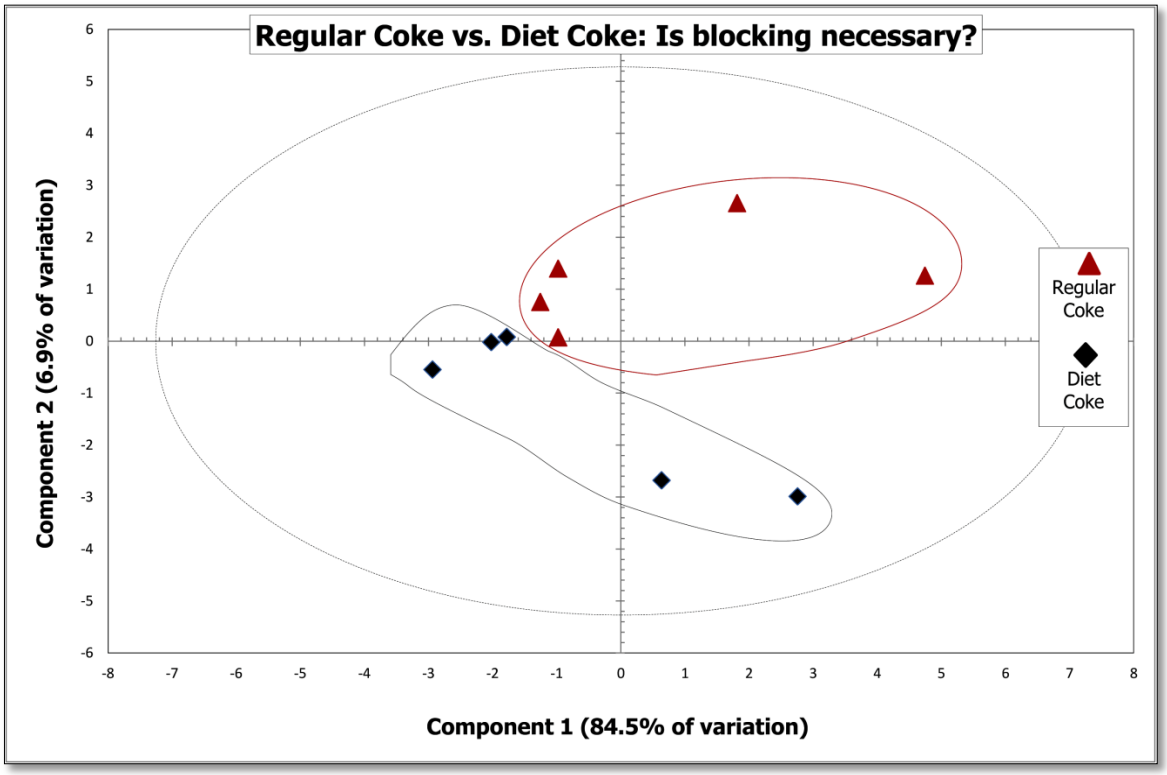

Figure 3.9.2 PCA of regular Coca-Cola and Diet Coke reacted with the un-blocked antibody-functionalized gold nanoparticles.

variation, the two samples are largely overlapped. This is consistent with the graph in figure 3.9.1 as the differences between the two averaged sample graphs are minor. This study implied that there is binding between the aspartame and un-reacted glutaraldehyde molecules. Therefore, it was determined that, blocking of the unreacted glutaraldehyde is required to avoid any cross interaction with interfering molecules. We further investigated this conclusion by investigating the interaction between the unblocked antibody- functionalized gold nanoparticles and the caffeine-free Diet Coke™ beverage.

3.9.2 **Caffeine free Diet Coke™ vs Unreacted Nanoparticles**

As the name implies, caffeine free Diet Coke™ contains no caffeine. However as for regular Diet Coke™ it is sweetened with aspartame. If there is no unreacted glutaraldehyde molecules available for cross binding with aspartame, the average spectra of this and the unreacted nanoparticles should be identical.

For this study we have performed a hierarchical PCA (HPCA). This technique allows us to include all of the spectral data for all samples. This allows any subtle differences to be accounted for, and is the most robust technique possible. HPCA was explained in the Materials and Methods chapter (section 2.6.5).

The results of this study are shown in figure 3.9.3 below. The HPCA had three significant components explaining 87.9% of the variation in spectral data. Component 1 comprised 48.5% of variation; component 2, 26.2% of variation and component 3, 13.1%.

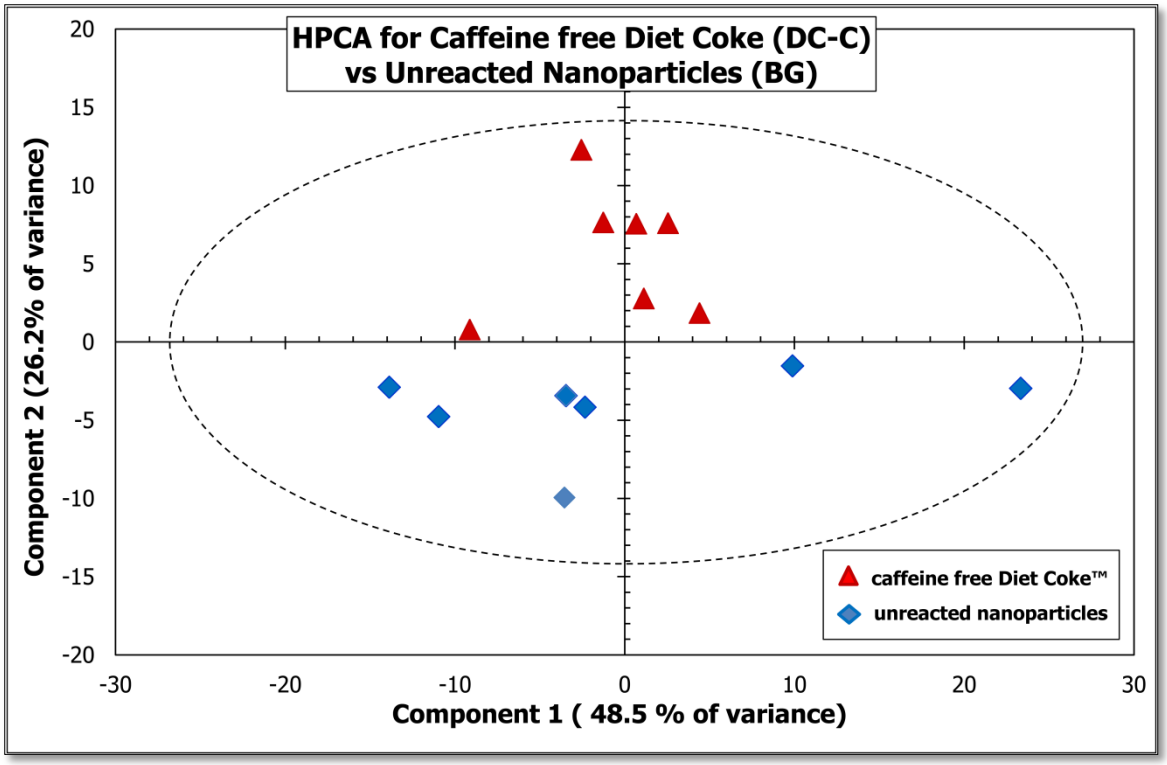

Figure 3.9.3 HPCA of the SERS spectra acquired from caffeine-free Diet Coke™ after interaction with the unblocked antibody-functionalized nanoparticles compared to the unreacted nanoparticles.

Figure 3.9.3 clearly confirms that component 1 shows no distinction between the two groups of samples. Component 3 also shows no distinction (not shown in fig. 3.9.3). However with component 2, all the unreacted nanoparticles are negative, while all the caffeine free Diet Coke™ samples are positive. This is a distinctive verification that there is unspecified reaction between aspartame and unreacted glutaraldehyde sites. Therefore it is established that blocking of the glutaraldehyde linker nanoparticles is required.

The above studies were repeated after blocking unreacted glutaraldehyde on the antibody-functionalized nanoparticles with ethylamine as per the procedure indicated in section 2.3.3. The retesting was carried out to investigate whether the blocking agent was successful in preventing the unwanted binding to interfering compounds.

3.10 CONFIRMATION OF BLOCKING ADEQUACY

The blocking adequacy was confirmed using firstly Coca-Cola™ vs Diet Coke™. As before, after that, unreacted nanoparticles and the caffeine free Diet Coke™ spectral data were obtained. The spectra for each study were averaged and compared for any variations in the corresponding spectra that would indicate the blocking was not adequate. This was followed up using PCA/HPCA respectively to further confirm the adequacy of the blocking step.

3.10.1 **Coke vs Diet Coke™**

The PCA for Coca-Cola™ vs Diet Coke™ is found in figure 3.10.1. It comprises one component that explains 98.2% of the variation in the data. The two groups of samples are significantly overlapped in this graph. This is a probable indication of blocking adequacy. However the overall tendency shows Diet Coke™ more negative than regular coke. So further verification needs to be done to confirm whether the blocking was inadequate or was something else causing the overall tendency of differences between these two products.

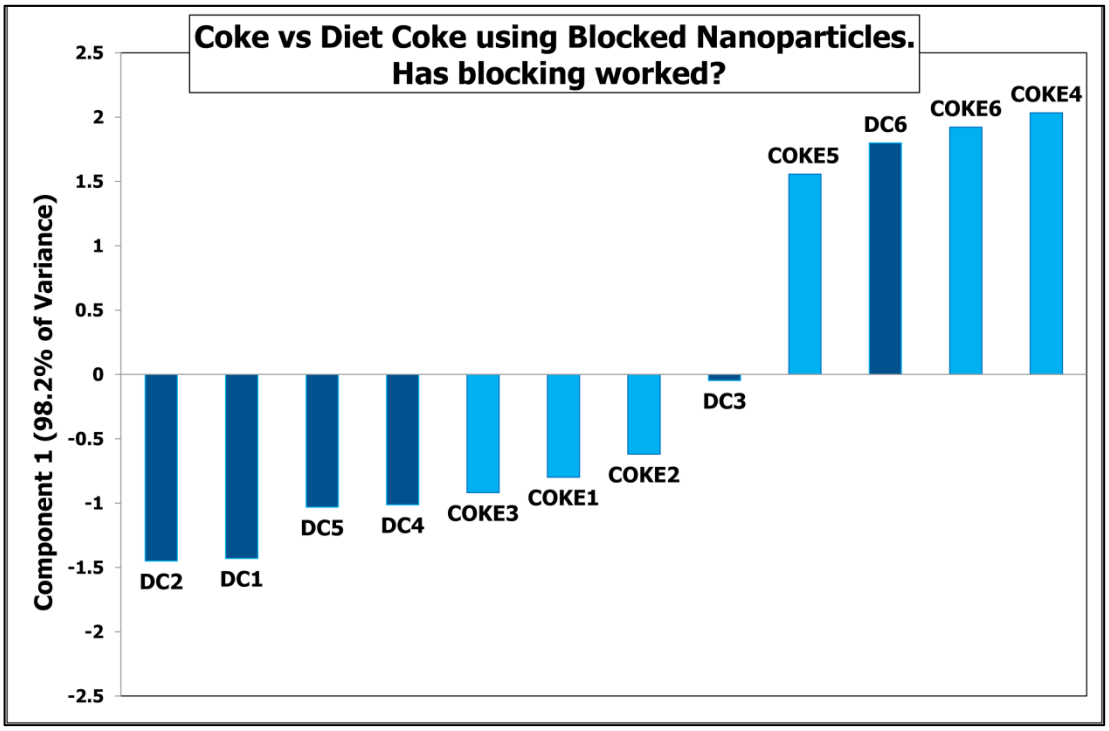

Figure 3.10.1 PCA of regular Coca-Cola™ vs Diet Coke™

3.10.2 **Caffeine free Diet Coke vs Unreacted Nanoparticles**

HPCA was used in this study to provide the most robust confirmation of blocking adequacy possible. Figure 3.10.2 shows the HPCA analysis of the acquired SERS spectra. The HPCA had four significant components explaining 95.9% of spectral data variance. Components 1-4 comprised 40.8%, 26.9%, 17.4% and 10.9% respectively of the spectral data variance.

Careful inspection of figure 3.10.2 shows that all four components are not able to distinguish between the unreacted nanoparticles and the caffeine free Diet Coke™ reacted nanoparticles. For the unreacted nanoparticle samples, some samples are negative and some positive in each component. This also holds for the caffeine free Diet Coke™ samples in components 2 and 4. For components 1 and 3 the caffeine free Diet Coke™ samples fall within the range of the unreacted nanoparticle samples. This means that the two groups of samples are equivalent, and that the blocking step was adequate to prevent unspecific cross reaction. This implies that the negative tendency of Diet Coke™ (fig. 3.10.1) may have other origins.

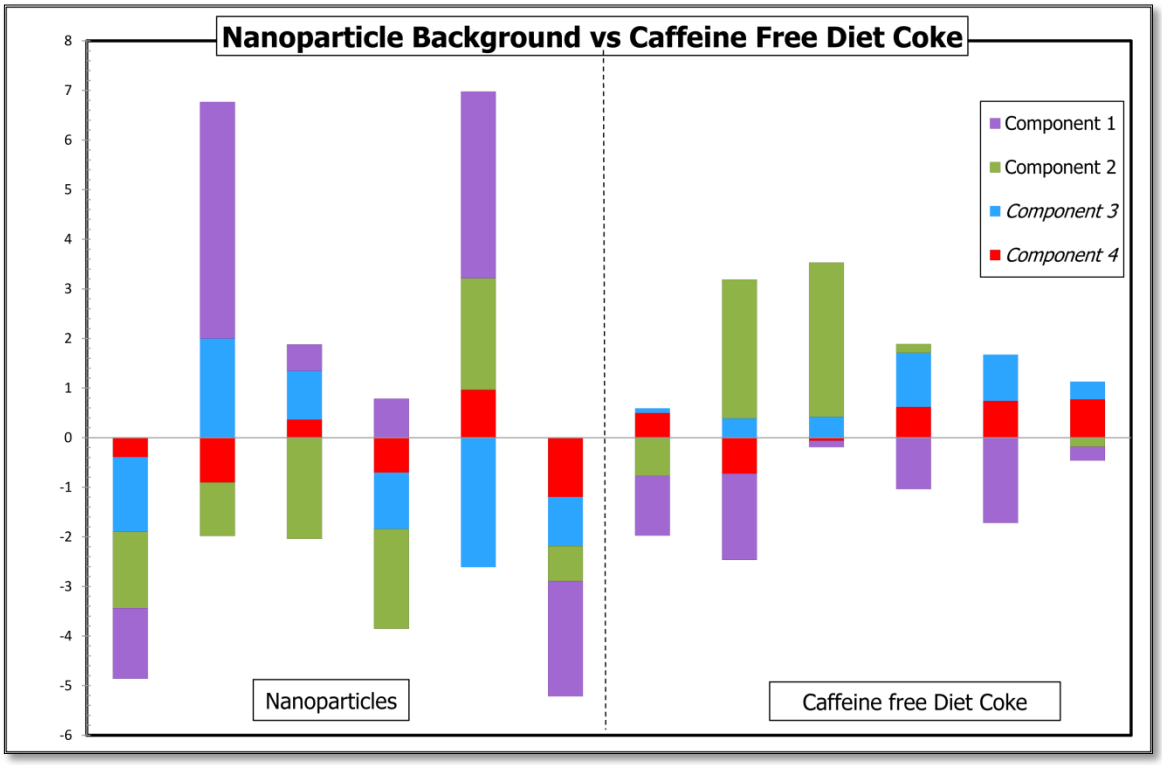

Figure 3.10.2 HPCA of caffeine free Diet Coke™ reacted with the caffeine antibody functionalized blocked nanoparticles compared to the unreacted nanoparticle, to confirm that the blocking has worked.

The ethylamine-blocked antibody-functionalized gold nanoparticles were then used in an overarching study involving a range of caffeinated beverages that contain different sweetening products as well as synthetic/naturally derived caffeine. This study was performed to determine if the nanoparticle could adequately distinguish caffeine in a range of complex matrices.

3.11 COMPARISON OF CAFFEINE CONTAINING BEVERAGES

The interference study was repeated using commercial beverages containing caffeine. These beverages were Cola flavoured beverages: regular Coca-Cola™ from Coca-Cola Company; along with two products with alternative sweeteners, Diet Coke™ from Coca-Cola Company containing aspartame as sweetener, and, Pepsi Next™ from PepsiCo containing Stevia extract as sweetener.

Two energy drinks were also investigated, Red Bull™ regular from Red Bull GmbH containing only synthetic caffeine, and Monster Energy™ from the Monster

Beverage Corporation containing both synthetic caffeine and naturally derived caffeine from Guarana seed extract. Coffee products were also used, they were, a short black (espresso) from a barista, and an instant coffee product -Italian Espresso Style coffee bag from Robert Timms. Figure 3.11.1 shows the spectra of the commercially available beverages included in this overarching study.

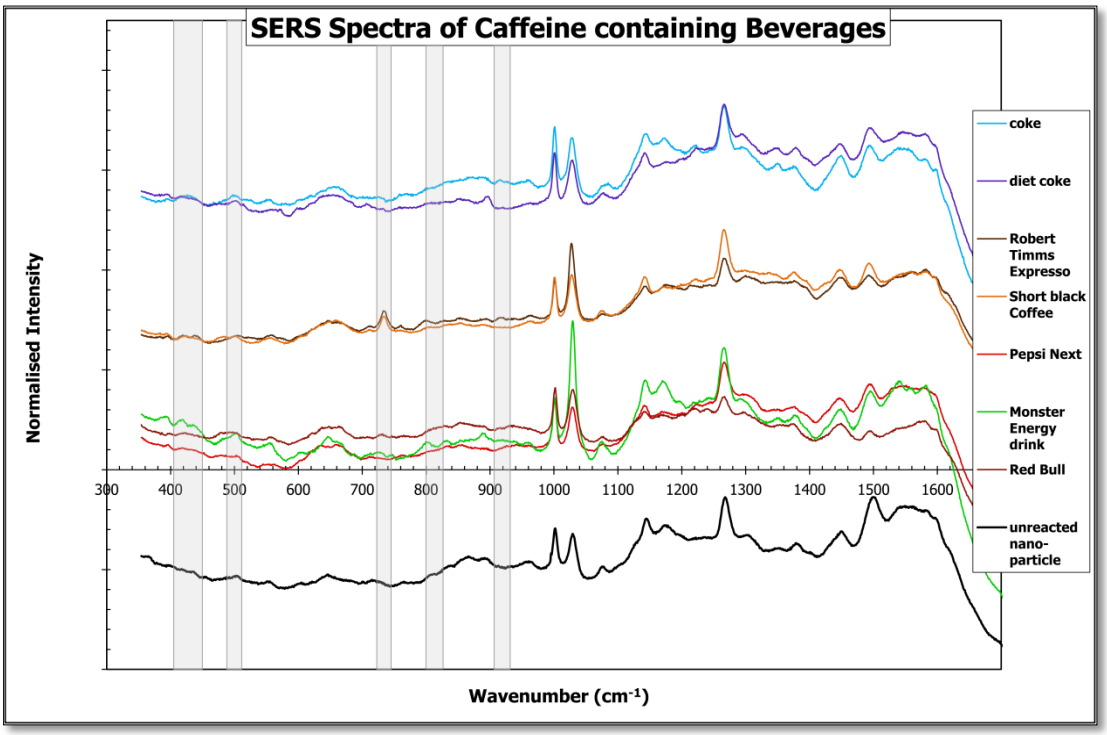

Figure 3.11.1 Stacked SERS spectra of caffeine containing beverages reacted with blocked antibody-functionalized gold nanoparticles.

NOTE: the antibodies used in this study were older so the nanoparticle background peaks differed from previous ones and difference from this background was used to determine caffeine binding.

3.11.1 **Caffeine in commercially available beverages**

The spectra acquired from reacting each of Coca-Cola™, Diet Coke™, Pepsi Next™, Red Bull™ and Monster energy™ beverages with the blocked antibody-functionalized gold nanoparticles were examined using PCA multivariate statistical analysis. The PCA for this study is shown in figure 3.11.2. The PCA model showed one significant component comprising 86% of the variance.

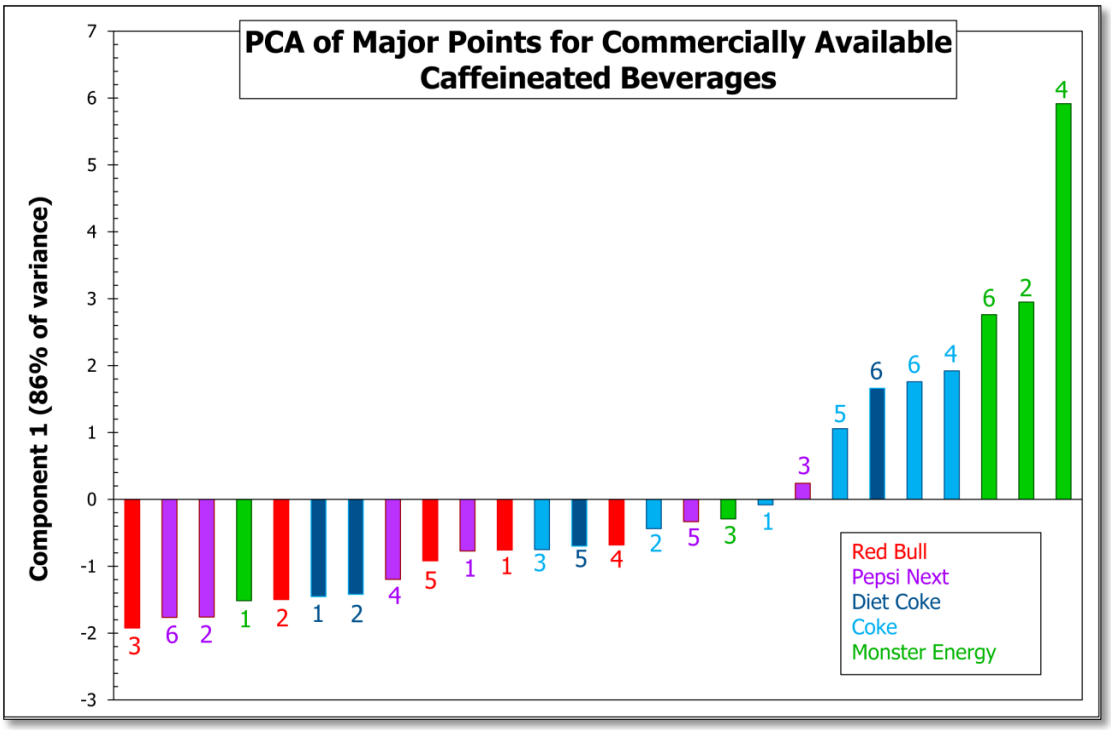

Figure 3.11.2 PCA for commercially available prepared caffeinated beverages using the major points of the caffeine is reaction with the caffeine antibody functionalized nanoparticle.

Red Bull™ is a product known to contain only synthetic caffeine. All the Red Bull™ samples are negative in component one. They are also found the furthest left of all the samples the PCA graph.

Monster Energy™ contains synthetic caffeine as well as an extract from the Guarana plant. The Guarana plant is a natural source of caffeine. Half of the Monster Energy™ samples are significantly positive in component one. One of the other two Monster Energy™ samples resembles that of the Red Bull™ samples. Other than this sample, all the Monster Energy™ samples are on the right hand side of the graph.

This mixed character of the Monster Energy™ samples reflects the mixed source of the caffeine in the product. One sample (on the far left) most likely primarily contains synthetic caffeine, three (on the far right) most likely contain only naturally derived caffeine and the other (towards the middle) probably contains a mixed source of caffeine.

A published study examined the caffeine in Guarana and found that it forms a complex with the tannins compound that is known to be found in

Guarana plants. the study proved that the interaction between caffeine and tannins was through the non-methylated nitrogen atom (N_9) and was most likely a hydrogen bond with a hydroxyl group on the tannin [43]. An earlier study of Guarana also came to this conclusion using a thin layer chromatographic technique and further analysis using mass spectroscopy, UV, IR and 'H NMR spectroscopy. They compared Guarana extract with the same extract after treatment with a method used to remove tannins. The treated Guarana extract reacted the same as caffeine in these techniques [65].

The actual ingredients of Coca-Cola™ are a trade secret.[66] However there has been a persistent rumour that historically Coca-Cola™ contained extracts from the Coke plant and the Kola plant, hence the name Coca-Cola™ derived from the two plant names with the K in Kola changed to C for marketing reasons.[67] There is no actual information available about the precise ingredients for Coca-Cola™ but the official UK Coca-Cola™ web page ingredients list for Coca-Cola™ includes "natural flavourings (containing caffeine)" [68]. This implies that Coca-Cola™ may contain an extract from Kola plant as its source of caffeine.

In figure 3.11.2 the Coca-Cola™ samples act far more similarly to those of the Monster Energy™ samples, which are assumed to contain naturally sourced caffeine, than they do to the Red Bull™ samples. The majority of the Coca-Cola™ samples are positive in component 1 and on the right hand side of the graph. This is evidence in support of the rumour that Coca-Cola™'s caffeine comes from the Kola plant.

The UK Coca-Cola™ web page ingredients list for Diet Coke™ has a subtle difference to that of the Coca-Cola™ web page (except obviously for the sweetener source). This is an omission of the word "natural" when describing the flavourings containing caffeine [69]. This implies that the source of the caffeine may be synthetic rather than natural even though the flavour is still that of Cola. Interestingly the Diet Coke™ samples in this study act very similarly to those of the Red Bull samples. All but one of the Diet Coke™ samples is closely similar to the corresponding Red Bull™ sample, i.e. negative in component 1 and on the

left-hand side of the graph. This is a confirmation of the hint from the UK Coca-Cola™ web page that the source of the caffeine in Diet Coke™ is different from that of Coca-Cola™ and is not natural.

The other beverage in this study is PepsiNext™. The Australian PepsiNext™ ingredients list contains caffeine and Natural flavours[70]. So the implication is that in PepsiNext™ the caffeine is of the synthetic variety. In this study the Pepsi Next™ samples act very much like the Red Bull™ samples even more so than those of Diet Coke™. This is strong confirmation that the caffeine source of Pepsi Next™ is synthetic. Consequently both Diet Coke™ and Pepsi Next™ will be omitted from the following study with naturally caffeinated beverages. Red Bull™ will be included only as a known source of synthetic caffeine for comparison purposes.

3.11.2 **Beverages with Naturally Occurring Caffeine**

The beverages included in this PCA Model were those commercial beverages identified in the last study as most likely containing naturally occurring caffeine i.e. Coca-Cola™ and Monster energy™. Also included were instant coffee from Robert Timms (Italian Espresso Style brand) and a short black (espresso) from a barista. As a comparison, Red Bull which is known to contain synthetic caffeine was included. SERS spectra of the beverages after their reaction with the blocked antibody-functionalized gold nanoparticles were processed and involved in the PCA model shown in figure 3.11.3.

This PCA model has two significant components explaining 96.4% of the spectral variance: component 1 with 76.4 % of the variance and component 2 with 20.0%. The red Bull samples in this model were tightly clustered and approximately centred on component one. They were all positive in component 2.

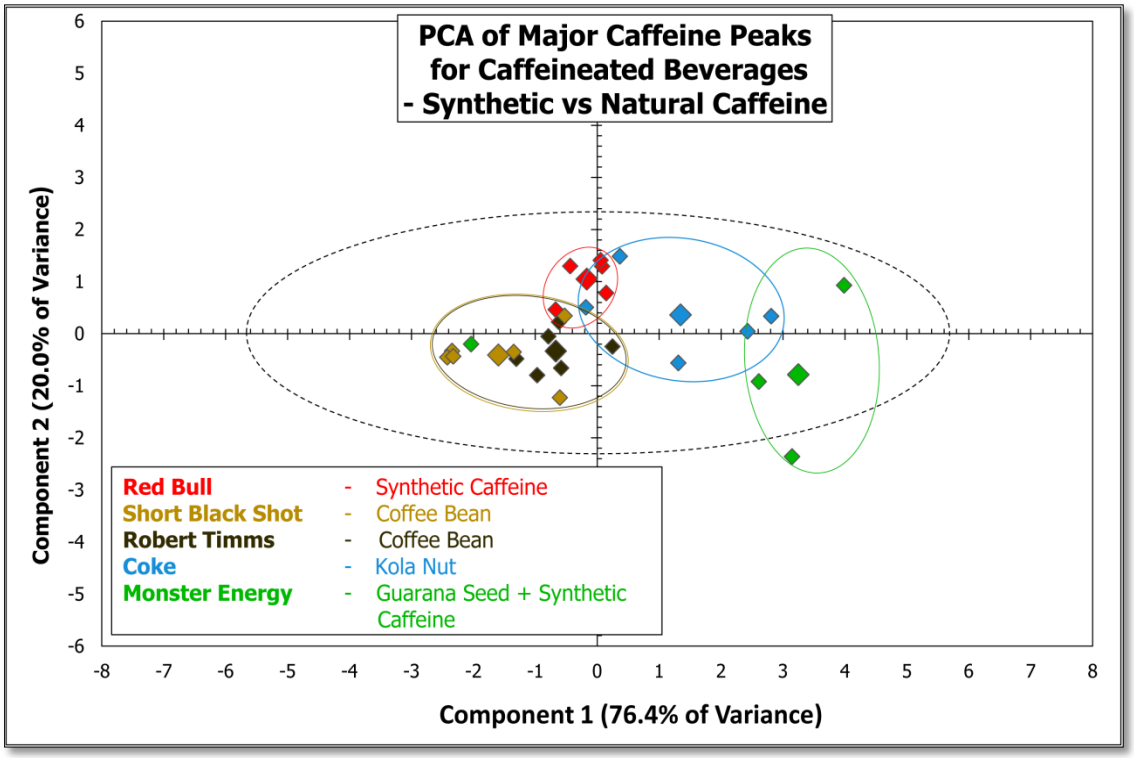

Figure 3.11.3 PCA of the all beverages containing naturally derived caffeine: Coca-Cola, Monster energy, instant coffee, short black (espresso). Red Bull is added to the list as a source of known synthetic caffeine for comparison.

All but one of the Monster energy samples were loosely clustered furthest right (i.e. positive on component 1). They were also mostly negative on component 2. As in the study with commercially available beverages one of the monster energy samples is significantly different to the rest.

The other group of samples whose average point is positive in component 1 is Coca-Cola. All but one of its samples is positive in component 1 with the remaining sample just negative, and consistent with synthetic caffeine the. Coca-Cola is the only group of naturally occurring caffeinated beverages whose average point is positive in component 2.

The two groups of coffee samples were intermingled, as would be expected. The instant coffee is more closed tightly clustered which is not unsurprising as this is a commercial product and therefore probably more processed with meticulously controlled ingredients. This instant coffee is also close in character to Red Bull, the synthetic caffeine containing beverage. The company (Robert Timms) that produces this instant coffee states on the

packaging that the coffee bag contains both ground and soluble coffee. This may mean that some of it has been sufficiently processed that part of the caffeine content is free of any molecular complexing, i.e. equivalent to synthetic caffeine.

The espresso samples (short black shot) showed an interesting pattern in this model. The coffee is known to be of a blended source[71]. The three of the samples were almost superimposed. Two of the remaining samples were on the other two points of a triangle, with the last sample almost equidistant between these three positions. This would be consistent with a mix of three different sources with three points of the triangle indicating the three separate sources, and the equidistant point a mix of all three sources. These results imply that this technique may be able to distinguish between coffee beans from different sources and may imply wider applications to other plants/beverages derived from them. This is an area that requires further investigation.

3.11.3 **All Caffeine containing Beverages**

The spectral data of all of the investigated beverages were included in a third PCA model [figure 3.11.4) with two significant components comprising 96% of the spectral data variation overall. Component 1 explains 71% of the variance while component 2 explains 25%. The model indicated that the majority of Monster energy samples were positive in component 1.

The Coca-Cola samples were placed very similarly to those in the previous models, but interesting findings about the Diet Coke can be seen. The Diet Coke samples were widely scattered in component 1 with the averaged data point practically neutral on component 2. The average data point for Diet Coke is almost superimposed upon the average data point of Pepsi Next, and both of them are very close to the Red Bull samples. Taking these points together it is further evidence that both of these cola flavoured drinks contain synthetic caffeine.

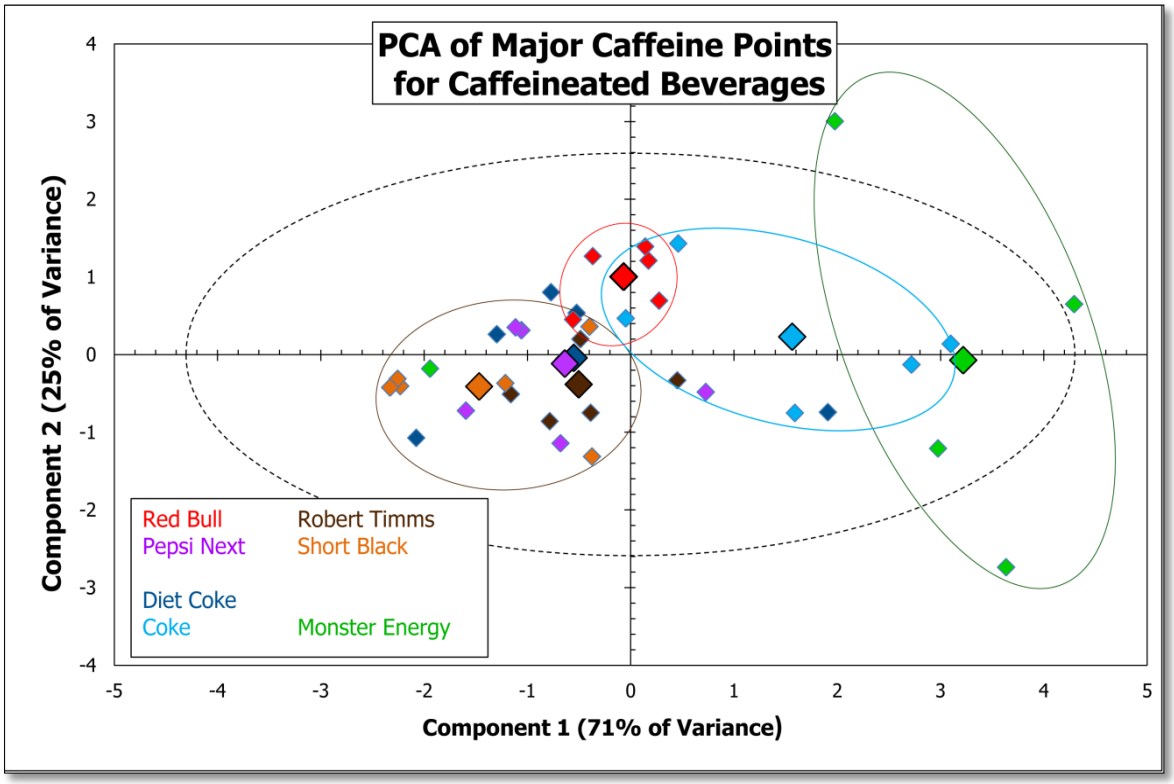

Figure 3.11.4 PCA of the major points in the Raman spectra of the caffeinated beverages reacted with the blocked caffeine antibody functionalized nanoparticles.

As before in the naturally caffeinated beverages model the two coffee samples were inter-disbursed with the instant (Robert Timms) coffee samples more tightly clustered. The PCA model also showed that the average instant coffee sample was very close in character to those of the Diet Coke and Pepsi Next, with one of the instant coffee samples so similar that it was concealed beneath that of the averaged Pepsi next. This is further evidence that the processing of the instant coffee may have produced at least some non-complexed caffeine approximating synthetic coffee.

The average espresso coffee sample was far more negative on component 1 than the average instant coffee sample, with half of the espresso coffee samples largely superimposed and the furthest left found. Both averaged coffee samples are, however, very similar on component 2.

3.12 PRELIMINARY CONCLUSIONS AND RECOMMENDATIONS FOR THE CAFFEINE MODEL

The caffeine study demonstrated that this new technique is suitable for ultra trace detection of caffeine and by extension other small molecules provided that a suitable antibody to the target analyte is used. The LLOQ found for caffeine standard solution was 1×10^{-10} M. This is magnitude significant improvement from of other techniques currently used for the detection of caffeine such as FT-Raman spectroscopy which has LLOD of 9.3×10^{-5} M [40].

In addition to its significant improvement in sensitivity and the non-destructive nature of the analysis, this technique requires at only 10 µL of sample from standard solution or commercial beverages (such as soft drink or energy drinks) while FT-Raman requires 10 mL of sample for the analysis [40]. The developed technique combines immuno-separation with direct SERS analysis of the target analyte. The technique does not suffer from the problems of other Raman techniques where the spectrum of the analyte is completely swamped by the remainder of the sample, or misidentification of the trace analyte due to the presence of interfering compounds in the sample within the sample[43, 45].

The new method does not require sample preparation and is applicable to liquid samples of complex matrices. These features along with the availability of commercial portable Raman spectrometers make the technique rapid, applicable to field screening scenarios and more user – friendly when compared to other techniques such as chromatography[40]. Therefore the developed technique has broad applicability in many fields such as pharmaceutical and food industries.

This model showed some interesting preliminary features that should be pursued with further analysis to verify. The guarana extract in Monster Energy™ with its complexed caffeine was different to the majority of other beverages that were trialled in this study as it is known to be complexed with tannins [43, 65]. The Monster Energy™ samples had extreme positions on the caffeinated beverages PCA analyses [figures 3.11.2, 3.11.3 and 3.11.4]. In a follow-on study, another source of Guarana extract will be used to verify that this result is not an artefact but is fundamental to Guarana analysis, and more broadly to

analysis of naturally derived caffeine. In addition, several other naturally caffeinated beverages, including tea and yerba maté will be used, to investigate the effects of the naturally derived caffeine on the developed method's caffeine detection.

This technique has been verified as suitable for ultra trace detection of small organic molecules, but for full applicability it needs to also be suitable for large and complex biomolecules. The following model will repeat this verification using erythropoietin and so demonstrate the technique's wide applicability.

Chapter 4: Erythropoietin Model

4.1 GENERAL BACKGROUND

4.1.1 What is Erythropoietin

Erythropoietin, otherwise known as EPO, is a hormone predominately produced by the kidneys (>90%) in response to low blood oxygen levels, released into the blood and carried to the bone marrow. Many other organs produce minor amounts of this hormone with the liver being the predominant alternative source of EPO production [72]. This hormone's primary role is to act as chemical messenger that indicates to the bone marrow that more red blood cells are required. This message starts a process that leads to the genesis of additional red blood cells and a higher oxygen carrying capacity [72, 73]. Erythropoiesis is the process for producing red blood cells. Substances that cause erythropoiesis are known as erythropoiesis stimulating agents (ESAs) [74].

EPO is a glycoprotein that has a protein core of 165 amino acids. EPO has three nitrogen-linked glycans (short carbohydrate chains) at amino acids number 24, 38, 83 and one oxygen-linked glycan chain at amino acid number 126. Various forms of branching within these glycan chains are found[74]. The glycan chains may or may not have a terminal sialic acid group, leading to the isoelectric point (pI) ranging between 3.7 and 4.7 for human EPO[75].

Because of the varying availability of glycosylation enzymes between organisms, each organism producing EPO has different patterns of branching in the glycan chains [76]. For example, while human cells can express sialyl-α 2-6 transferase, bisecting *N*-acetyl glucosamine transferase, and α 1-3/4 fucosyl transferase, Chinese Hamster Ovary (CHO) cells do not [77-79]. There are also subtle differences in branching patterns between cell types within the same organism.[73, 74, 76] These variations in charge or mass between individual molecules (isoforms) lead to characteristic differences in the recognition patterns of the various EPO isoforms, which are used by the current EPO detection methods to distinguish the various forms of EPO [80].

4.1.3 **Forms of recombinant EPO Available and why they are needed**

Patients with end-stage renal failure suffer from an unusual form of anaemia that presents as haemoglobin deficient anaemia but does not respond to iron supplementation. The diseased kidney is unable to produce the amount of EPO needed to signal the production of additional red blood cells. Several recombinant forms of EPO have been developed to fill this therapeutic need [58, 59, 67].

Various recombinant pharmaceutical preparations of EPO are currently available. Different host cells are used to produce these forms. The currently available recombinant Human EPO (rHuEPO) forms have been named using the term 'epoetin' followed by a letter of the Greek alphabet. Some early examples of these were epoetin alpha and beta, which are raised in CHO cells, and epoetin omega raised in baby hamster kidney (BHK) cells[77]. The first generation epoetins that are commercially available in Australia are Eprex (epoetin alpha, Janssen-Cilag Pty Ltd) and NeoRecormon (epoetin beta, Roche Australia Pty Ltd).

First generation epoetins are now out of patent protection, and these forms of rHuEPO, particularly epoetin alpha, have been produced by many companies in the world as generic products[81]. A new epoetin form known as epoetin delta, the first rHuEPO that had been raised in human cells (human ovary cells), appeared on the market about a decade ago but was withdrawn for commercial reasons in 2009 [74, 82].

In addition to these rHuEPO products, two other modified rHuEPO compounds, MINCERA™ and Aranesp™, have been produced. MINCERA™ is epoetin beta with a polyethylene glycol (PEG) group attached to a primary amine on one of either the N-terminals or the amino acid lysine, particularly amino acid number 45 or 52 [83]. The PEG attachment significantly increases the pharmacological half-life of the compound in blood, which means that the frequency of administration that is required is significantly decreased. PEG modification essentially doubles the molecular weight of the ESA to approximately 60 kDa [82].

Aranesp™ also has a similarly long biological half-life but achieves it by a different mechanism. Aranesp™ is epoetin alpha, which has amino acid substitutions in the EPO protein core. These substitutions allow for two extra glycan chains to be attached to the EPO core. The attached glycan chains resist degradation and removal of the enzyme by the kidneys [74]. The extra glycan chains increase the weight of Aranesp™ to 37 kDa.

4.1.4 **The history of athletes' exploitation of rHuEPO**

Athletes who wish to dope commonly exploit new medical developments to get better results than their competitors. RHuEPO was no exception. Athletes in endurance sports quickly realised the benefits of doping with rHuEPO to increase the capacity of their blood to carry oxygen and their endurance in competitions. Although rHuEPO was banned by a number of sporting bodies [76, 84] including the Olympic organisation in 1990 [85], there was no direct analytical test available to monitor rHuEPO doping. It was suspected that the illicit use of rHuEPO in sport became widespread in the late 1980s, soon after it became commercially available. In the late 1990s, a direct test for rHuEPO became available, however this test was unreliable [76]. The suspicion of rHuEPO doping was ultimately confirmed in 1998.

The 1998 Tour de France cycling competition was notorious for doping scandals, and is known as the Festiva affair. It started with the seizure of a significant haul of doping products, including rHuEPO, from a car belonging to a Festiva cycling team official, leading to searches of athlete hotel rooms and team investigations. Several teams, individual athletes and Coca-Cola, a major sponsor, subsequently withdrew from the race [86]. A spate of confessions by current and retired riders to the use of rHuEPO and other banned drugs followed. Officials of the Festiva cycling team, including team doctors, pharmacists and managers were arrested, tried and convicted with charges relating to "aiding and inciting the administration of illegal doping substances" [87] and fines and suspended sentences were handed down [87].

This pivotal event in anti-doping history highlighted the need for a global strategy to fight against doping in sport, and was the impetus for the founding of

the World Anti-Doping Agency (WADA) [85, 88]. The 1998 Tour de France is still the scandalous benchmark against which all sports doping is measured [89].

4.1.5 **The implications of doping for the athlete, sport and country**

Athletes involved in drug, protein or gene doping face long term and wide spread consequences. The athlete's integrity and reputation is enormously damaged when he/she is linked to illegal doping. If a ban is applied, the athlete potentially loses years of competition during the most productive years of his or her career and can fall out of the public eye for many years. This greatly diminishes his/her appeal to sponsors.

When multiple athletes within a sport are caught doping, the negative consequences extend beyond the individual athlete, and the reputation of the sport as a whole can also suffer. EPO and anabolic steroid doping in competitive cycling during the late 1990's threatened the continuation of the world's premier cycling event, the Tour de France. This is reflected in a statement written by a spectator on the pavement during this event: "EPO = mort du tour" (i.e. EPO is the death of the Tour)[86], and on the official Tour website: "Le Tour was rocked" describing the 1998 Tour [90].

In addition, as athletes often represent countries when they perform, the reputation of the nation and other associated athletes can suffer, as evidenced by the systematic doping of East German athletes in the 1970's and 1980's. While this was long suspected, it was only confirmed after the fall of the Berlin Wall [85, 91]. Germany has struggled to regain its sporting reputation in the decades that followed [92].

4.1.6 **Detrimental health effects of doping**

Many substances that are associated with illegal doping, including rHuEPO, impact negatively on the athlete's health; and can continue to plague the athlete many years after their athletic career ends. Former East German athletes involved in the state run doping program in the 1970's and 80's are still suffering the side effects of the abuse of steroids forced upon them [92].

The un-regulated use of rHuEPO can cause antibody-induced red blood cell aplasia (PRCA), which is an immune response to the artificial EPO [74, 93]. While rare, this condition is very debilitating, and expert handling and administration is need to minimise its occurrence [93]. Other grave and more common secondary effects of self-administered rHuEPO also exist.

EPO stimulates the production of red blood cells. This leads to increased blood viscosity[94], which can cause many cardiovascular problems including hypertension, strokes and heart attack. Patients undertaking rHuEPO therapy must have their blood pressure carefully monitored as the treatment with rHuEPO can lead to an increase in blood pressure, and the safe level of rHuEPO in therapy varies between patients [73, 94].

The misuse of rHuEPO has led to the sudden death of athletes in competition and training. Soon after rHuEPO became available in Europe, more than a dozen Dutch and Belgian cyclists died of sudden heart attacks at rest. This is thought to have been caused by doping with rHuEPO, although no test was available at the time to confirm this [91, 95].

4.2 CURRENTLY USED OR PROPOSED TECHNIQUES FOR DETECTION OF DOPING WITH rHuEPO

4.2.1 Double Blotting

The use of EPO by athletes was banned by the International Olympic Committee in 1990[76, 84]. However, it was 10 years later that the first analytical technique to detect EPO in athlete's urine was available. Prior to this, only indirect methods were available to suggest the possibility of EPO abuse. The indirect tests only indicated whether an athlete's haemoglobin level was higher than was normal. These tests were unable confirm actual doping, as the normal haemoglobin range can vary significantly [91].

In June, 2000 in a Brief Communication in *Nature*, the research group led by Françoise Lasne at the French National Anti-Doping Laboratory announced a direct detection technique for EPO in athlete's urine [76]. This involved a modification of the common isoelectric focusing (IEF) technique with a blotting

technique used in biochemistry, i.e. a western blot, where a second blot was taken of the original blot and the new method was called the double blotting technique [96].

Other modifications were later applied to improve this technique. This technique, with its modifications, constitute the basis of the current World Anti-Doping Association (WADA) approved analytical protocol for EPO detection (WADA Technical Document TD2013EPO) [80].

A gel electrophoresis method that uses sodium dodecyl sulphate polyacrylamide electrophoresis (SDS-PAGE) has also been developed and approved by the WADA protocol [80]. However multiple criticisms of these techniques have been raised.

4.2.2 **Criticisms of the current method**

The first criticism involves the antibody used to detect EPO. Several research groups have reported that the antibody (AE7A5, from R&D Systems), which is considered the critical reagent in this technique[80], is not specific to EPO [97-101]. Several other peptide hormones of similar profile (both in weight and pI) to EPO and found in human urine, cross react with AE7A5 [98]. This is important because the two techniques approved rely on these two characteristics. IEF relies on the differences in pI between molecules; and SDS-PAGE relies on the differences in weight [80].

Another criticism of the current technique is that the profile of EPO in urine can vary immediately after intense exercise. These changes may involve the identification of endogenous human EPO as rHuEPO [102].

The serum profile of endogenous EPO is similar to that of epoetin β, and the more basic isoforms of EPO that are not normally passed into the urine can be identified after exercise, as can other proteins (proteinuria) [97]. The main defence against this and the previous criticism is that experienced anti-doping scientists should be able to tell the difference between endogenous and recombinant EPO, even with these exercise induced EPO profiles [103-105].

Reproducibility between anti-doping laboratories was also criticised in the literature [106]. It has been argued that the same standards should be applied in anti-doping laboratories that are used in clinical laboratories, and that improvements can and should be made [107]. These topics are hotly debated, however, with the laboratories conducting these tests arguing adamantly that their tests are reliable [103-105], even with evidence to the contrary.

The limit of detection in the currently sanctioned test is also relatively high, which requires a large quantity of urine, 20 mL [84]. The sample must then be concentrated at least 200 times to make the EPO detection possible, which is both time and labour intensive [84]. In addition to narrowing the window of opportunity to detect doping, the above problems increase the potential of false negatives and false positives. False negative tests could result from careful planning of doping regimes by athletes so that the level of EPO in their urine is below the limit of detection on the day of competition, while still gaining benefit from increased red blood cell concentration and corresponding oxygen capacity [106, 108]. False positive results are minimised by careful and experienced analysts.

Other issues with the current technique include the difficulty to establish the presence of recombinant EPO when there is a low concentration of EPO in the urine and/or a combination of both endogenous and recombinant EPO are present [109]. Also, the cost and time required for the current testing regime severely limits its suitability for out of competition testing (the best way to catch and discourage athletes doping) [106].

Between batch variations have been reported for epoetins alpha and beta [110]. In addition, many different biosimilar EPO preparations have been made around the world, particularly forms of epoetin alpha [81]. The difference between batches of the same epoetin and between different epoetins is attributed in part to the cell lines used for the recombinant protein production, culture conditions and purification regimes [81, 109, 110]. These differences may cause the isoelectric point (pI) of endogenous EPO and rHuEPO to overlap, which potentially hampers the detection of rHuEPO by methods that rely on the pI

measurement. The difficulties in using the current technique to detect erythropoiesis stimulating agents (ESAs) and its limited ability to detect low levels of the analytes have spurred interest in developing new techniques for this purpose.

4.2.3 **Membrane-Assisted Isoform Immunoassay for EPO detection**

Recently, a new technique for the detection of EPO, Membrane -Assisted Isoform Immunoassay (MAIIA) was proposed [111]. In this technique the protein isoforms are first separated using lectin affinity chromatography [112]. The EPO isoforms are captured using an antibody specific to the protein and detected with a complimentary antibody that is attached to carbon black[113] The process uses a Lab-on-a-chip device and is read using a flatbed scanner[113]. This technique reportedly requires small volumes of urine samples, increases the ability to detect rHuEPO in the presence of endogenous EPO, lacks technical difficulty and uses relatively inexpensive equipment [111, 113-115].

However, a group of Australian researchers recently tested the MAIIA technique and reported reliability and sensitivity issues. These problems included the lack of reproducibility between repeated tests and the increased potential for human error due to the multistage nature of the technique [114].

When the MAIIA technique was evaluated again with an improved test kit, the researchers concluded that the MAIIA technique had the potential to detect EPO micro-dosing for at least 12 hours longer than the currently approved method can [116]. The disadvantages of the MAIIA technique include the difficult modification of the technique for on-site analysis and the requirement for laboratory testing.

Other improvements to the analysis of EPO include an EPO immunoaffinity column [117], which is used for EPO purification prior to the MAIIA analysis, and is also a useful and recommended pre-analysis step for the currently used technique [80]. The antibody used for this immunoaffinity separation (Anti-hEPO antibody 3F6) has been shown to be ideal for applications requiring high

association rates and low disassociation rates, and reacts with very low levels of EPO [115].

4.2.4 **Other proposed techniques for EPO and hormone detection**

Various techniques based in chromatography with mass spectrometry (MS) have been attempted for EPO analysis. Many of the chromatography-based methods have been unsuccessful for human doping purposes [118, 119]. However, when rHuEPO is used to dope horses there is sufficient difference between horse EPO and human EPO for this to be detected by chromatographic methods [119]. Guan et al. successfully used GC-MS for the detection of rHuEPO doping in racehorses [120-123]. However the reported methods were not sufficiently sensitive for the detection of extremely low concentrations of the glycoproteins in biological fluids [119].

Another technique, based on the distinctions of reactions between lectins and glycoprotein modifications of peptide hormones, has been proposed by Ukei *et al* [124, 125]. The technique is based on a lectin microarray.

The microarray includes three lectins that recognise sialyl alpha 2-6 linked galactose/ galactosamine moieties on the glycans. In this method, the lectins react only with endogenous EPO. rHuEPO does not contain these moieties as the cell line (CHO) used to raise rHuEPO lacks the enzymes required to express these linkages [77-79]. Therefore, it is possible to distinguish between endogenous and recombinant EPO. This technique is more sensitive than mass spectrometry based systems [125].

4.3 AIMS OF THIS EPO MODEL

The aims of this model for EPO detection by functionalized gold nanoparticles and SERS are twofold. The first is to develop a proof of concept for a new rapid, robust, easy and portable screening technique to detect ultra-trace amounts of EPO for anti-doping, forensic and bio-medical applications.

The second aim of this model is to demonstrate the applicability of the SERS-based method for high molecular weight complex biomolecules as well as

low molecular weight small molecules such as caffeine. This is intended to present the method to the diverse field of analytical and bioanalytical chemistry.

4.4 NANOPARTICLE CHARACTERISATION

The nanoparticles were characterised as described in section 2.4 of the materials and methods chapter (chapter 2). Briefly, they were analysed visually, then with UV-VIS spectroscopy, then further characterised using TEM.

4.4.1 **Visual Inspection**

The colour changes of the gold nanoparticles upon the immobilization of the anti-EPO antibodies and the ethylamine blocker were similar to those observed upon the development of the caffeine antibody-coated gold nanoparticles. The purple red colour of the silica-coated gold nanoparticles changed to bluish grey upon the addition of the glutaraldehyde linker and black with the anti-EPO antibody [Fig. 4.4.1].

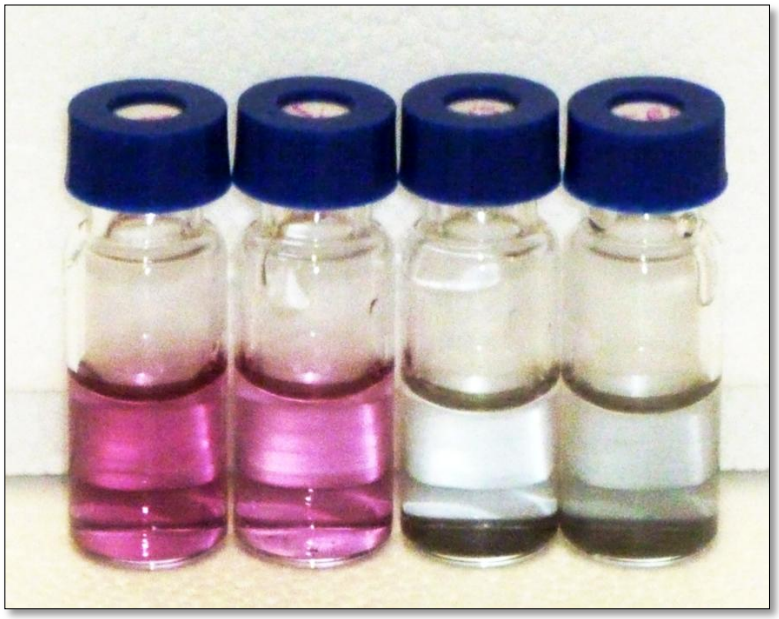

Figure 4.4.1 Photograph of (L-R) Bare Gold nanoparticles, Silica coated nanoparticles, Nanoparticles with Glutaraldehyde linker, and completed nanoparticle with EPO antibody attached and blocked.

4.4.2 **UV-Vis Characterisation**

UV-Vis spectroscopy of the nanoparticles showed that both the bare and silica-coated nanoparticles have the same absorption band at 525 nm. This is consistent with the preservation of colour between the two. The silica coated nanoparticles have a marginally wider peak width however. [See Fig. 4.4.2].

Both the glutaraldehyde linked nanoparticles and the completed nanoparticles with antibody and blocking show no visible peak. This is probably because there is a wide variation in size between nanoparticle clusters as was found in the caffeine model, and the nanoparticle clusters' light scattering. This result indicates the successful immobilization of the anti-EPO antibody onto the gold nanoparticles.

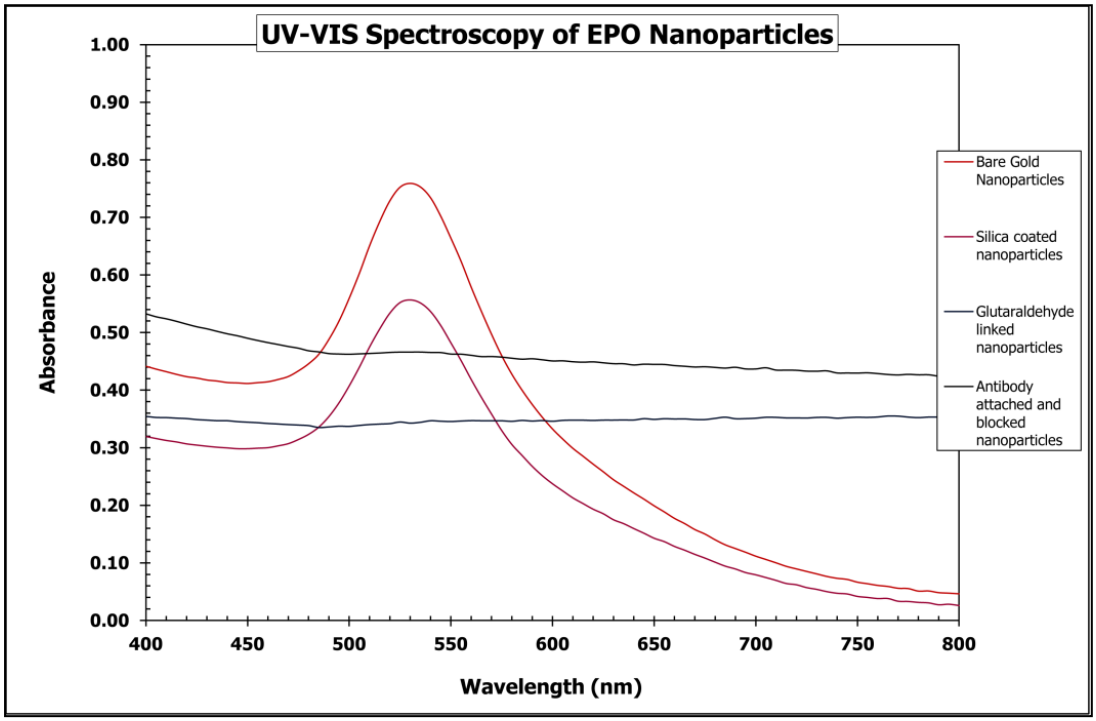

Figure 4.4.2 UV-Vis spectra of the bare gold nanoparticles, silica-coated nanoparticles, nanoparticles with glutaraldehyde linker attached and the completed nanoparticles with the EPO antibody (MAIIA, 3F6) and blocking

4.4.3 **TEM Characterisation**

Bare gold nanoparticles

The average bare gold nanoparticle was largely quasi-spherical (81%) with a further 8% appearing to be elongated spherical nanoparticles, as if they had joined early in the manufacture. [Note: The red boxed nanoparticle in the TEM of

silica coated nanoparticles (fig 4.4.6] appears to show this joining.] TEM photographs of the bare gold nanoparticles are shown in figure 4.4.3, and the corresponding graph analysing 140 of these nanoparticles in figure 4.4.4.

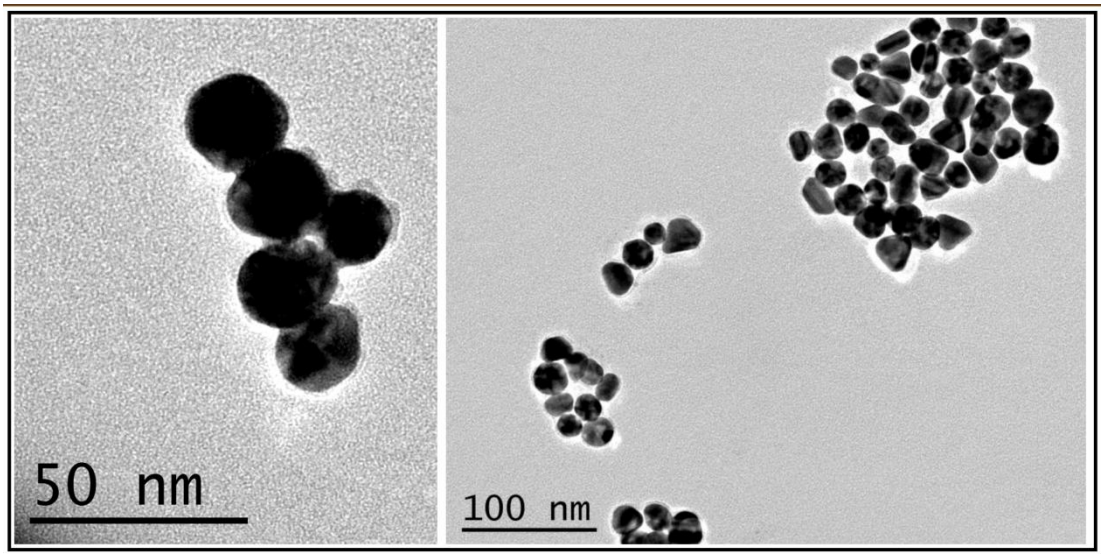

Figure 4.4.3 TEM of Bare gold Nanoparticles

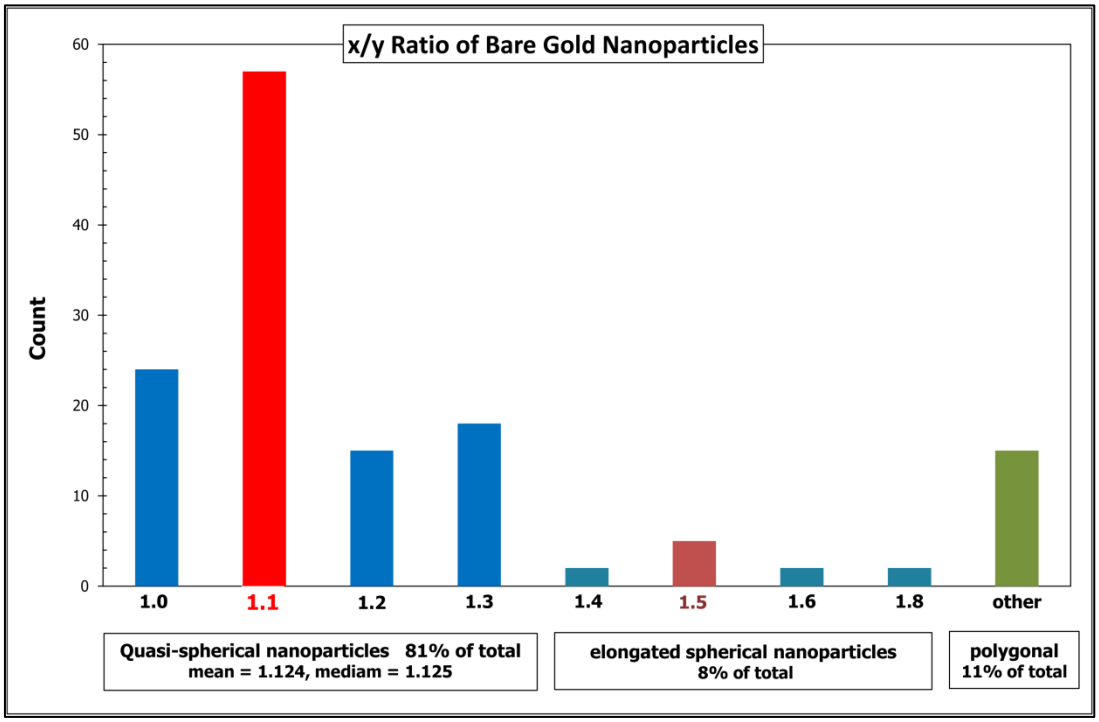

Figure 4.4.4 Determination of the sphericality of the nanoparticles. The nanoparticles are largely spherical or quasi-spherical (81%).

The nanoparticle diagonal sizes (mean and median) were 22.80 nm and 22.85 nm respectively, with a standard deviation (SD) of 3.2 nm [fig 4.4.5]. The size of the nanoparticles was calculated using the average of two dimensions for

spherical or elongated nanoparticles. For any polynomial nanoparticles the average was calculated using sum of Apex to middle of opposite side for all apexes, divided by the number of sides.

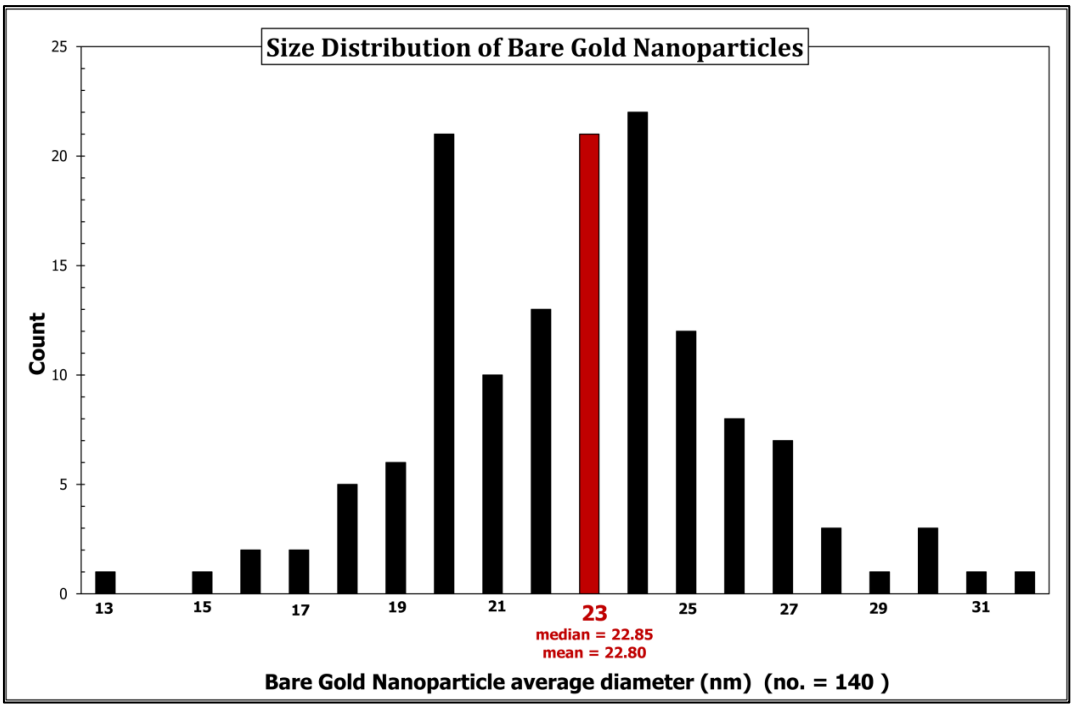

Figure 4.4.5 Distribution of the average diameter of the bare Gold nanoparticles

The majority of the peaks (89%) were sized between 18 and 27 nm which is +/-1.5 SD of the mean, with 74 % of total nanoparticles within 1 SD of the mean (19.6 - 26 nm). So the size distribution of the bare Gold nanoparticles is 22.8 +/- 3.2 nm using 1 SD as the error.

Silica Coated Nanoparticles

The TEM photos indicated that the thickness of the silica coating on the silica-coated nanoparticles was from 0.65 nm to 2.94 nm with the majority of the nanoparticles having a silica coating thickness of approximately 1.3 nm [fig. 4.4.6].

Tian *et al* have reported that the Raman spectrum is enhanced by a thin coating of silica on a gold nanoparticles [126]. The authors attributed their finding to the enhancement the nanoparticles electric field by the thin silica coating and the development of hotspots. The silica coat is a physical barrier

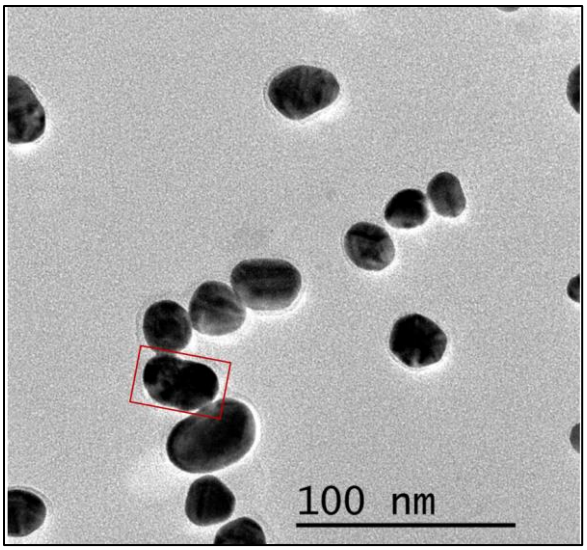

Figure 4.4.6 TEM of silica coated nanoparticles

preventing the 'dilution' of the LSPR by the movement of electrons between nanoparticles. The resulting two separated LSPR regions form a hotspot. Tian *et al* indicated that a silica coating of approximately 1 nm, leads to double the SERS enhancement that can be developed by un-coated (bare) gold nanoparticles. A similar effect was indicated by Liu *et al* for carbon coated silver nanoparticles [126-128]. The authors found that 0.5 nm coated nanoparticles had enhancement more than four times that of the bare nanoparticles. Therefore it is expected that the silica coating of the EPO antibody-functionalized gold nanoparticles to contribute positively to the SERS screening by the developed nanoparticles due to its ability to increase the SERS enhancement of the nanoparticles.

Addition of glutaraldehyde linker to the silica-coated nanoparticles

When glutaraldehyde was added to the APTMS primed silica-coated nanoparticles the formation of aggregates was noticed and lead to some nanoparticle clusters. Figure 4.4.7 shows a typical TEM of nanoparticles clusters. The clustering of the nanoparticles is attributed to the uncontrolled cross linking of some nanoparticles via the glutaraldehyde linker as the linker has two active aldehyde terminals that can interact with the silica coating of separate nanoparticles. This involves the reaction between glutaraldehyde and the terminal amine groups of the APTMS primed silica shell [38].

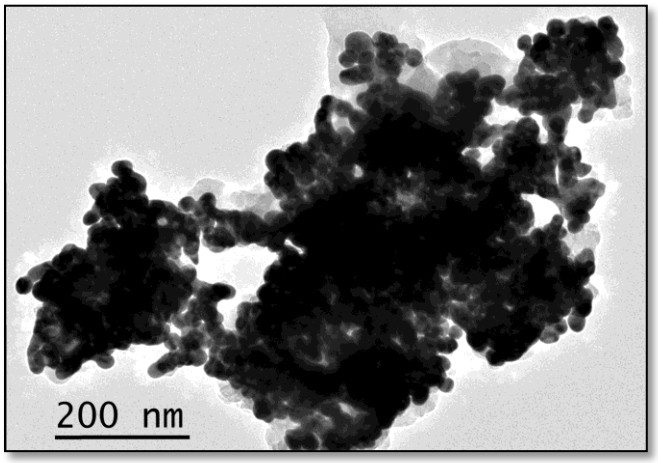

Figure 4.4.7 TEM of nanoparticles with linker

Immobilization of the EPO antibody onto the nanoparticles

The immobilization of the 3F6 EPO antibody onto the gold nanoparticles occurs by the formation of a linkage between an aldehyde moiety of the glutaraldehyde linker and any of the amine groups on the antibody molecule. As in the case of the addition of the glutaraldehyde linker to the gold nanoparticles colloid, some aggregation was also noticed upon the addition of the antibody to the nanoparticles colloid (figure 4.4.8). This can be attributed to the bridging between the nanoparticles through the glutaraldehyde and antibody bridges.

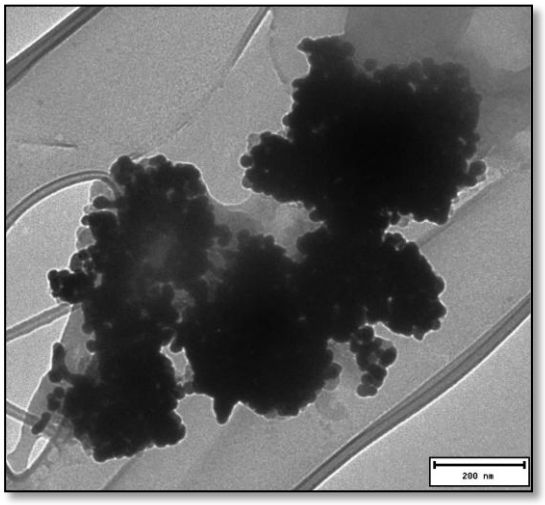

Figure 4.4.8 TEM of aggregates formed during the addition of the EPO antibody to the of the gold nanoparticles colloid

Figure 4.4.9 shows a schematic diagram of the proposed cross linking between the antibody-functionalized nanoparticles to form aggregates. While the aggregation of nanoparticles may be of value to surface enhanced Raman spectroscopy as it favours the formation of hot spots that cause significant signal enhancement, the use of a more controlled linker molecule other than glutaraldehyde would lead to a greater reproducibility of our proposed technique. A suitable linker that can be used to immobilize the antibody, while avoiding the uncontrolled aggregation of some of the nanoparticles, would be asymmetric molecule that link to the nanoparticles via one terminal group and binds to the antibody via a different terminal group.

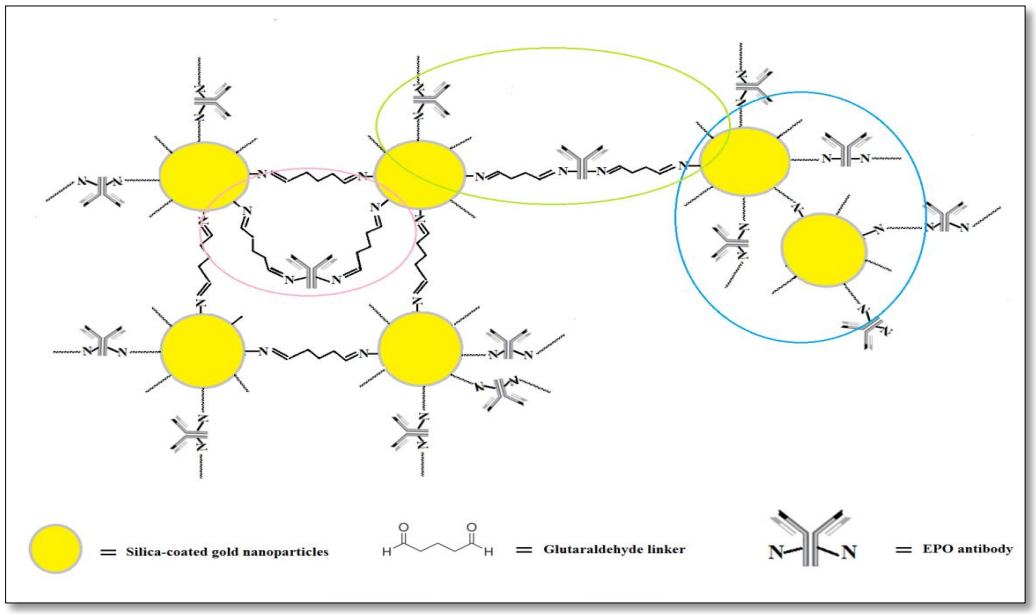

Figure 4.4.9 Schematic diagram of cross linking between gold nanoparticles via the glutaraldehyde and antibody bridges

For example, cysteamine is able to adhere to gold surface via its -SH moiety to form a thiol linkage. The other terminal of the cysteamine molecule is a primary amine group that can form a strong amide linkage with the carboxyl groups on the antibody. Therefore the cysteamine can be used to immobilize the antibody without inducing uncontrolled aggregation of the nanoparticles through the linker bridge.

The only possibility for cross linking between the nanoparticles, will be through the antibody as it has many carboxyl groups that can bind to cysteamine linker moieties on separate gold nanoparticles. The aggregation of the

nanoparticles will be more controlled in this case and may lead to the favoured hotspots without the formation of oversized clusters. Hotspots would only form if the gold nanoparticles were sufficiently close together.

Confirmation of nanoparticles clusters structure

To confirm the structure of the functionalized nanoparticles clusters, 3 aliquots of the functionalized nanoparticles colloid were boiled with deionised water, 1 M HCl and concentrated HCl (32%) respectively, for one hour. When the nanoparticles colloid was boiled in water no change in colour was observed. However the colloids that were boiled with the dilute and concentrated HCl showed a brownish colour which when viewed obliquely showed a reddish tint. The change in colour was rapid when the colloidal nanoparticles were boiled with the concentrated acid and occurred in few minutes but much slower with the dilute acid (Fig 4.4.10).

Figure 4.4.10. Functionalized colloidal nanoparticles after digestion for one hour in left) 1 M HCl, middle) deionised water and right) 32% HCl

4.5 INTERACTION BETWEEN THE ANTIBODY-FUNCTIONALIZED NANOPARTICLES AND HUEPO

In order to investigate the interaction between HUEPO and the EPO antibody-functionalized nanoparticles, the nanoparticles were reacted for 30 minutes with 10^{-8} M HUEPO standard solution and screened by SERS [fig. 4.5.1]. The SERS spectra of the un-reacted functionalized nanoparticles were also collected as the reference background. The spectra were visually inspected. This was carried out to identify the Raman spectral lines of the functionalized nanoparticles background and any new Raman bands that were developed due to the binding between HUEPO and the functionalized nanoparticles.

The EPO molecule is a large and complicated one. No spectral assignment has been attempted because the non-uniform orientation of the antibodies and the multiple isoforms lead to significant variability and difficulty in assignment of any spectral features. Rather only the differences to the unreacted nanoparticles spectra were noted.

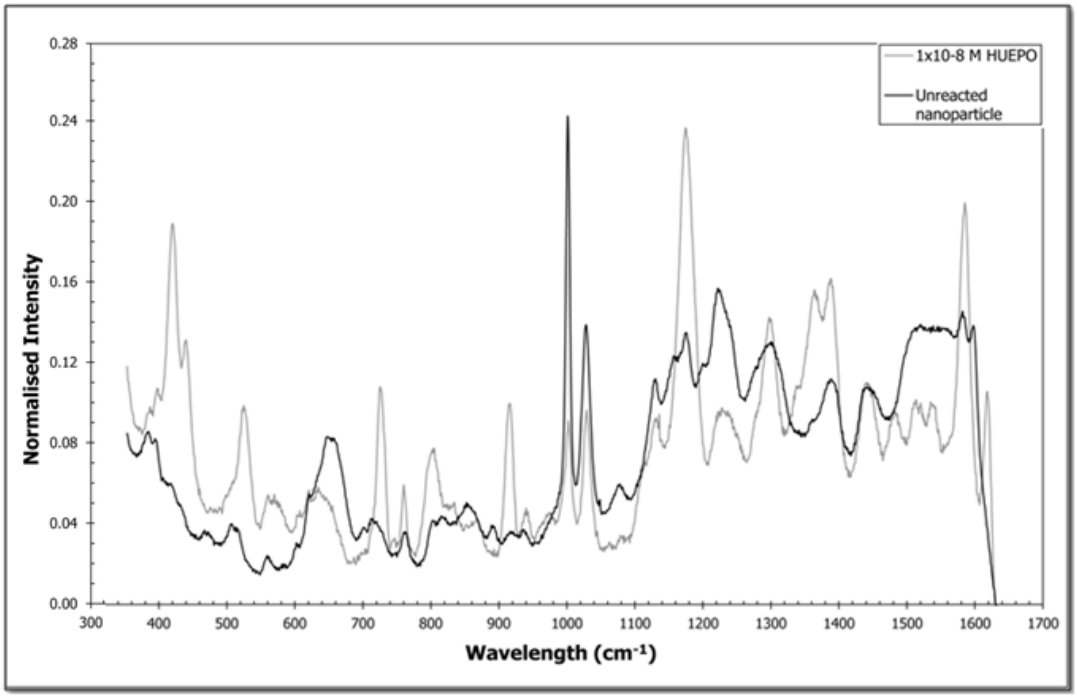

Figure 4.5.1 SERS spectra of un-reacted antibody-functionalized gold nanoparticles and antibody-functionalized nanoparticles reacted with 10^{-8} M HUEPO

After processing, the Raman bands at 422, 440, 916, 1176, and 1621 cm^{-1} were shown to be a result of the interaction between the HUEPO analyte and the

antibody-functionalized nanoparticles. Peaks at 525, 725, 802, 1365, 1385, 1515, 1538, 1585 cm^{-1} were also related to HUEPO but less prominent [Fig 4.5.1]. The prominent bands of the un-reacted nanoparticle were found at 660, 1000, 1030, 1045, 1224, 1514 and 1599 cm^{-1} [fig. 4.5.1].

PCA confirmed that there is a statistical difference between the SERS spectra of the unreacted nanoparticles and those reacted with HUEPO. The PCA model (Fig. 4.5.2) indicated that there is a clear separation of the two groups with both groups fitting comfortably within the model and no outliers from either group. This result confirms that proposed SERS screening by the EPO antibody-functionalized gold nanoparticles is able detect ultra-trace amounts of EPO in solutions.

Figure 4.5.2 also shows that the unreacted nanoparticles are tightly clustered, whereas the nanoparticles reacted with HUEPO are far less tightly clustered i.e. the spectra of the unreacted nanoparticles are more reproducible

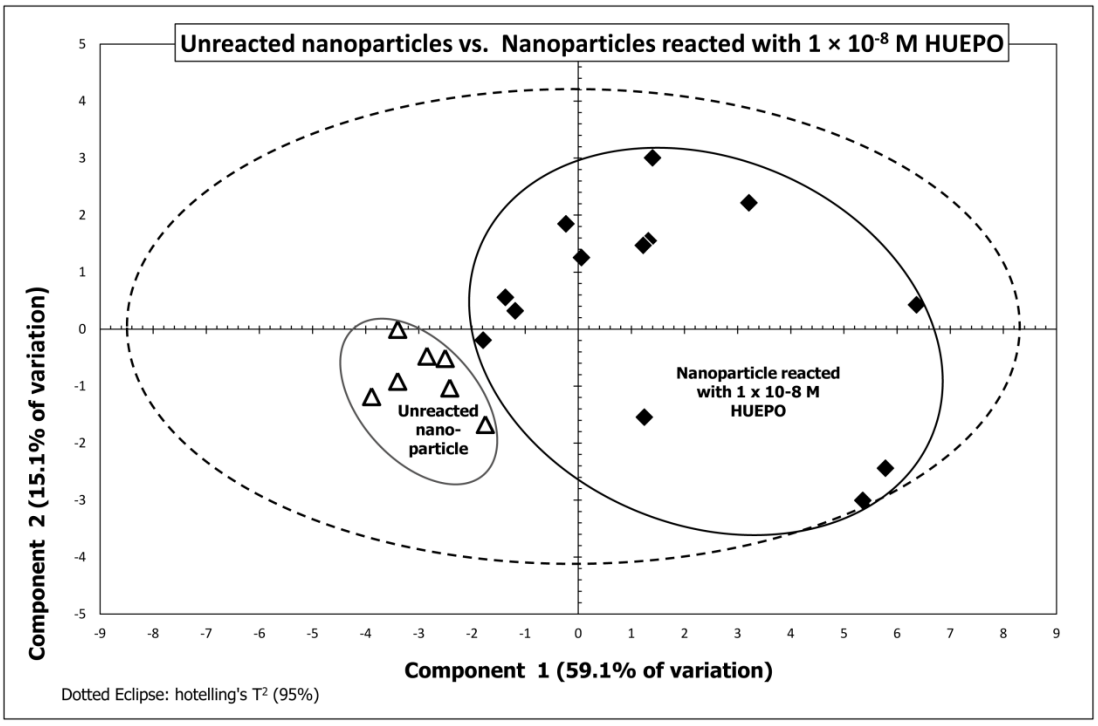

Figure 4.5.2 Distinction between unreacted nanoparticles and nanoparticles reacted with 1×10^{-8} M HUEPO.

than those of the reacted nanoparticles. This is not unexpected as the spectrum of the reacted nanoparticles would vary according to the orientation and location

of the antibodies in relation to the hotspots and which antibodies the HUEPO reacts with.

4.6 EFFECT OF TIME ON THE BINDING BETWEEN 10^{-8} M HUEPO AND ANTIBODY-FUNCTIONALIZED GOLD NANOPARTICLES

This study was performed to determine the optimal reaction time that gives maximum binding of the EPO analyte with its antibody-functionalized nanoparticle. A 10^{-8} M standard solution of EPO was mixed with its functionalized nanoparticle for a series of increasing times between 0 and 600 minutes before screening by SERS. The spectra were superimposed and the major peaks were visually inspected to determine when no significant change in peak heights with

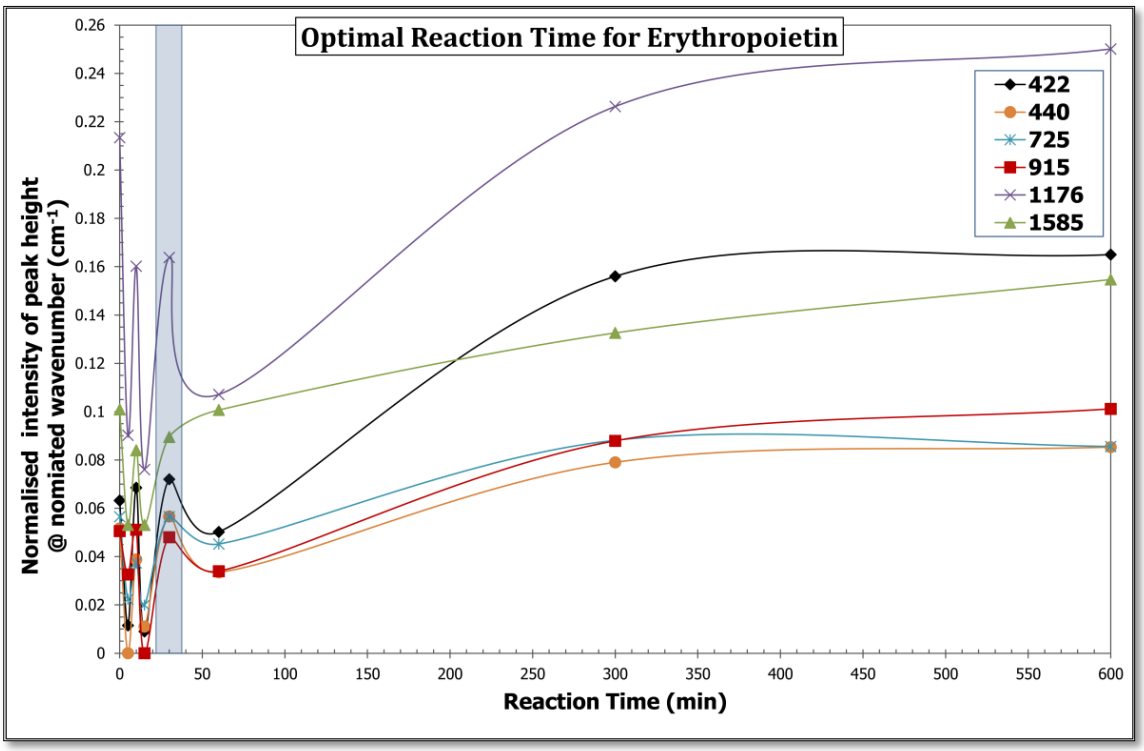

Figure 4.6.1 Determination of optimal reaction time between 1 x 10^{-8} M HuEPO standard and antibody-functionalized gold nanoparticles. The normalised peak intensities of various Raman bands (indicated by the inset) are plotted against the reaction time.

increasing time was observed. (This is shown in Figure 4.6.1 with Reaction time plotted against Peak height.) This was observed after 30 minutes of interaction between the analyte and the functionalized nanoparticles. Therefore the optimal reaction time was determined to be 30 minutes.

NOTE: The immobilized antibody was anti-EPO antibody 3F6 from MAIIA. This antibody was demonstrated by the manufacturers to have a very rapid reaction with its EPO analyte [115]. This allowed the peak found at 0 min in figure 4.6.1.

4.7 DILUTION SERIES USING STANDARD SOLUTIONS

This study was performed to develop a calibration curve of the analyte. After careful inspection of the qualitative data, the bands at 422 cm^{-1} and 440 cm^{-1} were found to fulfil the criteria outlined (RSQ ≥ 70%). PLS of these two points was also attempted to determine whether it would yield a better result than univariate regression. The PLS R^2 values were worse than the RSQ values for the nominated peaks. Figure 4.7.1 shows the log linear relationship between the peak intensity at 422 cm^{-1} and the EPO concentration (on a log scale) in the range $2x10^{-10}$M to (LLOQ) $3.5x10^{-13}$ M using the inflection point. If 3*SD of

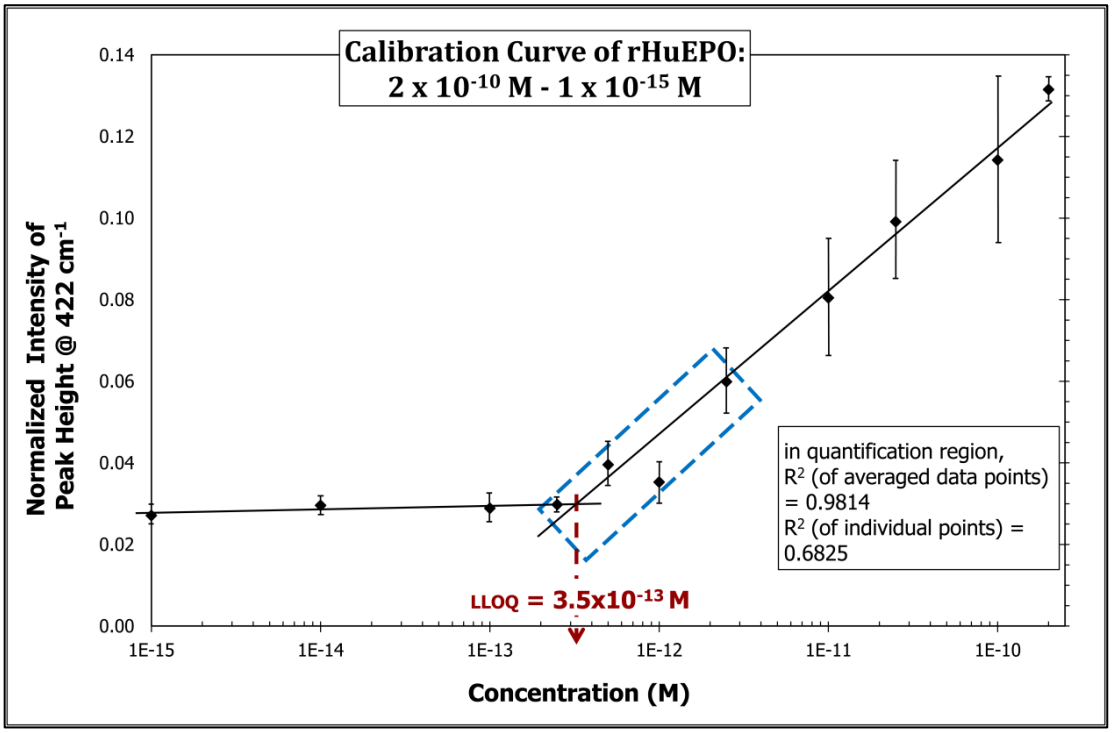

Figure 4.7.1 Log_{10} calibration curve using area-normalised peak intensity at 422 cm^{-1} of EPO solutions in the range 2 x 10^{-10} M to Lower Limit of Quantification (LLOQ) = $3.5x10^{-13}$ M.

background is used as the LLOQ this gives a LLOQ of $1.3x10^{-13}$ M (using the equation of the quantification region).

Taking the larger of these two measurements we determine the LLOQ to be $3.5x10^{-13}$ M.

The lowest concentration measured was 10^{-15} M (Fig. 4.7.1) at intensity of 0.0271, while the average nanoparticle background is 0.0092. A robust definition for the limit of detection is:

$$LLOD = mean_{(background)} + 1.654*SD_{(background)} + 1.654*SD_{(low\ concentration\ sample)} [129]$$

If 1×10^{-15} M is used as the low concentration sample, LLOD is 0.0243, (7.4×10^{-19} M i.e. ~16 molecules of EPO) using the equation of the curve after the inflection point. While this is not unobtainable with parameters maximised, (i.e. the thin pacification layer, significant clustering of the nanoparticles, optimal orientation of the antibody and multiple hotspots within the sampled area), we conservatively nominate the lowest concentration measured (1×10^{-15} M) as the LLOD.

The average EPO concentration in human serum is 2.5×10^{-12} M and 2.5×10^{-13} M in urine respectively. These concentrations were within the linear range of

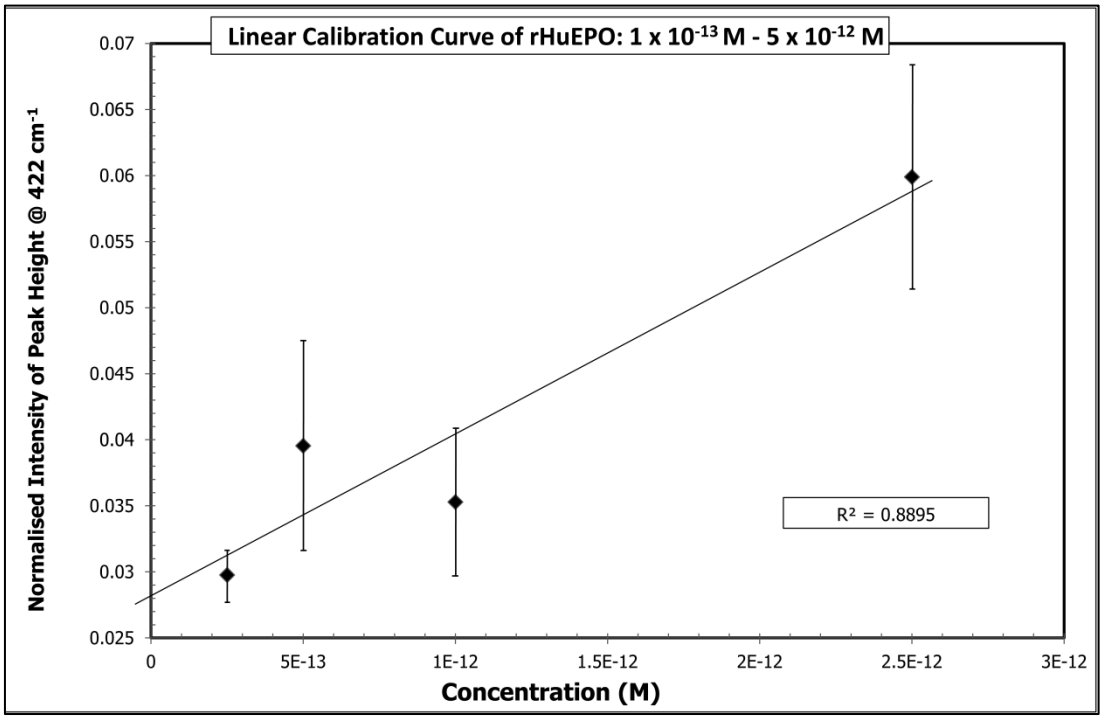

Figure 4.7.2 Linear calibration range $2.5X10^{-12}$M to 2.5×10^{-13}M (on log scale), corresponding to blue dotted box in fig 4.7.1

the calibration curve shown in figures 4.7.2, (Corresponding to blue dotted box in 4.7.1). This indicated the applicability of the developed method for the detection of EPO in biological samples of ultra trace concentration levels below.

4.8 CROSS REACTIVITY OF THE EPO ANTIBODY-FUNCTIONALIZED NANOPARTICLES WITH PROTEIN MATRIX

This study was carried to determine whether the EPO antibody-functionalized gold nanoparticles interact non-selectively with other proteins that may co-exist in a complex matrix such as biological fluids. Non selective interaction with proteins other than EPO would typically lead false positives. Therefore it was necessary to investigate the cross reactivity of the antibody-functionalized gold nanoparticles despite the fact that the immobilized 3F6 anti EPO antibody is certified by, MAIIA diagnostics, to be of very high selectivity towards EPO [76].

For this study, the EPO antibody-functionalized gold nanoparticles were mixed with skim milk. The skim milk matrix consists of a variety of proteins that would react with the EPO antibody only if the antibody has cross reactivity towards these proteins. In addition the skim milk proteins contain primary amines that would react with any un-blocked aldehyde group of the glutaraldehyde linker. It worth reminding that, the antibody-functionalized nanoparticles are always reacted with ethylamine upon their development. This is carried out as described in chapter 2 "materials and methods" to block any residual un-reacted aldehyde group of the glutaraldehyde linker after the immobilization of the antibodies.

SERS spectra (12 measurements per sample) were obtained from the blocked antibody-functionalized gold nanoparticles after their reaction with milk sample and from un-reacted nanoparticles. The spectra were compared for any variations that would indicate cross reactivity with the 3F6 antibody and/or binding to the glutaraldehyde linker. The spectra (Fig 4.8.1) showed no major variation between the unreacted and the reacted antibody- functionalized gold nanoparticles. One spectrum for each group had a noticeably different

background, see figure 4.8.1). The peak positions for the outlier spectrum coincided with the other spectra, however. So, this result indicated that there was most likely no cross reaction between the skim milk proteins and the 3F6 antibody.

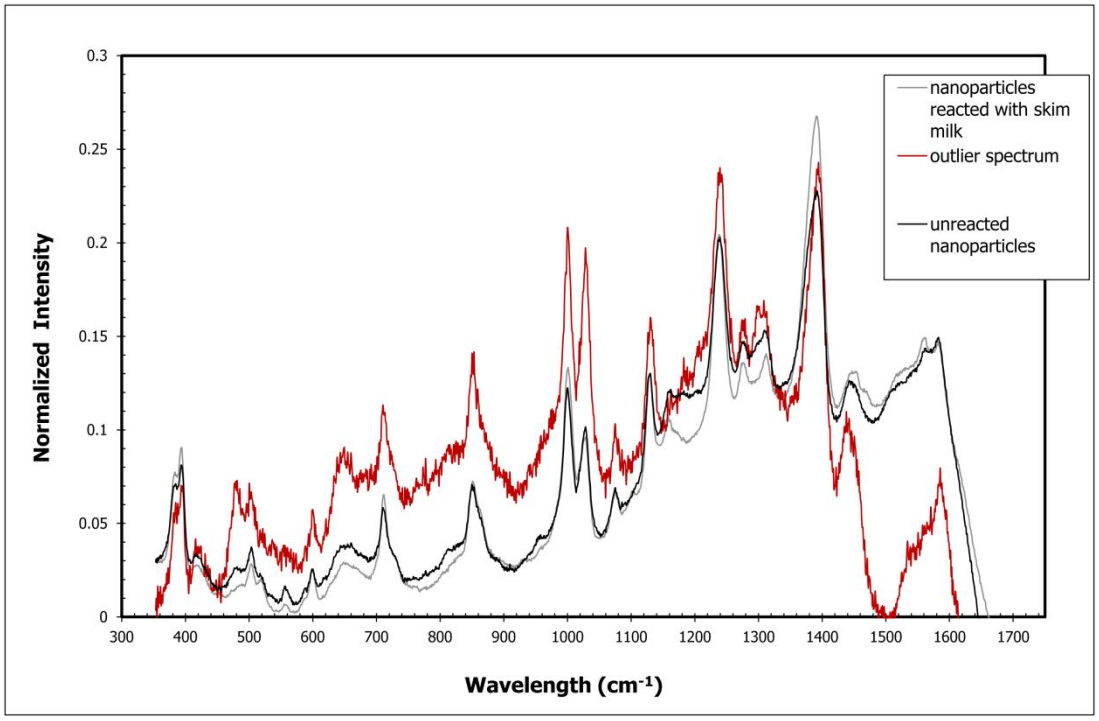

Figure 4.8.1 SERS spectra of the blocked EPO antibody-functionalized nanoparticles (un-reacted with skim milk), the nanoparticles after reaction with skim milk and a representative outlier spectrum. Close correspondence of major peaks heights and positions is noticed.

For further substantiation, HPCA was performed using the entire spectral data from repeated SERS measurements of the un-reacted and reacted nanoparticles. The developed HPCA model (Fig 4.8.2) confirmed that the spectral data from both the unreacted and reacted nanoparticles were very closely clustered with only two outliers. The two outliers in the HPCA model correspond to the outlier spectra, (fig 4.8.1). The difference in background baseline contributed in part to the non-clustering of these samples with the rest of the spectra despite the fact that there were no noticeable differences in the peak positions of the two samples, however they are similar to each other. Therefore, it is confirmed that there were no unblocked linkers available to cross react with the milk proteins. This result gave confidence that the developed EPO antibody-functionalized gold nanoparticles can be used for the selective detection of EPO in biological samples such as urine.

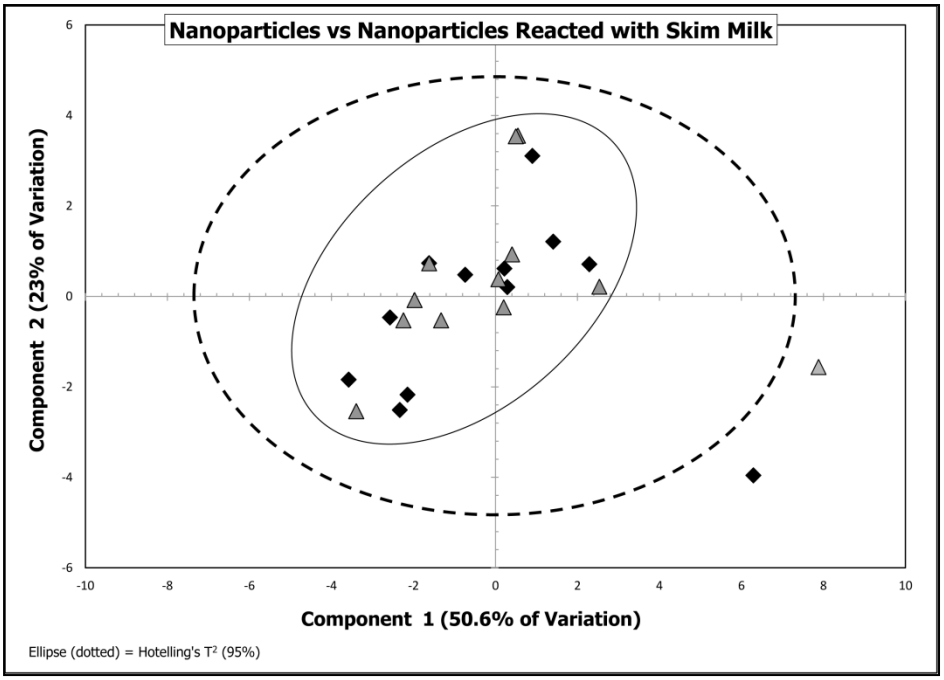

Figure 4.8.2 Hierarchical PCA (HPCA) of Raman spectra (354 -1627 cm^{-1}). Black diamonds are un-reacted nanoparticles; grey triangles are nanoparticles reacted with skim milk.

4.9 APPLICATION OF THE DEVELOPED METHOD TO THE DETECTION OF EPO IN BIOLOGICAL SAMPLES

4.9.1 **Can the nanoparticle separate EPO from urine?**

To investigate the use of functionalized nanoparticles for the detection of EPO in a urine matrix, the functionalized nanoparticles were reacted with a self-donated (from a person not receiving EPO treatment) urine sample. Another aliquot of the functionalized nanoparticles was reacted with a 1×10^{-9} M HUEPO IS solution in PBS buffer (pH 7.4). The spectral data in figure 4.9.1 showed that the major peaks indicative of the EPO binding to the functionalized nanoparticles also existed in the SERS spectrum of the tested urine sample. The close wavenumber correspondence between the HUEPO spectrum and the urine spectrum clearly indicate that the EPO antibody-functionalized nanoparticles were able to detect the natural EPO that is excreted in human urine.

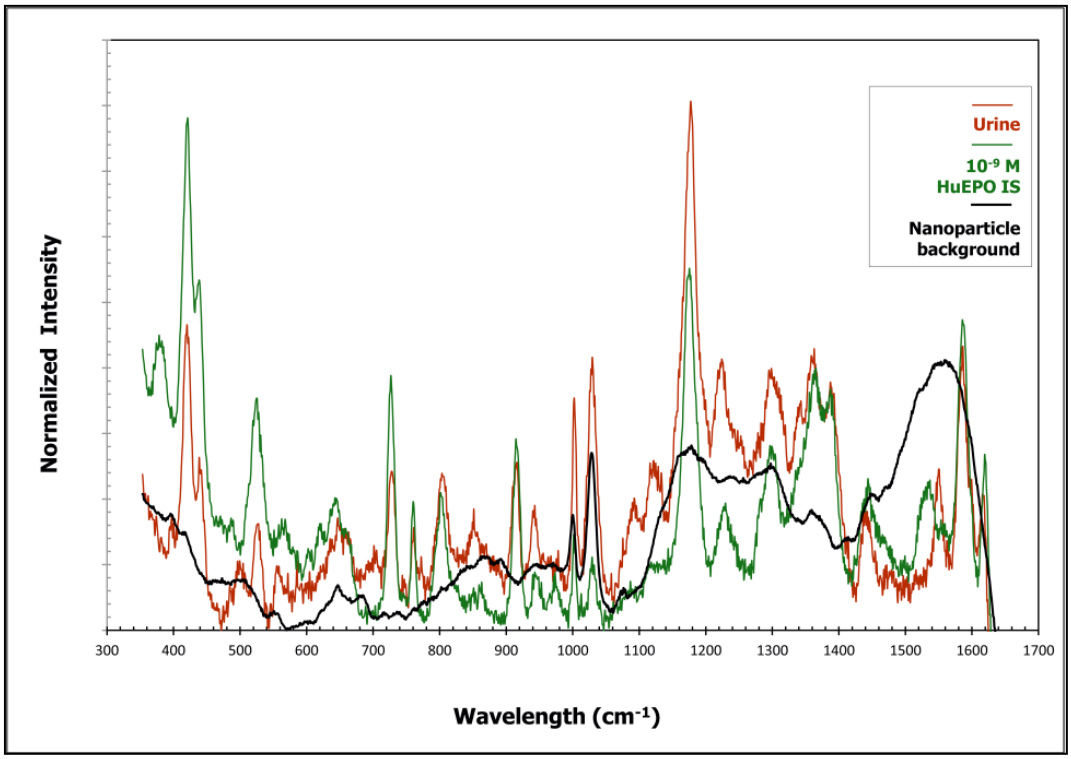

Figure 4.9.1 Comparison between a spectrum of 1 x 10^{-9} M HUEPO and a spectrum of human urine (from a donor not receiving EPO treatment). The major peaks indicative of the EPO binding to the blocked antibody-functionalized gold nanoparticles are found at 422, 440, 525, 725, 760, 800, 915, 1176, 1585 and 1620 cm^{-1}

4.9.2 **Using standard solutions**

This interference study was an initial test to determine whether endogenous and recombinant EPO could be distinguished. It was performed using the 2nd international reference standard for HUEPO and the 3rd international reference standard for rHuEPO both at the concentration of 1 x 10^{-13} M. The SERS spectra are shown in figure 4.9.2.

The spectra were found to be very similar to each other and indicated the successful binding between the EPO standards and the functionalized nanoparticles. However, there is some minor variation between the HUEPO IS and the rHuEPO IS at approximately 1540 cm^{-1}. See Fig. 4.9.2 below.

The consistency between the HUEPO and rHuEPO spectrum is not surprising. HUEPO and rHuEPO (epoetin α) have only minor differences in the branching patterns of their glycan chains. Therefore it would be expected that

the Raman spectra of these two molecules when reacted with the functionalized nanoparticles to be largely similar.

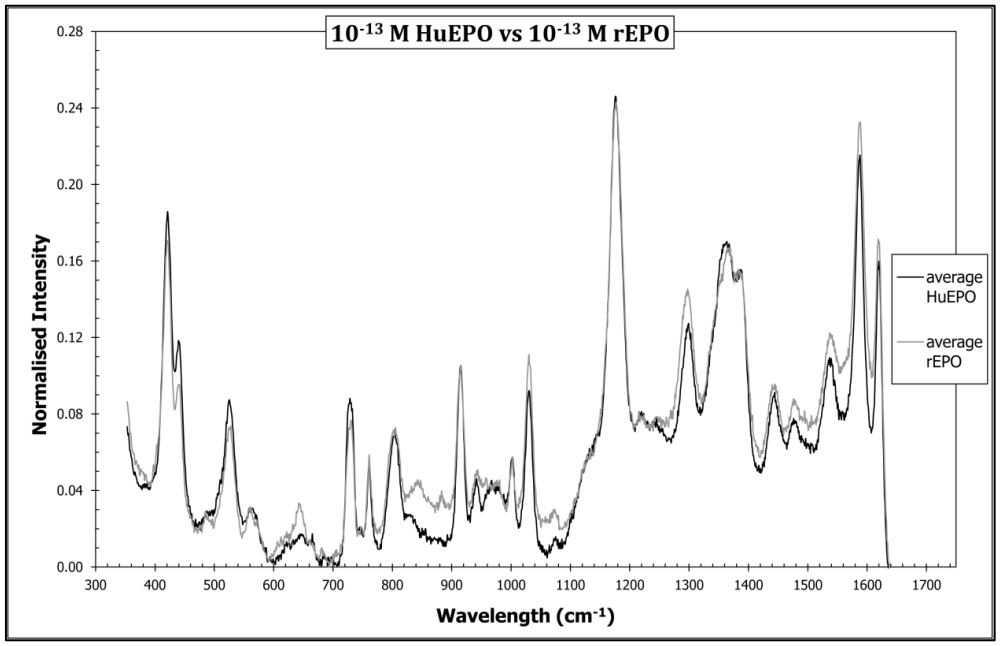

Figure 4.9.2 Comparison of 1 x 10^{-13} M international standards of HUEPO and rHuEPO

4.9.3 **Spiked vs non-spiked urine samples**

Urine vs. urine spiked with rHuEPO

Urine samples were spiked with 10^{-12} and 10^{-14} M rHuEPO respectively, interacted with the EPO antibody-functionalized nanoparticles for 30 minutes and screened by SERS. For comparison, another urine sample, with no added rHuEPO, was also reacted with the functionalized nanoparticles and screened by SERS. The collected spectra (Fig 4.9.3) were inspected visually and a series of preliminary PCA were done selecting blocks of the spectra that were known to vary with EPO binding and not the nanoparticle. Upon careful study of the spectra subtle differences are present in spectral region 1515 cm^{-1} to 1580 cm^{-1} (the grey-shaded region in Fig 4.9.3). The PCA performed using this region showed the best distinctions between the human and recombinant EPO.

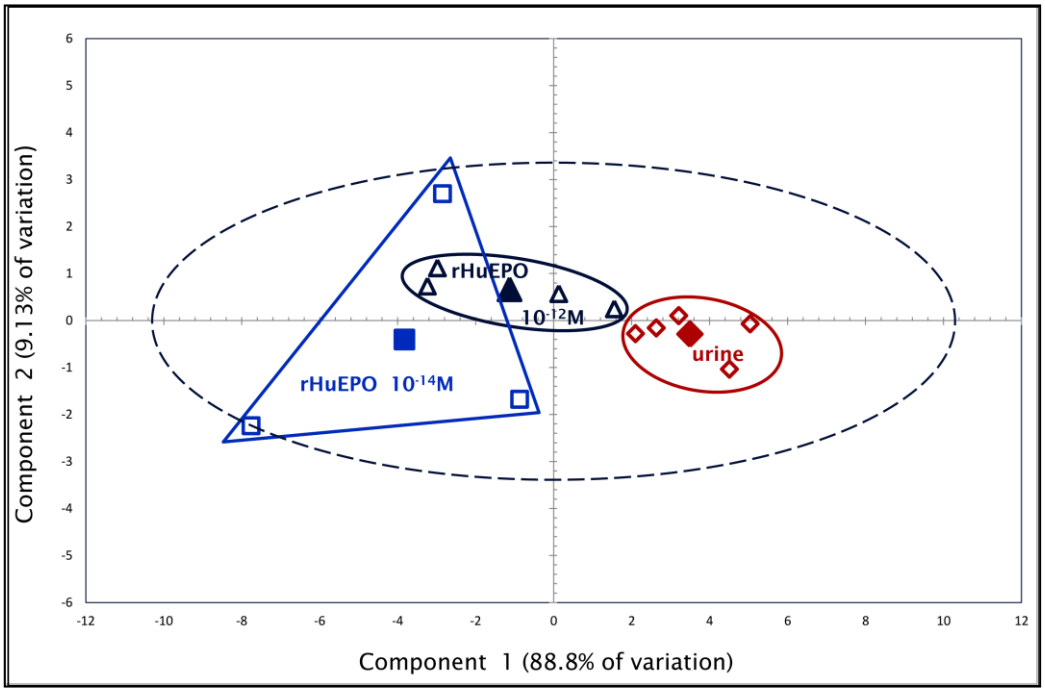

Figure 4.9.3 SERS spectra of un-spiked urine sample and urine spiked with 10^{-12}, 10^{-14} M rHuEPO.

In the PCA model, (fig 4.9.4) the larger data points are the average of six measurements of each of the three samples, un-spiked urine, urine spiked with 10^{-12} M, 10^{-14} M. The PCA model confirmed that rHuEPO can be detected in urine at ultra low concentration. The model also shows that the spectral data from un-spiked urine samples are distinguishable from the rest of the data even though there were some measurements that are outliers to the model. The separation between clusters indicated that the SERS detection is able to differentiate between human endogenous EPO and rHuEPO in urine. This discrimination may be attributed to the marginally higher affinity of the 3F6 anti EPO antibody towards rHuEPO over natural EPO [72, 74, 76, 79-82]

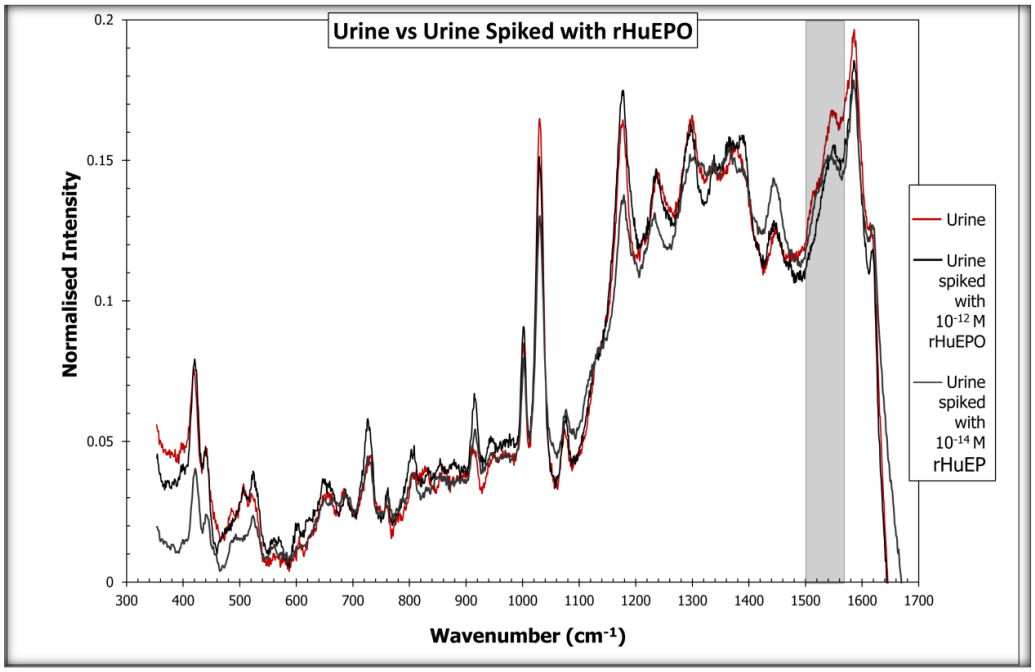

Figure 4.9.4 PCA of Raman spectra (1515 -1580 cm-1). All urine samples are diluted 1:1. The larger data points are the average of six measurements. They are well separated even though they each contain measurements that are outliers to the model. Urine with: PBS pH 7.4, rHuEPO at 1x10-12 M in PBS and rHuEPO at 1x10-14 M in PBS respectively.

Urine spiked with HUEPO IS vs. rHuEPO IS at 1x10^{-12} M

The PCA of urine spiked with HUEPO IS compared with the urine spiked with rHuEPO IS at the concentration of 1×10^{-12} M shows a good separation between the two sets of data points and particularly between their average data points. (fig 9.4.5) The ratio between the concentrations of HUEPO and rHuEPO is 1:2.5 in the sample spiked with rHuEPO (using the same assumptions about endogenous EPO concentrations as in the above study). This corresponds with 28.7% HUEPO in the sample spiked with rHuEPO vs. 100% HUEPO in the other sample.

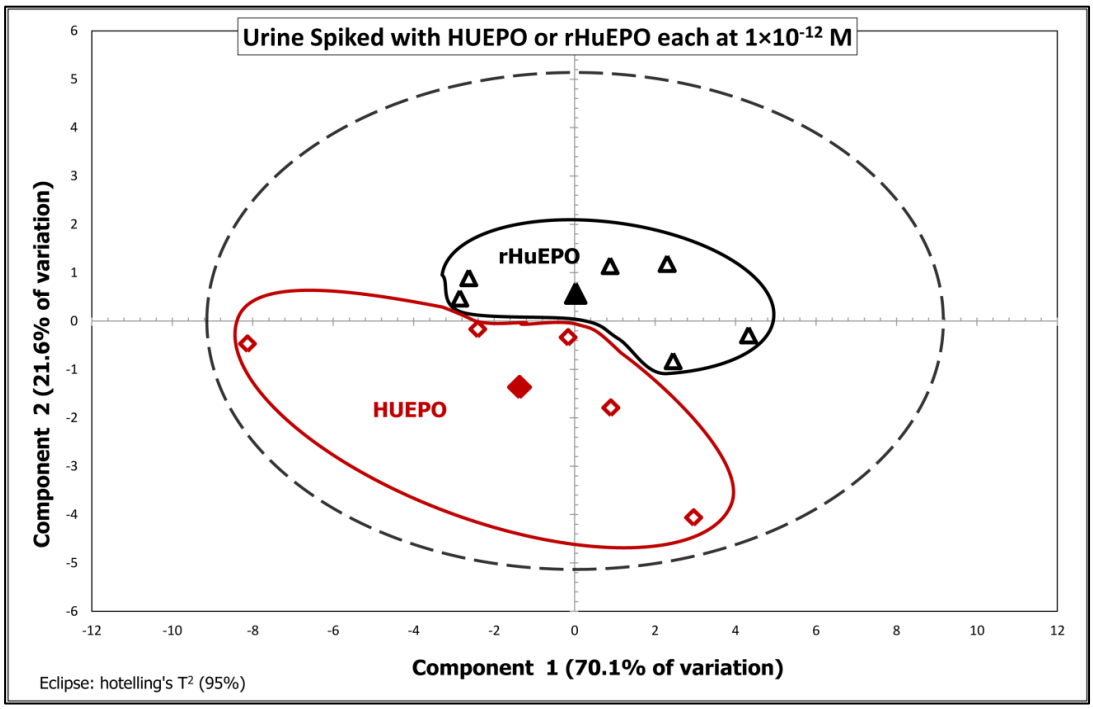

Figure 4.9.5 PCA of region 1515 -1580 cm-1 from Raman spectra of urine spiked with HUEPO or rHuEPO at 1 x 10^{-12} M.

Urine spiked with HUEPO IS vs. rHuEPO IS at 1x10^{-14} M

The separation of urine spiked with HUEPO IS compared with the urine spiked with rHuEPO IS in the PCA at the concentration of 1×10^{-14} M (fig4.9.6) is similar to previous model. It shows a generally good separation between the two sets of data points and their average data points. The exceptions to this are one data point for rHuEPO, which lies close to and overlaps the data points for HUEPO; and another data point which is an outlier to the model.

That a rHuEPO data point is found with the HUEPO data points is not surprising as the ratio between the concentrations of HUEPO and rHuEPO is 1: 0.025 in the sample spiked with rHuEPO (using the same assumptions about endogenous EPO concentrations as in the above studies). This corresponds with 2.5% rHuEPO in the sample spiked with rHuEPO vs. 100% HUEPO in the other sample. With such a low concentration of rHuEPO in the sample it is not surprising that at least one data point contains no rHuEPO. However if averages are taken of the six data points these two groups are well separated even with the outlier and the sample containing no rHuEPO included.

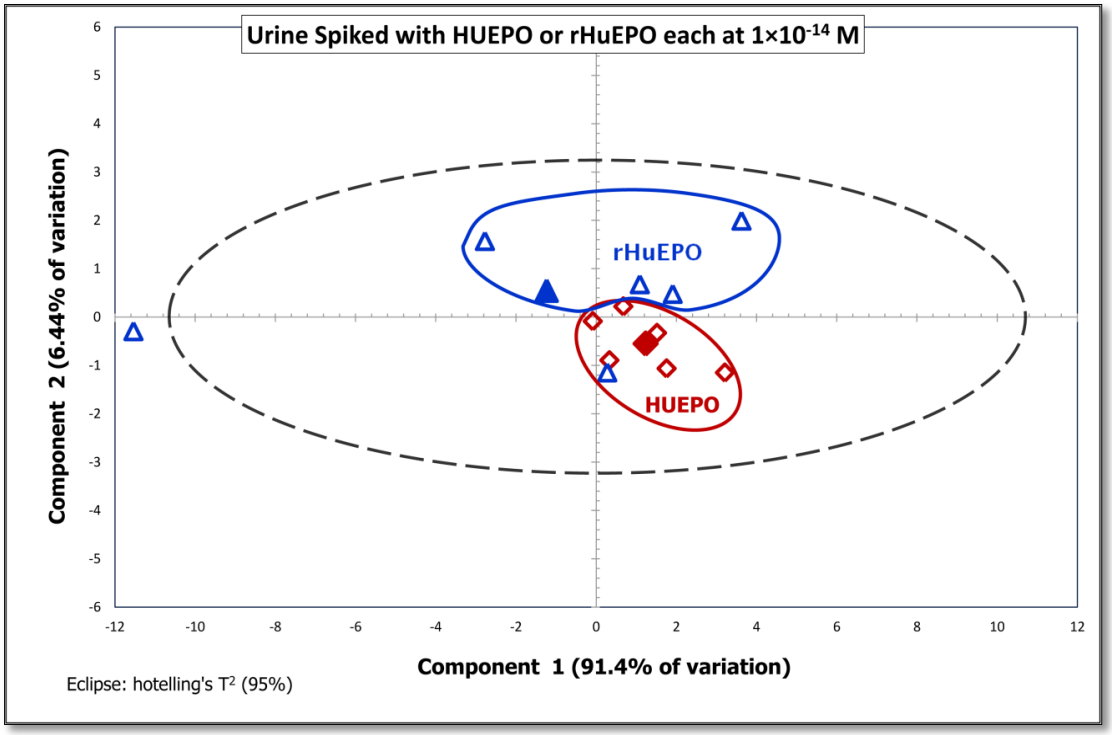

Figure 4.9.6 PCA of region 1515 -1580 cm-1 from Raman spectra of urine spiked with HUEPO or rHuEPO each at 1 x 10^{-14} M.

The Raman instrument used has a very small spot size at one µm, and in this type of experiment this is a disadvantage. The collection of six data points and averaging them approximates the large majority of Raman instruments which have larger spot sizes. This experiment shows that this technique can distinguish between rHuEPO and HUEPO when only 2.5% of the sample is rHuEPO. This is a very significant improvement upon the current technique where approximately 71% of the sample must be rHuEPO before it can be detected [125], and is still a significant improvement on the MAIIA technique where 40% rHuEPO is required before it can be detected [109].

4.10 PRELIMINARY CONCLUSIONS

More than 80% of the bare gold nanoparticles were quasi-spherical, with the remainder appearing to have joined early in the reduction. The size range is pseudo-monodisperse with 74% of nanoparticles being within one standard deviation of the mean size. Two thirds of the nanoparticles had a silica coating less than 1.6 nm which is the level quoted by Tian *at el* [126] as the limit for extra enhancement.

The attachment of the glutaraldehyde linker leads to a considerable amalgamation of nanoparticles which is further exacerbated when the antibodies are attached. While limited clustering, producing hotspots, is essential for maximum enhancement of the SERS signal, this unrestrained clustering would need to be controlled for batch to batch reproducibility. This could be achieved via a bifunctional linker.

The silica pacification layer and the blocking of unreacted glutaraldehyde sites were shown to prevent any non-specific cross reaction.

The wavenumbers of spectra difference between EPO and unreacted nanoparticles was: 422, 440, 525, 725, 760, 800, 915, 1176, 1585 and 1620 cm^{-1}. The volume required for the analysis: 10 µL for standard solutions and 30 µL for biological fluids, compares favourably with the current technique: 20 mL and the proposed MAIIA technique: 5 mL of urine [109].

The technique was also found to be log linear quantitative: 2×10^{-10} M – 3×10^{-13} M (LLOQ). It was linear quantitative at the concentration where EPO is naturally found in both urine and serum.

The nanoparticles were found to react with both HUEPO and rHuEPO and to be able to distinguish between the two. The spectral region between 1519 and 1580 cm^{-1} showed this difference. The technique was able to distinguish rHuEPO spiked in urine where the concentration of the recombinant EPO was as low as 2.5% of the total EPO. This is a significant improvement over the current techniques (71%) [130] and the new proposed MAIIA technique (40%) [109].

Chapter 5: Conclusions and Recommendations for Further Studies

The aim of this work was to develop a simple, rapid and cost-effective technique for the detection of ultra-trace amounts of simple organic molecules as well as complex biomolecules in aqueous and biological fluids. This chapter outlines the outcomes of this work in comparison to other techniques currently used or suggested for the detection of ultra-trace amounts caffeine and EPO in various matrices, and its many applications such as doping control and quality assurance of food products. This chapter also proposes future improvements of the presented technique.

In this work, I have indicated the applicability of the developed SERS antibody-functionalised nanoparticle technique to a wide range of applications. This was demonstrated by applying the developed technology to both small organic molecules (caffeine) and complex biological macromolecules (EPO). These two exemplars demonstrated several key advantages of antibody-functionalised gold nanoparticles over existing technologies, including sensitivity, specificity, simplicity, portability and cost effectiveness. In both the caffeine and EPO models, the technique amply qualified the analyte over many orders of magnitude (2×10^{-10} M to 3.5×10^{-13} M for EPO and 1×10^{-4} M to 1×10^{-9} M for caffeine). The achieved levels of quantifications encompassed those required for the analysis of the nominated analytes in their relevant field applications (such as, food analysis, clinical diagnostics, racing and sports industry).

In both the caffeine and EPO models, this technique demonstrated significant improvement of conservatively six orders of magnitude in lower levels of detection for the required sample over the currently used techniques in the respective industry: detection of caffeine improved from 2×10^{-4} g (10 mL at 9.3×10^{-5} M) for the FT-Raman technique [40] down to 2×10^{-13} g (10 µL at 1×10^{-10} M); and detection of EPO improved from 7×10^{-11} g (20 mL at $3\text{x }10^{-9}$ M) for IEF [84] down to 3×10^{-16} g (10 µL at 1×10^{-15} M).

This technique simplifies the analysis, as the antibody-functionalised nanoparticles utilises the highly selective antibody recognition to bind to the target analyte and extract it from solution in a single step capture and pre-concentration process. Consequently, there is no need for complicated pre-treatment procedures to isolate and concentrate the analyte from large sample volumes, as is required for most of the other currently used methods. Once the analyte was bound to the antibody-functionalized nanoparticles, the nanoparticles were easily isolated from solution by centrifugation. The washed nanoparticles were then subjected directly to trapped analyte detection by SERS.

The antibody-functionalised gold nanoparticle technique functions as an autonomic immuno-separation technique, which eliminates interfering substances that co-exist with the target analyte within the sample without a separate purification step. This was evident in the 'real life' samples of both the caffeine and EPO models, in which no interference was detected by SERS measurement from the potentially problematic complex biological matrix in which the analytes are naturally found, and the EPO antibody functionalised nanoparticles were extracted successfully from skim milk without any cross reaction evidenced by indistinguishable Raman spectra and completely intermingled HPCA.

The enhanced sensitivity attributed to the thin silica coating allowed the analytes to be successfully detected and analysed by surface-enhanced Raman spectroscopy without the requiring the incorporation of a Raman reporter, which represents is a significant improvement over other Raman techniques. As there are no extraction procedures required to remove the analyte from the sample matrix, this technique eliminates the use of toxic and environmentally unfriendly solvents.

As sensitive and inexpensive portable Raman instruments are becoming commercially available, the antibody-functionalised gold nanoparticle technique can be adapted for field use as necessary. In this scenario, a kit, including the relevant functionalized-nanoparticles and portable instrumentation, could be used onsite to concentrate, separate and rapidly analyse the sample for the target analyte.

This technique has been shown to be a simple rapid and cost-effective method, however improvements are needed in the nanoparticle manufacturing process. Glutaraldehyde, the linker used in this study, has two aldehyde groups, binds nanoparticles bilaterally and thereby forms uncontrollably large nanoparticle aggregates. While some aggregation is necessary for maximum sensitivity the degree of aggregation found is counter-productive. Consequently, there is a need to identify a bi-functional linker that will specifically bind the nanoparticle at one end and the antibody at the other end.

A bi-functional linker would allow an increased number of the antibody molecules to be loaded onto the nanoparticles, as there would be more surface area available on non-aggregated nanoparticles. Increasing the antibody load on the nanoparticle surface would increase the analyte capturing capacity and effectively increase the SERS signal intensity. Cysteamine, which forms a strong thiol bond with gold and an amide bond with carboxyl groups (antibody), would be useful if a polymer based pacification strategy is used, or other suitable linkers would need to be found if using silica for this purpose.

Strategies for more controlled minimal aggregation may need to be explored as well, to compensate for loss of aggregation. Hence, these aggregation control techniques would be an important improvement to the nanoparticle but would have to be optimised for maximum sensitivity.

Another optimisation, that would enhance the nanoparticle, is modifying its structure to include a magnetic-core. Magnetic-core gold nanoparticles, with an iron oxide core and a gold shell allow isolation of the nanoparticles from solution by the simple use of a magnetic separator. Antibody-functionalized, magnetic core gold nanoparticles reacted with the target analyte, form a simple magnetic separator to extract analytes from the matrix. This would greatly decrease the time required to separate the analyte from complicated biological matrices, from an hour with separation via the current centrifugation protocol to just a few minutes [131, 132], and would allow technique automation.

Magnetic-core gold nanoparticles have another benefit as they improve the efficiency of the synthesis and coating procedures by reducing the labour and time required for cleanup procedures.

Nanoparticles improved by inclusion of a magnetic core and efficient and optimised aggregation with maximised antibody loading should give the most sensitive results. There is one proviso; this technique has been developed on a research grade laboratory-based Raman instrument whereas for the most applicability it should be a portable technique that can be taken to the site of analysis. Therefore, its applicability to several models of available portable instrumentation must also be evaluated to exploit the advantages of a portable technique.

Applications where this technology could be applied are many and varied. Its applicability in anti-doping, for industrial quality control and providence has been demonstrated here. This technique might also be easily adapted and applied to medical diagnostics and monitoring, environmental surveillance, food toxicology and microbiology, as well as forensic and security applications, just to name a few.

BIBLIOGRAPHY

1. Krishnan, R.S. and R.K. Shankar, *Raman effect: History of the discovery.* Journal of Raman Spectroscopy, 1981. **10**(1): p. 1-8.
2. American Chemical Society and Indian Association for the Cultivation of Science. *American Chemical Society International Historical Chemical Landmarks. The Raman Effect. -Commemorative Booklet*. 1998 [cited August 5,2013]; Available from: http://www.acs.org/content/dam/acsorg/education/whatischemistry/landmarks/ramaneffect/the-raman-effect-commemorative-booklet.pdf.
3. Nobelprize.org. *The Nobel Prize in Physics*. 1930 [cited August 5,2013]; Available from: http://www.nobelprize.org/nobel_prizes/physics/laureates/1930/.
4. Raman, C.V., *The Molecular Scattering of Light.* Nobel Lectures, Physics 1922-1941, Elsevier Publishing Company, Amsterdam 1965
5. Le Ru, E. and P. Etchegoin, *Principles of Surface-Enhanced Raman Spectroscopy : and related plasmonic effects*, 2008 Elsevier Science Amsterdam, Boston
6. Fleischmann, M., P.J. Hendra, and A.J. McQuillan, *Raman spectra of pyridine adsorbed at a silver electrode.* Chemical Physics Letters, 1974. **26**(2): p. 163-166.
7. Albrecht, M.G. and J.A. Creighton, *The Anomalously intense Raman spectra of pyridine at a silver electrode.* Journal of the American Chemical Society, 1977. **99**(15): p. 5215-5217.
8. Haynes, C.L., et al., *Surface-enhanced Raman sensors: early history and the development of sensors for quantitative biowarfare agent and glucose detection.* Journal of Raman Spectroscopy, 2005. **36**(6-7): p. 471-484.
9. Jeanmaire, D.L. and R.P. Van Duyne, *Surface raman spectroelectrochemistry: Part I. Heterocyclic, aromatic, and aliphatic amines adsorbed on the anodized silver electrode.* Journal of Electroanalytical Chemistry and Interfacial Electrochemistry, 1977. **84**(1): p. 1-20.
10. Pahlow, S., et al., *Bioanalytical application of surface- and tip-enhanced Raman spectroscopy.* Engineering in Life Sciences, 2012. **12**(2): p. 131-143.
11. Le Ru, E.C. and P.G. Etchegoin, *Single-Molecule Surface-Enhanced Raman Spectroscopy.* Annual Review of Physical Chemistry, 2012. **63**(1): p. 65-87.
12. Kneipp, K., H. Kneipp, and J. Kneipp, *Surface-Enhanced Raman Scattering in Local Optical Fields of Silver and Gold Nanoaggregates - From Single-Molecule Raman Spectroscopy to Ultrasensitive Probing in Live Cells.* Accounts of Chemical Research, 2006. **39**(7): p. 443-450.
13. Tam, N.C.M., et al., *Porphyrin-lipid Stabilized Gold Nanoparticles for Surface Enhanced Raman Scattering based Imaging.* Bioconjugate Chemistry, 2012.

14. Li, J.F., et al., *Shell-isolated nanoparticle-enhanced Raman spectroscopy.* Nature, 2010. **464**(7287): p. 392-395.
15. Natan, M.J., R.G. Freeman, and W. Doering. *SERS nanotags for point of care diagnostics*. in *2007 NSTI Nanotechnology Conference and Trade Show - NSTI Nanotech*. 2007. Santa Clara, CA; United States. Available from: http://www.scopus.com/inward/record.url?eid=2-s2.0-34547969876&partnerID=40&md5=41ff45317973bcd1290bdf731fc04ae1.
16. Guarrotxena, N., et al., *Antitags: Nanostructured Tools for Developing SERS-Based ELISA Analogs.* Advanced Materials (Weinheim, Germany), 2010. **22**(44): p. 4954-4958.
17. Neng, J., et al., *Surface-enhanced Raman scattering (SERS) detection of multiple viral antigens using magnetic capture of SERS-active nanoparticles.* Biosensors and Bioelectronics, 2013. **41**(0): p. 316-321.
18. Chen, K., et al., *A practicable detection system for genetically modified rice by SERS-barcoded nanosensors.* Biosensors and Bioelectronics, 2012. **34**(1): p. 118-124.
19. Domenici, F., A.R. Bizzarri, and S. Cannistraro, *Surface-enhanced Raman scattering detection of wild-type and mutant p53 proteins at very low concentration in human serum.* Analytical Biochemistry, 2012. **421**(1): p. 9-15.
20. Neng, J., et al., *A versatile SERS-based immunoassay for immunoglobulin detection using antigen-coated gold nanoparticles and malachite green-conjugated protein A/G.* Biosensors and Bioelectronics, 2010. **26**(3): p. 1009-1015.
21. Huet, A.C., et al., *Simultaneous determination of (fluoro)quinolone antibiotics in kidney, marine products, eggs, and muscle by enzyme-linked immunosorbent assay (ELISA).* Journal of Agricultural and Food Chemistry, 2006. **54**(8): p. 2822-2827.
22. Kim, I., et al., *SERS-based multiple biomarker detection using a gold-patterned microarray chip.* Journal of Molecular Structure, 2012. **1023**(0): p. 197-203.
23. Chen, S.-H., et al., *Using oligonucleotide-functionalized Au nanoparticles to rapidly detect foodborne pathogens on a piezoelectric biosensor.* Journal of Microbiological Methods, 2008. **73**(1): p. 7-17.
24. Wang, S., et al., *Rapid Colorimetric Identification and Targeted Photothermal Lysis of Salmonella Bacteria by Using Bioconjugated Oval-Shaped Gold Nanoparticles.* Chemistry – A European Journal, 2010. **16**(19): p. 5600-5606.
25. Tsai, Y.-H., M.-J. Bair, and C.-C. Hu, *Determination of Levofloxacin in Human Urine with Capillary Electrophoresis and Fluorescence Detector.* Journal of the Chinese Chemical Society (Taipei, Taiwan), 2007. **54**(4): p. 991-995.
26. Wang, X.-L., et al., *Ultrasensitive Detection of Protein Using an Aptamer-Based Exonuclease Protection Assay.* Analytical Chemistry, 2004. **76**(19): p. 5605-5610.

27. Lin, C., et al., *Self-Assembled Signaling Aptamer DNA Arrays for Protein Detection.* Angewandte Chemie International Edition, 2006. **45**(32): p. 5296-5301.
28. Shao, X., et al., *Flow injection chemiluminescence determination of levofloxacin in medicine and biological fluids based on its enhancing effect on luminol-H 2O2 reaction.* Spectroscopy, 2009. **23**(3-4): p. 209-216.
29. Wong, F.A., S.J. Juzwin, and S.C. Flor, *Rapid stereospecific high-performance liquid chromatographic determination of levofloxacin in human plasma and urine.* Journal of Pharmaceutical and Biomedical Analysis, 1997. **15**(6): p. 765-771.
30. Centi, S., et al., *Aptamer-Based Detection of Plasma Proteins by an Electrochemical Assay Coupled to Magnetic Beads.* Analytical Chemistry, 2007. **79**(4): p. 1466-1473.
31. Yoon, J., et al., *Highly sensitive detection of thrombin using SERS-based magnetic aptasensors.* Biosensors and Bioelectronics, 2013. **47**(0): p. 62-67.
32. Harris, D.C., *Quantitative Chemical Analysis*. 6 ed2003, New york: Freeman.
33. Turkevich, J., P.C. Stevenson, and J. Hillier, *A study of the nucleation and growth processes in the synthesis of colloidal gold.* Discussions of the Faraday Society, 1951. **11**: p. 55-75.
34. Xia, H., et al., *Synthesis of Monodisperse Quasi-Spherical Gold Nanoparticles in Water via Silver(I)-Assisted Citrate Reduction.* Langmuir, 2009. **26**(5): p. 3585-3589.
35. Liz-Marzan, L.M., M. Giersig, and P. Mulvaney, *Synthesis of nanosized gold-silica core-shell particles.* Langmuir, 1996. **12**(18): p. 4329-4335.
36. Li, J.-F., et al., *Synthesis and characterization of gold nanoparticles coated with ultrathin and chemically inert dielectric shells for SHINERS applications.* Applied Spectroscopy, 2011. **65**(6): p. 620-626.
37. Freitag, I., et al., *Preparation and characterization of multicore SERS labels by controlled aggregation of gold nanoparticles.* Vibrational Spectroscopy, 2012. **60**: p. 79 - 84.
38. Migneault, I., et al., *Glutaraldehyde: behavior in aqueous solution, reaction with proteins, and application to enzyme crosslinking.* BioTechniques, 2004. **37**(5): p. 790-802.
39. Goh, C.Y., W. van Bronswijk, and C. Priddis, *Rapid Nondestructive On-Site Screening of Methamphetamine Seizures by Attenuated Total Reflection Fourier Transform Infrared Spectroscopy.* Applied Spectroscopy, 2008. **62**: p. 640-648.
40. Armenta, S., S. Garrigues, and M. de la Guardia, *Solid-phase FT-Raman determination of caffeine in energy drinks.* Analytica Chimica Acta, 2005. **547**(2): p. 197-203.
41. Pavel, I., et al., *Theoretical and pH dependent surface enhanced Raman spectroscopy study on caffeine.* Biopolymers, 2003. **72**(1): p. 25-37.
42. Russell, D.W., et al., *Caffeine, a naturally occurring acaricide.* Journal of Allergy and Clinical Immunology, 1991. **87**(1, Part 1): p. 107-110.

43. Edwards, H.G.M., et al., *FT-Raman spectroscopic studies of guarana and some extracts.* Analytica Chimica Acta, 2005. **532**(2): p. 177-186.
44. Edwards, H.G.M., T. Munshi, and M. Anstis, *Raman spectroscopic characterisations and analytical discrimination between caffeine and demethylated analogues of pharmaceutical relevance.* Spectrochimica Acta Part A: Molecular and Biomolecular Spectroscopy, 2005. **61**(7): p. 1453-1459.
45. Baranska, M. and L.M. Proniewicz, *Raman mapping of caffeine alkaloid.* Vibrational Spectroscopy, 2008. **48**(1): p. 153-157.
46. Aucamp, J.P., Y. Hara, and Z. Apostolides, *Simultaneous analysis of tea catechins, caffeine, gallic acid, theanine and ascorbic acid by micellar electrokinetic capillary chromatography.* Journal of Chromatography A, 2000. **876**(1–2): p. 235-242.
47. Goto, T., et al., *Simultaneous analysis of individual catechins and caffeine in green tea.* Journal of Chromatography A, 1996. **749**(1–2): p. 295-299.
48. Yang, M.J., M.L. Orton, and J. Pawliszyn, *Quantitative determination of caffeine in beverages using a combined SPME-GC/MS method.* Journal of Chemical Education, 1997. **74**(9): p. 1130-1132.
49. Meinhart, A.D., et al., *Optimisation of a CE method for caffeine analysis in decaffeinated coffee.* Food Chemistry, 2010. **120**(4): p. 1155-1161.
50. Paradkar, M.M. and J. Irudayaraj, *A Rapid FTIR Spectroscopic Method for Estimation of Caffeine in Soft Drinks and Total Methylxanthines in Tea and Coffee.* Journal of Food Science, 2002. **67**(7): p. 2507-2511.
51. Gunasekaran, S., G. Sankari, and S. Ponnusamy, *Vibrational spectral investigation on xanthine and its derivatives—theophylline, caffeine and theobromine.* Spectrochimica Acta Part A: Molecular and Biomolecular Spectroscopy, 2005. **61**(1–2): p. 117-127.
52. Paradkar, M.M. and J. Irudayaraj, *Rapid determination of caffeine content in soft drinks using FTIR–ATR spectroscopy.* Food Chemistry, 2002. **78**(2): p. 261-266.
53. Huck, C.W., W. Guggenbichler, and G.K. Bonn, *Analysis of caffeine, theobromine and theophylline in coffee by near infrared spectroscopy (NIRS) compared to high-performance liquid chromatography (HPLC) coupled to mass spectrometry.* Analytica Chimica Acta, 2005. **538**(1–2): p. 195-203.
54. Lee, S., et al., *Rapid and sensitive phenotypic marker detection on breast cancer cells using surface-enhanced Raman scattering (SERS) imaging.* Biosensors and Bioelectronics, 2014. **51**(0): p. 238-243.
55. Kleinman, S.L., et al. *Structural and optical characterization of single nanoparticles and single molecule SERS*. in *Plasmonics: Metallic Nanostructures and Their Optical Properties VIII*. 2010. San Diego, CA; United States. Available from: http://www.scopus.com/inward/record.url?eid=2-s2.0-79952685762&partnerID=40&md5=84b9f57fe13406feb5d1c3fde020571b.

56. Deegan, R.D., et al., *Capillary flow as the cause of ring stains from dried liquid drops.* Nature, 1997. **389**(6653): p. 827-829.
57. Wong, T.-S., et al., *Nanochromatography Driven by the Coffee Ring Effect.* Analytical Chemistry, 2011. **83**(6): p. 1871-1873.
58. Pahlow, S., et al., *Isolation and Enrichment of Pathogens with a Surface-Modified Aluminium Chip for Raman Spectroscopic Applications.* ChemPhysChem, 2013. **14**(15): p. 3600-3605.
59. Pagba, C.V., et al., *Direct detection of aptamer-thrombin binding via surface-enhanced Raman spectroscopy.* Journal of Biomedical Optics, 2010. **15**(4): p. 047006-047006-8.
60. Sanles-Sobrido, M., et al., *Label-free SERS detection of relevant bioanalytes on silver-coated carbon nanotubes: The case of cocaine.* Nanoscale, 2009. **1**(1): p. 153-158.
61. Muniz-Miranda, M., G. Cardini, and V. Schettino, *Surface-enhanced Raman spectra of pyridine and pyrazolide on silver colloids: chemical and electromagnetic effects.* Theoretical Chemistry Accounts, 2004. **111**(2-6): p. 264-269.
62. Hardy, P.M., A.C. Nicholls, and H.N. Rydon, *The nature of the cross-linking of proteins by glutaraldehyde. Part I. Interaction of glutaraldehyde with the amino-groups of 6-aminohexanoic acid and of [small alpha]-N-acetyl-lysine.* Journal of the Chemical Society, Perkin Transactions 1, 1976(9): p. 958-962.
63. Hardy, P.M., G.J. Hughes, and H.N. Rydon, *The nature of the cross-linking of proteins by glutaraldehyde. Part 2. The formation of quaternary pyridinium compounds by the action of glutaraldehyde on proteins and the identification of a 3-(2-piperidyl)-pyridinium derivative, anabilysine, as a cross-linking entity.* Journal of the Chemical Society, Perkin Transactions 1, 1979(0): p. 2282-2288.
64. Y_tambe *Immunoglobulin basic unit*, 2007 licensed under the Creative Commons Attribution-Share Alike 3.0 license. [cited 4/10/13] Available from: http://en.wikipedia.org/wiki/File:Immunoglobulin_basic_unit.svg.
65. Bempong, D.K., P.J. Houghton, and K. Steadman, *The Xanthine Content of Guarana and Its Preparations.* Pharmaceutical Biology, 1993. **31**(3): p. 175-181.
66. Coca-Cola Company press release. *Coca-Cola Moves Its Secret Formula to The World of Coca-Cola* 2011 [cited 8 October,2013]; Available from: http://www.coca-colacompany.com/press-center/press-releases/coca-cola-moves-its-secret-formula-to-the-world-of-coca-cola.
67. Coca-Cola Company. *Coke Lore: Trademark Chronology* 2012 [cited 8 October,2013]; Available from: http://www.coca-colacompany.com/stories/coke-lore-trademark-chronology.
68. Coca-Cola UK. *Coca-Cola webpage*. [cited 8 October,2013]; Available from: http://www.coca-cola.co.uk/brands/coca-cola.html.
69. Coca-Cola UK. *Diet Coke webpage*. [cited October 8,2013]; Available from: http://www.coca-cola.co.uk/brands/diet-coke.html.

70. Pepsi Australia. *Pepsi Next - Ingredients list and nutrition panel*. 2013 [cited 6 November,2013]; Available from: http://pepsinext.com.au/info.html#ing.
71. Head barista of the coffee shop. Personal communication regarding composition of the coffee. Communicated to Juanita Hughes, September 2013.
72. Krantz, S., *Erythropoietin.* Blood, 1991. **77**(3): p. 419-434.
73. Lappin, T.R., A.P. Maxwell, and P.G. Johnston, *EPO's Alter Ego: Erythropoietin Has Multiple Actions.* STEM CELLS, 2002. **20**(6): p. 485-492.
74. Shahrokh, Z., et al., *Erythropoietin Produced in a Human Cell Line (Dynepo) Has Significant Differences in Glycosylation Compared with Erythropoietins Produced in CHO Cell Lines.* Molecular Pharmaceutics, 2010. **8**(1): p. 286-296.
75. Lasne, F., et al., *Detection of recombinant human erythropoietin in urine for doping analysis: Interpretation of isoelectric rofiles by discriminant analysis.* Electrophoresis, 2007. **28**(12): p. 1875-1881.
76. Lasne, F. and J. de Ceaurriz, *Recombinant erythropoietin in urine - An artificial hormone taken to boost athletic performance can now be detected.* Nature, 2000. **405**(6787): p. 635-635.
77. Skibeli, V., G. Nissen-Lie, and P. Torjesen, *Sugar profiling proves that human serum erythropoietin differs from recombinant human erythropoietin.* Blood, 2001. **98** (13): p. 3626-3634.
78. Svensson, E.C., B. Soreghan, and J.C. Paulson, *Organization of the beta-galactoside alpha 2,6-sialyltransferase gene. Evidence for the transcriptional regulation of terminal glycosylation.* Journal of Biological Chemistry, 1990. **265**(34): p. 20863-8.
79. Grabenhorst, E., et al., *Genetic engineering of recombinant glycoproteins and glycosylation pathway in mammalian host cells.* Glycoconjugate Journal, 1999. **16**(2): p. 81-97.
80. WADA EPO Working Group, *Harmonisation of Analysis and Reporting of Recombinant Erythropoietin (I.E. Epoetins) and Analogues (E.G. Darbepoetin, Pegeserpoetin, Peginesatide, EPO-Fc) by Electrophoretic Techniques.*, 2012 Available from: http://www.wada-ama.org/Documents/World_Anti-Doping_Program/WADP-IS-Laboratories/Technical_Documents/WADA-TD2013EPO-Harmonization-Analysis-of-Recombinant-Erythropoietins-EN.pdf.
81. Park, S.S., et al., *Biochemical assessment of erythropoietin products from Asia versus US Epoetin alfa manufactured by Amgen.* Journal of Pharmaceutical Sciences, 2009. **98**(5): p. 1688-1699.
82. Dehnes, Y. and P. Hemmersbach, *Effect of single doses of methoxypolyethylene glycol-epoetin beta (CERA, Mircera™) and epoetin delta (Dynepo™) on isoelectric erythropoietin profiles and haematological parameters.* Drug Test Anal, 2011. **3**(5): p. 291-9.
83. Roche Products Pty Limited, *Mircera Product Information sheet*, 2011 Available from: http://www.roche-australia.com/fmfiles/re7229005/downloads/anaemia/mircera-pi.pdf.

84. Lasne, F., et al., *Detection of isoelectric profiles of erythropoietin in urine: differentiation of natural and administered recombinant hormones.* Analytical Biochemistry, 2002. **311**(2): p. 119-126.
85. World Anti-Doping Agency webpage - about WADA -history. *A Brief History of Anti-Doping*. [cited April 11,2013,]; Available from: http://www.wada-ama.org/en/About-WADA/History/A-Brief-History-of-Anti-Doping/.
86. the Guardian UK. *The Festina affair France, 1998: On its 10th anniversary, we look back at the doping scandal which rocked the Tour de France*. 1998 [cited April 11,2013,]; Available from: http://www.guardian.co.uk/sport/gallery/2008/jul/09/tourdefrance.cycling?picture=335585245#/?picture=335585204&index=8.
87. BBC Sport online. *Festina ruling 'not tough enough'*. 22 December, 2000 [cited 28/11,2013]; Available from: http://news.bbc.co.uk/sport2/hi/other_sports/1082730.stm.
88. Davis, J. *Ten Years Later, Festina Doping Affair Still Not Forgotten*. 2008 [cited April 11,2013,]; Available from: http://www.bicycle.net/2008/ten-years-later-festina-doping-affair-still-not-forgotten.
89. Channel Nine Wide World of Sports. *Doping in rugby 'as bad as cycling'*. 2013 [cited April 11,2013]; Available from: http://wwos.ninemsn.com.au/article.aspx?id=8637988.
90. *official website of Le Tour De France;- Great moments in the history of the Tour, year 1998*. [cited April 11,2013]; Available from: http://www.letour.fr/2011/TDF/HISTO/us/index.html#.
91. Vogel, G., *A Race to the Starting Line.* Science, 2004. **305**(5684): p. 632-5.
92. Deutsche Welle (DW). *Sports Doping Statistics Reach Plateau in Germany* 2003 [cited April 11,2013]; Available from: http://www.dw.de/sports-doping-statistics-reach-plateau-in-germany/a-786574-1.
93. Bennett, C.L., et al., *Pure Red-Cell Aplasia and Epoetin Therapy.* New England Journal of Medicine, 2004. **351**(14): p. 1403-1408.
94. Adamson, J.W. and J.W. Eschbach, *Treatment of the Anemia of Chronic Renal Failure with Recombinant Human Erythropoietin.* Annual Review of Medicine, 1990. **41**(1): p. 349-360.
95. Noakes, T.D., *Tainted Glory — Doping and Athletic Performance.* New England Journal of Medicine, 2004. **351**(9): p. 847-849.
96. Lasne, F., *Double-blotting: a solution to the problem of non-specific binding of secondary antibodies in immunoblotting procedures.* Journal of Immunological Methods, 2001. **253**(1-2): p. 125-131.
97. Beullens, M., J.R. Delanghe, and M. Bollen, *False-positive detection of recombinant human erythropoietin in urine following strenuous physical exercise.* Blood, 2006. **107**(12): p. 4711-4713.
98. Khan, A., et al., *New urinary EPO drug testing method using two-dimensional gel electrophoresis.* Clinica Chimica Acta, 2005. **358**(1-2): p. 119-130.

99. Beullens, M., J.R. Delanghe, and M. Bollen, *False-positive detection of rhEpo remains a real concern.* BLOOD, 2006. **108**(5): p. 1779,1780.
100. Franke, W.W. and H. Heid, *Pitfalls, errors and risks of false-positive results in urinary EPO drug tests.* Clinica Chimica Acta, 2006. **373**(1–2): p. 189-190.
101. Peltre, G. and W. Thormann, *Evaluation report of the urine epo test*, 2003, WADA: Paris and Bern.
102. Lamon, S., et al., *Effects of Exercise on the Isoelectric Patterns of Erythropoietin.* Clinical Journal of Sport Medicine, 2009. **19**(4): p. 311-315.
103. Lasne, F., *No doubt about the validity of the urine test for detection of recombinant human erythropoietin.* Blood, 2006. **108**(5): p. 1778-1779.
104. Catlin, D., et al., *False-positive Epo test concerns unfounded.* Blood, 2006. **108**(5): p. 1778.
105. Rabin, O.P., et al., *New urinary EPO drug testing method using two-dimensional gel electrophoresis.* Clinica Chimica Acta, 2006. **373**(1–2): p. 186-187.
106. Lundby, C., et al., *Testing for recombinant human erythropoietin in urine: problems associated with current anti-doping testing.* Journal of Applied Physiology, 2008. **105**(2): p. 417-419.
107. Banfi, G., et al., *A world apart: Inaccuracies of laboratory methodologies in antidoping testing.* Clinica Chimica Acta, 2010. **411**(15–16): p. 1003-1008.
108. Ashenden, M., et al., *The effects of microdose recombinant human erythropoietin regimens in athletes.* Haematologica-the Hematology Journal, 2006. **91**(8): p. 1143-1144.
109. Lönnberg, M., et al., *Rapid detection of erythropoiesis-stimulating agents in urine and serum.* Analytical Biochemistry, 2012. **420**(2): p. 101-114.
110. Storring, P.L., et al., *Epoetin alpha and beta differ in their erythropoetin isoform compositions and biological properties.* British Journal of Haematology, 1998. **100**(1): p. 79-89.
111. Lonnberg, M. and J. Carlsson, *Membrane assisted isoform immunoassay - A rapid method for the separation and determination of protein isoforms in an integrated immunoassay.* Journal of Immunological Methods, 2000. **246**(1-2): p. 25-36.
112. Fraguas, L.F., J. Carlsson, and M. Lonnberg, *Lectin affinity chromatography as a tool to differentiate endogenous and recombinant erythropoietins.* Journal of Chromatography A, 2008. **1212**(1-2): p. 82-88.
113. Lonnberg, M. and J. Carlsson, *Quantitative detection in the attomole range for immunochromatographic tests by means of a flatbed scanner.* Analytical Biochemistry, 2001. **293**(2): p. 224-231.
114. Ashenden, M., et al., *Evaluation of the MAIIA dipstick test to detect recombinant human erythropoietin in plasma.* Journal of Pharmaceutical and Biomedical Analysis, 2012. **67–68**(0): p. 123-128.

115. Lonnberg, M., M. Drevin, and J. Carlsson, *Ultra-sensitive immunochromatographic assay for quantitative determination of erythropoietin.* Journal of Immunological Methods, 2008. **339**(2): p. 236-244.
116. Mørkeberg, J., et al., *Detection of microdoses of rhEPO with the MAIIA test.* Scandinavian Journal of Medicine & Science in Sports, 2013: p. n/a-n/a.
117. Dehnes, Y., S. Lamon, and M. Lönnberg, *Erythropoietin (EPO) immunoaffinity columns--a powerful tool for purifying EPO and its recombinant analogues.* Journal of Pharmaceutical and Biomedical Analysis, 2010. **53**(4): p. 1028-32.
118. Reichel, C., *Recent developments in doping testing for erythropoietin.* Analytical and Bioanalytical Chemistry, 2011. **401**(2): p. 463-481.
119. Kay, R.G. and C.S. Creaser, *Application of mass spectrometry-based proteomics techniques for the detection of protein doping in sports.* Expert Review of Proteomics, 2010. **7**(2): p. 185-8.
120. Guan, F., et al., *Confirmatory Analysis of Continuous Erythropoietin Receptor Activator and Erythropoietin Analogues in Equine Plasma by LC−MS for Doping Control.* Analytical Chemistry, 2010. **82**(21): p. 9074-9081.
121. Guan, F., et al., *Identification of Darbepoetin Alfa in Human Plasma by Liquid Chromatography Coupled to Mass Spectrometry for Doping Control.* International Journal of Sports Medicine, 2009. **30**(02): p. 80,86.
122. Guan, F., et al., *Differentiation and Identification of Recombinant Human Erythropoietin and Darbepoetin Alfa in Equine Plasma by LC−MS/MS for Doping Control.* Analytical Chemistry, 2008. **80**(10): p. 3811-3817.
123. Guan, F., et al., *LC−MS/MS Method for Confirmation of Recombinant Human Erythropoietin and Darbepoetin α in Equine Plasma.* Analytical Chemistry, 2007. **79**(12): p. 4627-4635.
124. Ueki, M., Y. Kishikawa, and T. Ohtsuki, *"Novel methods for identification of recombinant glycoprotein hormones"*, 2011, World Anti-Doping Agency Sponsored Grant Available from: http://www.wada-ama.org/Documents/Science_Medicine/Funded_Research_Projects/2011/11B26MU%20Dr.%20Ueki.pdf.
125. Ueki, M., *Multiplexing of Protein Detection Capabilities*, in *Developments and Challenges in the Detection of Doping with Peptide Hormones Symposium* 2011, WADA and the Italian Federation of Sports Medicine (FMSI): Rome Available from: http://www.wada-ama.org/Documents/Science_Medicine/Scientific%20Events/Rome%202011/Dr.%20UEKI.pdf.
126. Tian, X.D., et al., *SHINERS and plasmonic properties of Au Core SiO2 shell nanoparticles with optimal core size and shell thickness.* Journal of Raman Spectroscopy, 2013. **44**(7): p. 994-998.

127. Liu, F., et al., *Ultrathin Diamond-like Carbon Film Coated Silver Nanoparticles-Based Substrates for Surface-Enhanced Raman Spectroscopy.* ACS Nano, 2010. **4**(5): p. 2643-2648.
128. Liu, F., et al., *Released Plasmonic Electric Field of Ultrathin Tetrahedral-Amorphous-Carbon Films Coated Ag Nanoparticles for SERS.* Scientific Reports, 2014. **4**.
129. Armbruster, D.A. and T. Pry, *Limit of Blank, Limit of Detection and Limit of Quantitation.* The Clinical Biochemist Reviews, 2008. **29**((Suppl 1)): p. S49-S52.
130. Mallorqui, J., et al., *New screening protocol for recombinant human erythropoietins based on differential elution after immunoaffinity purification.* J. Pharm. Biomed. Anal., 2010. **51**: p. 255-259.
131. Huang, C., et al., *Trapping Iron Oxide into Hollow Gold Nanoparticles.* Nanoscale Res Lett, 2011. **6**(1): p. 43.
132. Bao, F., J.-L. Yao, and R.-A. Gu, *Synthesis of Magnetic Fe2O3/Au Core/Shell Nanoparticles for Bioseparation and Immunoassay Based on Surface-Enhanced Raman Spectroscopy.* Langmuir, 2009. **25**(18): p. 10782-10787.

APPENDIX

Modified citrate reduction method for gold nanoparticle production video

movie link